8-2011

ANALYTICAL SOLUTIONS USING HIGH ORDER COMPOSITE LAMINATE THEORY FOR HONEYCOMB SANDWICH PLATES WITH VISCOELASTIC FREQUENCY DEPENDENT DAMPING

Nan Shan
Clemson University, nshan@clemson.edu

ANALYTICAL SOLUTIONS USING HIGH ORDER COMPOSITE LAMINATE THEORY FOR HONEYCOMB SANDWICH PLATES WITH VISCOELASTIC FREQUENCY DEPENDENT DAMPING

A Thesis
Presented to
The Graduate School of
Clemson University

In Partial Fulfillment
of the Requirements for the Degree
Master of Science
Mechanical Engineering

---

by
Nan Shan
August 2011

Accepted by:
Dr. Lonny L. Thompson, Committee Chair
Dr. Mohammed Daqaq
Dr. Jaehyung Ju

ABSTRACT

Analytical methods allow parametric changes in geometric and material properties of a honeycomb sandwich plate for studies of stiffness, mass, and damping characteristics with low computational cost. However, studies based on analytical methods are still limited with frequency independent damping models. Specifically, previous analytical models have not consider the frequency dependent damping for viscoelastic honeycomb core sandwich composites, while some work has been done on studying the honeycomb sandwich plate using finite element method, which can be computationally expensive for multiple parameter studies. Therefore, in this work, the honeycomb sandwich plate is studied analytically based on the cellular material theory, together with composite laminate theory. In initial analytical studies, first-order shear deformation theory (FSDT) is used for symmetric honeycomb sandwich plate in order to capture important transverse shear effects in the core.

In order to obtain a frequency response which includes frequency dependent viscoelastic damping properties, the study is based on a time harmonic analysis of the sandwich plate in the frequency domain. Two materials are compared for the core; aluminum and polycarbonate. For the aluminum honeycomb core, frequency independent damping is included and results compared with the results of different damping ratios. For the polycarbonate honeycomb core, the viscoelastic behavior is modeled using the generalized Maxwell damping model expressed in terms of the Prony series.

The study begins with a simplified case of a simply supported honeycomb sandwich plate subject to a uniform distributed transverse time harmonic loading, which has infinite length such that the deformation in the width direction is independent of the length. The undamped natural frequencies are also derived analytically based on the free vibration problem and compared to the damped resonance frequencies in the frequency response of the plate. Comparisons are made between regular and two types of auxetic honeycomb cores. Regular honeycomb is defined by cellular geometry with effective Poisson's ratio of approximately one, whereas auxetic honeycomb has negative Poisson's ratio. Both regular and auxetic have special orthotropic properties.

The case study is then generalized to a simply-supported sandwich honeycomb plate for a two dimensional problem. The response of the sandwich plate with regular honeycomb core is then compared with the responses of the two types of auxetic cores. Results for frequency response show shifts in resonance frequencies due to differences in stiffness and mass of the sandwich plate with different cores. Results from a composite sandwich plate finite element model using ANSYS with effective honeycomb core orthotropic properties was used to validate the analytical models in the case of no damping.

A refined higher order shear deformation theory (RSDT), based on a piecewise kinematic axial displacement component assumption, for sandwich honeycomb composite beam model is also compared to a model based on FSDT. Results show that the RSDT is more accurate at higher frequencies.

DEDICATION

This thesis is dedicated to my parents, Mr. Yuanpeng Zhao and Mrs. Xiaolu Huang.

ACKNOWLEDGMENTS

I offer my deepest gratitude to my research advisor Dr. Lonny L. Thompson who was abundantly helpful and offered invaluable assistance, support and guidance throughout this research project and for my thesis writing. I attribute the level of my Masters degree to his encouragement and effort without which this thesis would not have been completed. I would like to thank Dr. Mohammed Daqaq and Dr. Jaehyung Ju for serving on my committee and for their valuable suggestions for improving my thesis.

TABLE OF CONTENTS

LIST OF TABLES

LIST OF FIGURES

CHAPTER ONE– INTRODUCTION

Composite materials are made from two or more materials with significantly different material properties [18]. After certain processing techniques, these material laminates stick together but still remain the original material properties.

A sandwich plate (As seen in Figure 1.1), also called the sandwich composite structure, is one category in the composite material family. It is constructed by two thin face sheets and a thick core. Usually, the face sheet is composed of material with high stiffness (glass, carbon fiber, metal.). The core is composed of low stiffness material (polyvinylchloride, polyurethane, polycarbonate.). The three layers are attached together using an adhesive. In the early period, the core of a sandwich plate was normally composed of corrugated paper.

Figure 1.1: A sandwich plate [19]

Nowadays, various geometric structures are used to build the core. Honeycomb structure (As seen in Figure 1.2) is a very popular choice among them. This kind of structural design stemmed from the shape of beehive and had a very long history. A common honeycomb structure has hollow cells which all have the same shape and they are attached by thin walls. The cells' shape is often hexagonal.

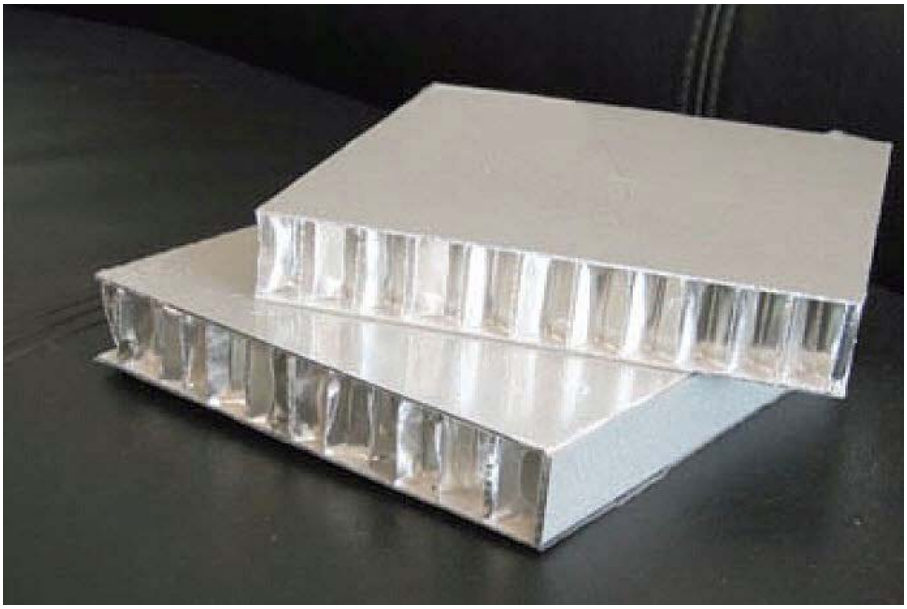

Figure 1.2: A honeycomb sandwich composite plate [20]

The normal way to create a honeycomb sandwich plate on a production line is by pressing the face sheets and honeycomb core together with an epoxy adhesive agent added on the contact surface. The face sheets itself may be constructed by composite material for various applications. A 3D model example of honeycomb sandwich plate is shown in Figure 1.3

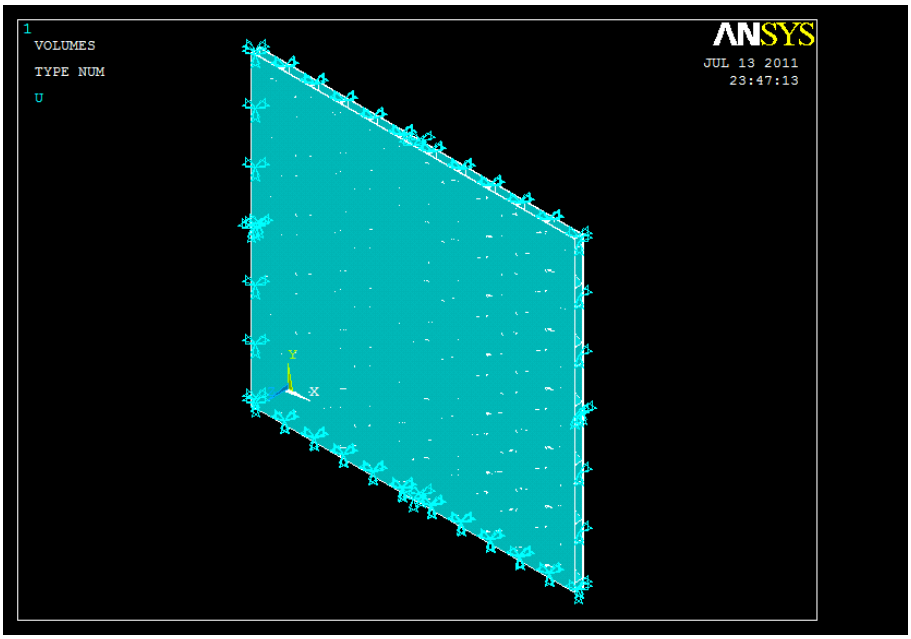

Figure 1.3: A 3D honeycomb sandwich plate model

1.1 Characteristics of a honeycomb sandwich plate

A sandwich plate possesses several important characteristics.

1. The lightweight feature is achieved by the special structure of the honeycomb sandwich plate. A honeycomb sandwich plate can be much lighter than composite panels with solid cores. Due to the high fuel price nowadays, fuel efficiency becomes a key factor in automotive design. Many manufacturers in automotive industry begin to use sandwich composite plate to replace the original structure because light weight construction becomes more important than before. Land Rover applied composite material to their new vehicles' instrument panel and door modules which made their new models' weight

under 1600kg [21]. In the transportation industry, honeycomb plates can reduce much weight out of a trailer, which increases fuel efficiency. This feature of a sandwich plate is also taken advantage of in ship building reducing tons of vessel weight which makes the vessel safer and more fuel efficient.

2. The special structure of a honeycomb sandwich plate also reduces the amount of material used comparing to regular composite plates.
3. Based on the material used, a honeycomb plate can have high strength to weight ratio and high stiffness to weight ratio. Depending on different needs, a sandwich plate can be manufactured using a wide range of materials. For low performance needs, paper or thermoplastics can be used. For high performance circumstances, metal or carbon-fiber will be used. As a result, honeycomb sandwich plates are often used in sports. Racing boats as well as racing cars use honeycomb sandwich plates for shell building.
4. A honeycomb sandwich plate can also have good damping property when certain materials are chosen to build the core. Therefore it is a widely used for sound absorption.
5. Other features may include corrosion and chemical resistance, non-conductive, fire resistance, reusability based on different materials. These properties are needed in industries like packaging design. Engineers will use honeycomb plates as void fillers.

Honeycomb sandwich plates are also widely used in aircraft and aerospace (The feet of the Apollo 11 landing module used honeycomb structure [15].), furniture design, building construction where such features are needed.

1.2 Previous works and study on honeycomb sandwich composite plates

Because of the utility value, much research relating to the honeycomb structure has been done in the past few decades. The mechanical property of the honeycomb structure is a research topic which many researchers focus on. The most popular way to derive the mechanical property, also called the effective property, of a honeycomb structure is to use the linear cell wall's bending model. This theory is called the cellular materials theory (CMT) which will be discussed in detail in following chapters.

The out-of-plane properties of a honeycomb structure is often used in design when normal or shear loads are high in that the out-of-plane properties are often much larger than the in-plane properties. What fascinates researchers most is that the honeycomb sandwich plate has anisotropic mechanical properties. These properties can be varied when geometric properties of a honeycomb structure are changed. The cellular geometry of the core considered for the present study is shown in Figure 1.4. t stands for cell wall thickness. l and h are inclined and vertical edge lengths. θ is called the cell wall angle. For a regular hexagonal cell, $h=l$ and $\theta=30°$.

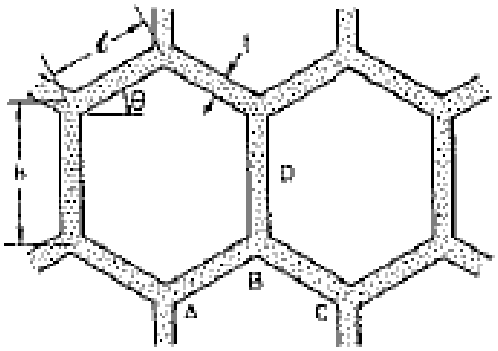

Figure 1.4: A hexagonal honeycomb core

Scarpa and Tomlinson [1] did research on the anisotropic mechanical properties of a honeycomb sandwich plate using the CMT theory. They found that the out-of-plane shear moduli of a honeycomb sandwich structure can be altered significantly when the geometric properties are changed, especially for a honeycomb core with a negative cell wall angle (Auxetic cell). They also found that the density of a sandwich plate with negative cell angle was higher than that with a regular honeycomb core. They studied the natural frequency of the structure with different cell wall angle and concluded that the dynamic behavior of a honeycomb sandwich structure could be significantly improved with a properly designed honeycomb cell. In their study, the first order shear deformation theory (FSDT) is used to derive the governing equations and the fundamental frequencies of sandwich plates. However, this theory could be inaccurate in some conditions.

Dobyns [2] studied the behavior of laminated composite plates subject to static and dynamic loads analytically. He derived the expression of the fundamental natural frequency of a general composite plate subject to simply supported boundary condition and studied the behavior of the plate when transient loadings were applied. He also

studied the behavior of the plate when these loadings were applied on different areas on the plate.

Chandra, Singh and Gupta [3] wrote a review on current research on damping in composite material. They found that the strain energy approach was very popular in predicting damping of a composite material when considering viscoelastic property. They also pointed out areas which still required further study. There were few models established including transverse and shear damping effects. Study on the interlaminar stress was limited. Damping optimization study in a composite structure was also needed.

Latheswary, Valsarajan, Sadasiva Rao [4] did research on laminated composites with focus on the effects of various design parameters on the dynamic behavior of a laminated composite plate. The research including transient analysis and time harmonic analysis was based on finite element method. The design parameters studied were damping ratio, width-to-thickness ratio, material anisotropy, fiber orientation, number of layers and aspect ratio. The harmonic response of the plate was studied with various damping ratios. It was found that the damping ratio had a significant effect on the resonance response, but the change of fiber orientation and width-to-thickness ratio did not have any influence on the response.

Araújo, et al [5] formulated a new finite element model for anisotropic laminated plate structure. The new model which contained 17 degrees of freedom in the displacement was based on a combination of FSDT and HSDT which meant to use FSDT for face sheet and HSDT for core. Their study involved viscoelastic material in designing the core. They used the complex modulus method to simulate viscoelastic property of the

core material. They studied the modal loss factor, the ratio of the imaginary part of the complex eigenvalue to the real part, for the free vibration problem. Having the modal loss factor, they did research on the damping optimization of the plate with both single and multiple objectives using the new model and an alternative ABAQUS model and found that the results matched. Their research showed that the present technique can improve the modal loss factor of the plate as to increase damping in the system. The new model was also proved to be more efficient in that the computational effort it took was 15 times less than the ABAQUS model's.

Meunier and Shenoi [6] studied Reddy's higher order shear deformation theory (HSDT). They derived the equations of motion of the system using Hamilton's principle. They then added the viscoelastic material property into the model and determined the natural frequencies and modal loss factors. During the study, they found that the dynamic properties of the materials had significant effect on the behavior of the plate.

Nayak, Shenoi and Moy [7] made modifications in Reddy's higher order shear deformation theory by adding two degrees of freedom into the displacement field and successfully let the requirement change from C^1 continuity finite element based on Reddy's HSDT to C^0. In their research, both frequency independent and frequency dependent damping of viscoelastic material were considered. During the study, they found that the resulting equations which were derived using the variational principle based on the new displacement field were very similar to the FSDT except for the higher order terms. The research results showed that the elements based on the new displacement field can be used to handle a wide range of problems.

Researchers are interested in refining the deformation theory used to define the behavior of a sandwich plate. Makhecha, Ganapathi and Patel [8] studied HSDT. They concluded that there were 3 kinds of HSDT used in the study of sandwich composites (HSDT7, HSDT11 and HSDT13). The number stands for the degrees of freedom involved in the displacement field. They then did research using the finite element method with viscoelastic material property taken into consideration. Their results showed that HSDT13 was the most accurate theory in simulating the response of the plate. Their research proved that the higher order terms in HSDT has significant effect in simulating the behavior of the plate.

Another method to simulate the response of the plate is to establish the displacement field layer by layer. Siala, Abdennadher, Hammami and Haddar [9] used this kind of displacement field to model the plate. In the study, they assumed a linear in-plane variation in the displacement through the thickness in the face sheet and a quadratic variation in the core. This method also showed high accuracy.

Studies of honeycomb sandwich panel made of other materials like paper have also been done. Zhu [10] did research on realizing the dynamic properties of a paper honeycomb panel. In his study, the plate model was based on a single degree of freedom system. Both viscous damping and linear viscoelastic damping were considered in the study.

The honeycomb sandwich plate in this work is created using aluminum and polycarbonate material for face sheet and honeycomb core respectively. The material behavior of aluminum and polycarbonate will be discussed in following chapters.

1.3 Honeycomb sandwich plate analysis in ANSYS

It is also feasible to use finite element commercial software to analyze honeycomb sandwich plates. A 3D model of honeycomb sandwich plate created using ANSYS v13 [17] is shown in Figure 1.5.

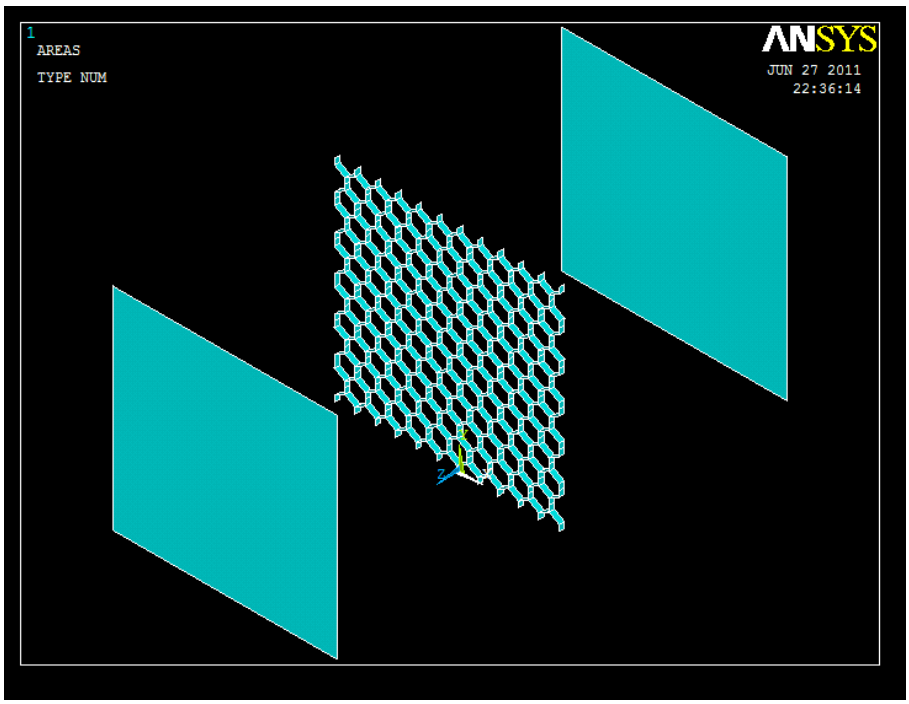

Figure 1.5: 3D finite element model built using ANSYS v13

There are several possible methods to create a honeycomb sandwich plate model using ANSYS. The most accurate way to model a honeycomb sandwich plate is to create the model in a fully detailed manner as shown in Figure 1.6. This way of modeling is called discrete modeling. It may be suitable for modeling one portion of a large

honeycomb sandwich plate. However, the computational consumption will be very high because a model like this may contain more than 40000 elements.

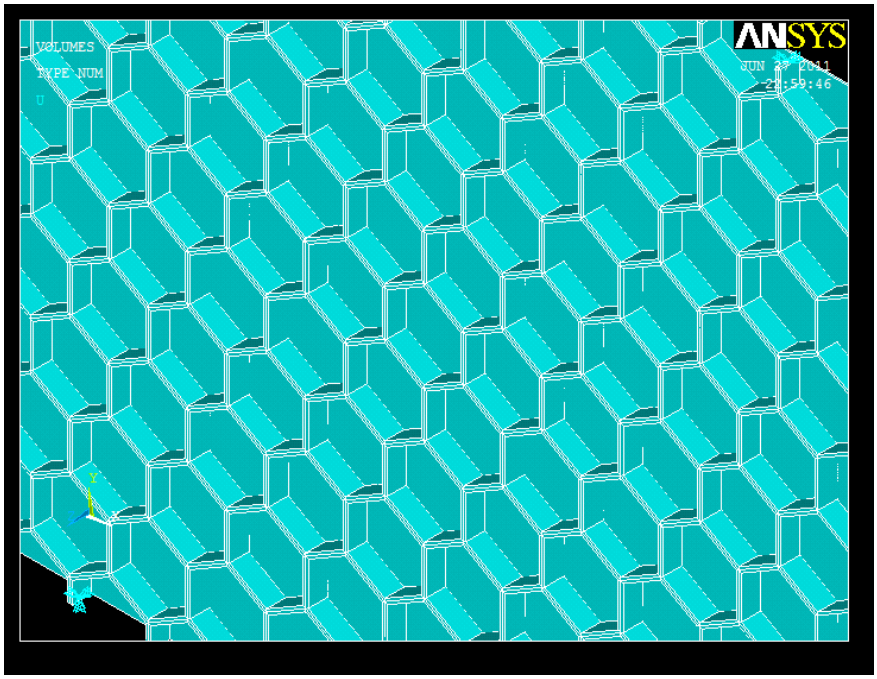

Figure 1.6: A fully modeled honeycomb sandwich plate

The way Figure 1.5 used is another way for discrete modeling. The honeycomb core in Figure 1.5 is modeled using a shell element with cell wall thickness input before the modeling process. This method could reduce the time needed for calculation.

A more simplified way to model a honeycomb sandwich plate is to replace the honeycomb layer with a homogeneous plate as shown in Figure 1.7. This method will use only shell elements during the process. But the researcher will be required to have a firm

understanding in the effective properties of a honeycomb core. This modeling technique will save much more time than the discrete modeling.

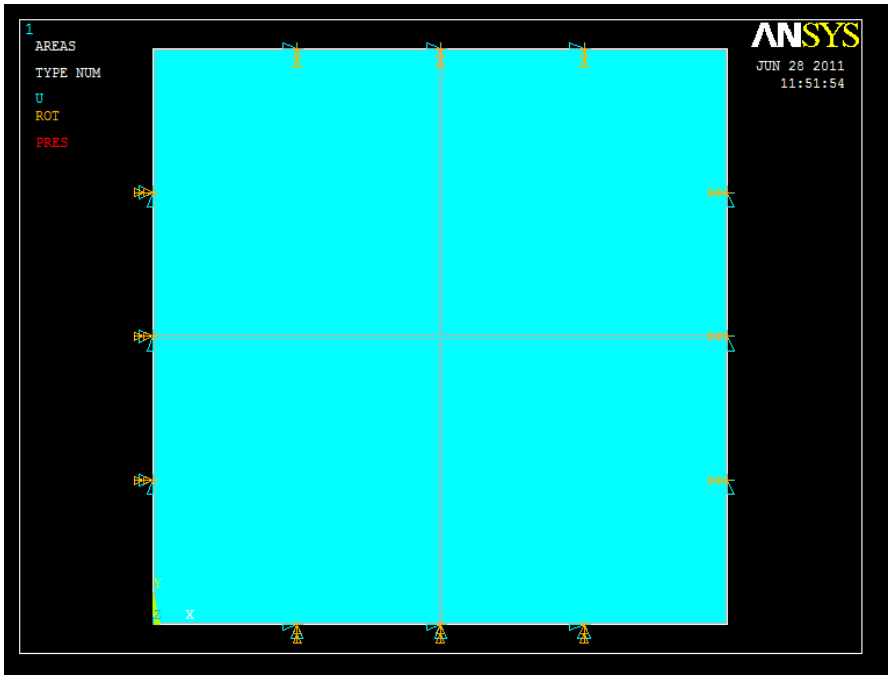

Figure 1.7: A honeycomb sandwich plate model using effective properties

1.4 Thesis objectives

Much work has been done on studying the honeycomb sandwich plate using commercial software. However, studies based on analytical methods are limited. Therefore, in this work, the honeycomb sandwich plate is studied analytically based on the composite material theory and first order shear deformation theory. The case study begins with a simplified sandwich beam which is simply supported on all edges. The beam is subject to a uniform distributed time harmonic loading. The behavior

(displacement field) of the beam is analyzed in the frequency domain. The natural frequency of the beam is also derived based on the free vibration case.

Viscoelastic material has been used in other studies based on finite element method. In this work, the viscoelastic material property is used for analytical study. The frequency dependent material properties are studied. Different material combinations are also used for core and face sheet to study the damping effect of the plate. Then the case study is generalized to a simply supported sandwich plate.

The first order shear deformation theory is commonly used in composite plate study. In this study, the accuracy of the FSDT is measured with another higher order shear deformation theory based on the sandwich beam case.

ABAQUS is often used in finite element modeling of honeycomb sandwich plates. However, it is not viable to establish a homogeneous plate model in ABAQUS in that users are not allowed to input Poisson' ratios larger than 0.5. Therefore, a homogenous plate model is established using ANSYS in this study for the simply supported sandwich plate case.

The contents of each chapter are shown below.

In Chapter 2, the original and the refined composite material theories are introduced. The material properties used in this study are defined. The frequency dependent viscoelastic material property is studied.

In Chapter 3, the governing equations of a sandwich beam (plate) are introduced. The results for the displacement field are given with different material combinations for face sheet and core. The damping effect is studied based on FSDT.

In Chapter 4, an HSDT is introduced. The results of the displacement field are compared between HSDT and FSDT. The accuracy of FSDT is discussed

In Chapter 5, a finite element model of a simply supported sandwich plate is provided for modal analysis and time harmonic analysis using ANSYS. The result is compared with FSDT.

CHAPTER TWO - THE PROPERTIES OF HONEYCOMB STRUCTURES AND MATERIALS

2.1 Chapter overview

Researchers need to have in depth knowledge of the mechanical effective properties of a honeycomb structure in order to study the behavior of a honeycomb sandwich plate, because this is the basis of the honeycomb sandwich plate theory. Therefore, the mechanical effective properties of a honeycomb structure will be discussed in this chapter.

The research in this thesis will be based on two kinds of materials which are aluminum and polycarbonate. The polycarbonate material contains viscoelastic material property. Its special characteristics will be discussed in detail in this chapter.

2.2 The effective properties of honeycomb cells

Figure 2.1 shows a regular hexagonal honeycomb shaped layer. The in-plane stiffness and strength (the X_1-X_2 plane in Figure 2.1) is very low in that in-plane stresses will cause cell walls to bend. The out-of-plane stiffness and strength (the X_2-X_3 plane and the X_1-X_3 plane in Figure 2.1) are higher because axial extension or compression of the cell walls which is much more difficult to deform is required. Therefore, the salient high stiffness feature of a honeycomb sandwich plate in design is represented by the out-of-plane stiffness.

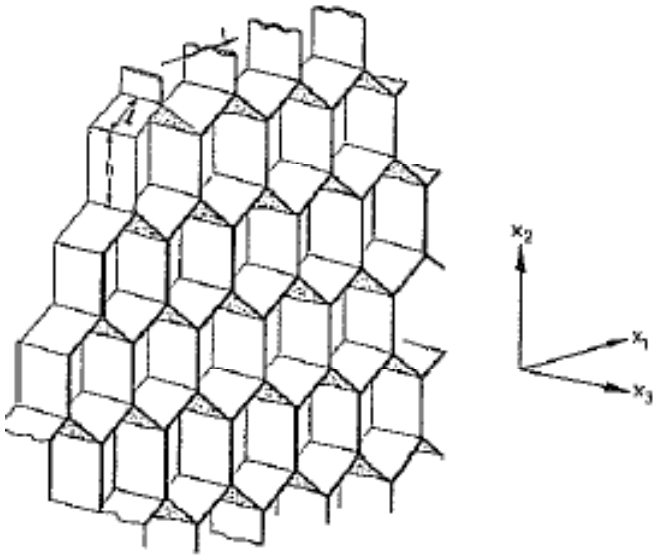

Figure 2.1: A honeycomb structured layer with regular hexagonal cells

Figure 2.2 shows a regular honeycomb cell. The honeycomb cell will show isotropic in-plane material properties if the following requirements are met:

1. The honeycomb cell has a regular hexagonal shape (All sides equal. The angle between two adjacent sides is 120°). The angle between two adjacent sides can be defined by $90^{\circ} + \theta$, so that for regular honeycomb, $\theta = 30^{\circ}$.
2. The cell has equal wall thickness on all sides.

There will be two independent moduli for this circumstance which are the effective Young's modulus *E* and the effective shear modulus *G*. However, when one or two of the two requirements are not met, there will be more independent moduli as the material shows an anisotropic behavior. Then four moduli are needed which are the

Young's modulus in X_1 direction E_1, the Young's modulus in X_2 direction E_2, the in-plane shear modulus G_{12} and the Poisson's ratio v_{12}.

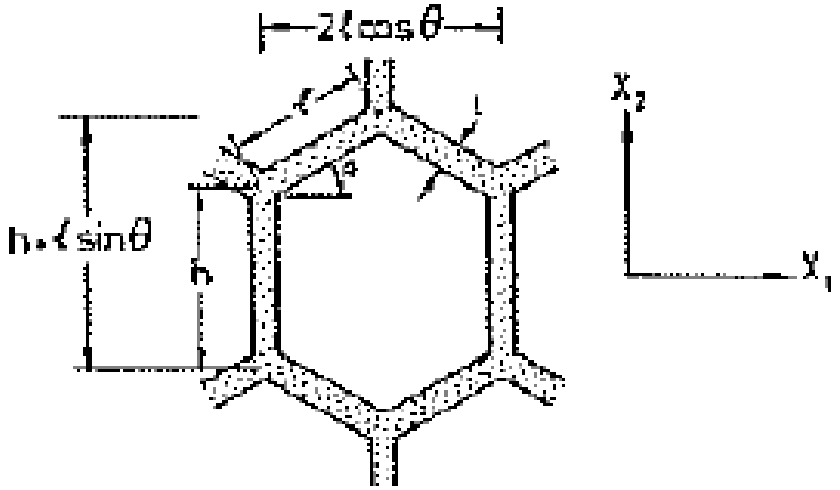

Figure 2.2: A regular hexagonal shaped honeycomb cell

The density of the honeycomb as shown below is derived by geometric calculation. The ratio of h to l is defined as α, i.e. $\alpha = h/l$. β is the ratio of t to l, i.e. $\beta = t/l$.

$$\frac{\rho_c}{\rho_m} = \frac{\beta(\alpha + 2)}{2\cos\theta(\alpha + \sin\theta)}$$

where ρ_c stands for the density of the honeycomb and ρ_m stands for the density of the core material. The definition of other dimensions can be found in Figure 2.2.

If the honeycomb structure is loaded in either X_1 or X_2 direction, and deforms in a linear-elastic way, there will be one more moduli in addition to the four moduli mentioned above, which is v_{21}. However, there is a reciprocal relation as seen below

$$E_1 v_{21} = E_2 v_{12}$$

which reduce the independent moduli number by one.

The two Young's moduli are derived by the method as seen in Figure 2.3.

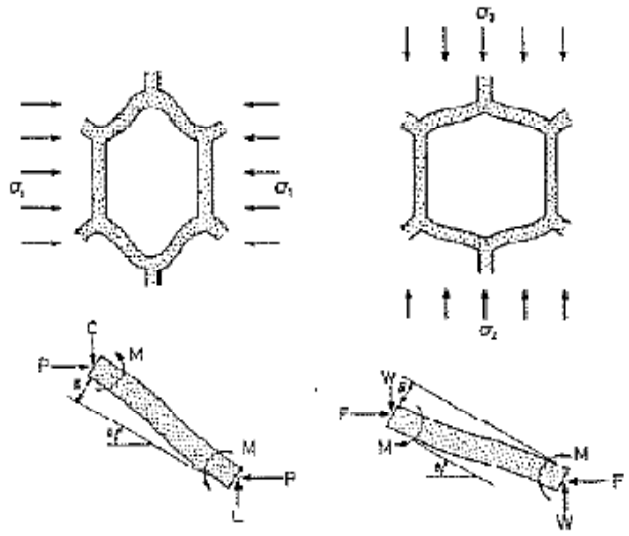

Figure 2.3: Bending caused by loading in X1 and X2 direction

The moment M tending to bend the cell wall is

$$M = \frac{Pl\sin\theta}{2}$$

where

$$P = \sigma_1 (h + l\sin\theta) b$$

where b is the depth of the honeycomb core.

The wall deflects by

$$\delta = \frac{Pl^3 \sin\theta}{12E_m I}$$

where I is the second moment of inertia of the cell wall and E_m is the Young's moduli of the core material.

The strain in X_1 direction is given by

$$\varepsilon_1 = \frac{\delta \sin\theta}{l\cos\theta} = \frac{\sigma_1 (h + l\sin\theta) bl^2 \sin^2\theta}{12E_m I \cos\theta}$$

Then the Young's modulus in X_1 direction can be derived as

$$\frac{E_1}{E_m} = (\beta)^3 \frac{\cos\theta}{(\alpha + \sin\theta)\sin^2\theta}$$

Loading in the X_2 direction is also shown in Figure 2.3. The moment can be derived as below

$$M = \frac{Wl\cos\theta}{2}$$

The wall deflects by

$$\delta = \frac{Wl^3 \cos\theta}{12E_m I}$$

The strain is the X_2 direction is given by

$$\varepsilon_2 = \frac{\delta\cos\theta}{h + l\sin\theta} = \frac{\sigma_2 bl^4 \cos^3\theta}{12E_m I(h + l\sin\theta)}$$

The Young's modulus in the X_2 direction can be derived as

$$\frac{E_2}{E_m} = \beta^3 \frac{(\alpha + \sin\theta)}{\cos^3\theta}$$

For a regular hexagon with homogeneous walls

$$\frac{E_1}{E_m} = \frac{E_2}{E_m} = 2.3\beta^3$$

As we can see, honeycomb layer with a regular hexagon shape will have isotropic in-plane properties.

Having the strains in X_1 and X_2 direction, we can derive the Poisson's ratio by taking the negative ratio of them, which is

$$\nu_{12} = -\frac{\varepsilon_2}{\varepsilon_1} = \frac{\cos^2\theta}{(\alpha + \sin\theta)\sin\theta}$$

The in-plane Poisson's ratio for a regular hexagon will be seen as 1. However, this may not be true for a refined theory which will be discussed later. Knowing v_{12}, v_{21} can be derived in the same way which is the reciprocal of v_{12}. An interesting phenomenon can be seen considering the Poisson's ratio. That is, when the cell wall angle of the honeycomb cell is negative, the Poisson's ratio will be negative which is very rare. This means that when an extensional force is applied in X_1 or X_2 direction, the normal in-plane side will , rather than contracting, expand. This phenomenon is disscussed in detail in Scarpa and Tomlinson's research[1] which was mentioned in the first chapter.

For regular honeycomb, since

$$E_1 = E_2, \quad E_1\nu_{21} = E_2\nu_{12}$$

then $\nu_{12} = \nu_{21}$.

The in-plane shear modulus is derived by the method as seen in Figure 2.4 and Figure 2.5.

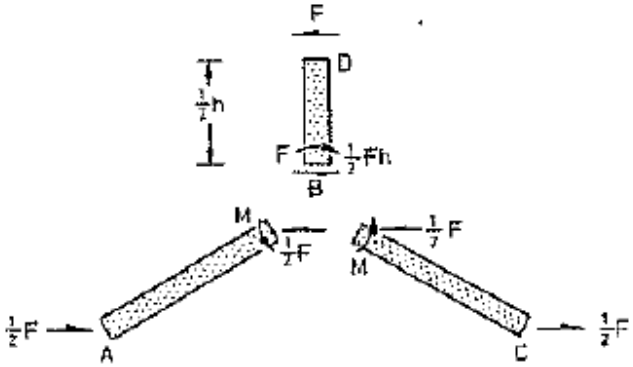

Figure 2.4: Loads and moments caused by a shear stress

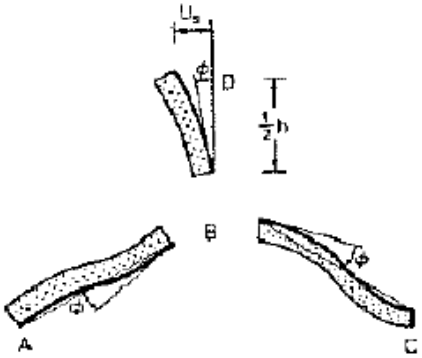

Figure 2.5: Displacements and rotations caused by a shear stress

The shear deflection is caused by bending of BD and the rotational angle. Therefore, the shear strain is given by

$$\gamma = \frac{2u_s}{(h + l\sin\theta)} = \frac{Fh^2}{24E_m I}\frac{(l+2h)}{(h+l\sin\theta)}$$

The shear stress is given by

$$\tau = \frac{F}{2lb\cos\theta}$$

The shear modulus can be derived by

$$\frac{G_{12}}{E_m} = (\beta)^3 \frac{(\alpha + \sin\theta)}{(\alpha)^2(1+2\alpha)\cos\theta}$$

The out-of-plane properties of a honeycomb structure are more important in that for hexagonal honeycomb structure, the out-of-plane properties are much larger than in-plane properties. This is due to the fact that when loaded in the X_3 direction, cell walls will be extended or compressed. The load is assumed to be applied in the X_3 direction, or on the surface normal to the X_3 direction which can be seen in Figure 2.6.

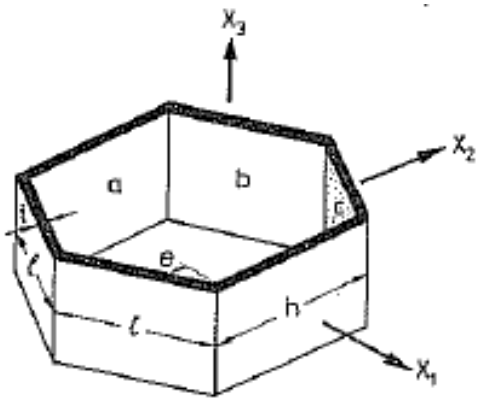

Figure 2.6: A honeycomb cell with loading in the X3 direction

A low density honeycomb layer is assumed. The cell walls have the same thickness. Five more moduli are needed to describe the out-of-plane properties. The Young's modulus in the X_3 direction E_3 is given by

$$\frac{E_3}{E_m} = \frac{\alpha + 2}{2(\alpha + \sin\theta)\cos\theta}\beta = \frac{\rho_H}{\rho_m} \approx \beta$$

The Poisson's ratios v_{31} and v_{32} are equal to the Poisson's ratio of the core material

$$v_{31} = v_{32} = v_m$$

Then v_{13} and v_{23} are found by using the reciprocal relations mentioned above

$$E_1 v_{31} = E_3 v_{13}, \quad E_2 v_{32} = E_3 v_{23}$$

For honeycomb, $E_1 / E_3 = v_{13} / v_{31} \approx (t/l)^2$. Typically the ratio of cell wall thickness to cell length, $\beta = t/l$, is small, $E_1 \ll E_3$ and

$$v_{13} = v_{23} \approx 0$$

The out-of-plane shear moduli were derived using the theorems of minimum potential energy and minimum complementary energy. The first theorem gives an upper bound, which are

$$\frac{G_{13}}{G_m} \le \frac{\cos\theta}{\alpha + \sin\theta}\beta$$

$$\frac{G_{23}}{G_m} \le \frac{1}{2}\frac{\alpha + 2\sin^2\theta}{(\alpha + \sin\theta)\cos\theta}\beta$$

For regular hexagons, it becomes

$$\frac{G_{13}}{G_m} = 0.577\beta$$

The second theorem gives a lower bound, which are

$$\frac{G_{13}}{G_m} \ge \frac{\cos\theta}{\alpha + \sin\theta}\beta$$

$$\frac{G_{23}}{G_m} \geq \frac{\alpha + \sin\theta}{(1+2\alpha)\cos\theta}\beta$$

For regular hexagons, it becomes

$$\frac{G_{23}}{G_m} = 0.577\beta$$

This is another proof that a honeycomb structure with regular hexagonal shaped cells has isotropic in-plane material properties.

There is also an refined theory to calculate E_1, E_2, v_{12}, v_{21} and G_{12} which become useful when $t/l > 0.2$. In this theory, axial and shear deformation effects are considered during the deriving process. For this theory, E_1 is given by

$$E_1 = E_m\beta^3 \frac{\cos\theta}{(\alpha+\sin\theta)\sin^2\theta} \frac{1}{1+(2.4+1.5\nu_m+\cot^2\theta)\beta^2}$$

E_2 is given by

$$E_2 = E_m\beta^3 \frac{\alpha+\sin\theta}{\cos^3\theta} \frac{1}{1+(2.4+1.5\nu_m+\tan^2\theta+\frac{2\alpha}{\cos^2\theta})\beta^2}$$

v_{12} is given by

$$\nu_{12} = \frac{\cos^2\theta}{(\alpha+\sin\theta)\sin\theta} \frac{1+(1.4+1.5\nu_m)\beta^2}{1+(2.4+1.5\nu_m+\cot^2\theta)\beta^2}$$

v_{21} can be derived using the reciprocal relation. Using this refined theory, for regular honeycomb, $\nu_{12} = \nu_{21} \neq 1$, like it was using the simple theory discussed earlier, which neglected transverse shear and axial effects.

G_{12} is given by

$$G_{12} = \frac{E_m \beta^3 (\alpha + \sin\theta)}{\alpha^2 \cos\theta} \frac{1}{F}$$

where F is

$$F = 1 + 2\alpha + \beta^2 \left\{ \begin{array}{l} \frac{1}{\alpha}(2.4 + 1.5\nu_m)(2 + \alpha + \sin\theta) \\ + \frac{\alpha + \sin\theta}{\alpha^2}[(\alpha + \sin\theta)\tan^2\theta + \sin\theta] \end{array} \right\}$$

This refined theory is useful in that most current commercial software like ANSYS and ABAQUS will not allow users to input Poisson's ratios larger than 1 or 0.5, respectively. Therefore, if researchers want to establish a model using the effective properties to save computational time as mentioned in the first chapter, the moduli provided by the refined theory can be accepted because of the slight difference.

2.3 Material properties

As mentioned in the first chapter, two kinds of materials will be used during the study in this dissertation, which are aluminum and polycarbonate. Aluminum is often used in building honeycomb cores and faces in that the sandwich plates built using this material will possess many salient features mentioned in the first chapter. Therefore, it is worthwhile to study the behavior of aluminum honeycomb sandwich plates.

Polycarbonate is used as the honeycomb core material in this study. This is due to the fact that this material is stiff enough to be used as the core material while it possesses good viscoelastic material property. Therefore, polycarbonate is chosen to study the viscoelastic damping behavior of the honeycomb sandwich plate.

In this study, two types of material combination will be used which are honeycomb sandwich plate built by aluminum face sheets and honeycomb cores, sandwich plate built by aluminum face sheets and polycarbonate cores. The aluminum alloy used in this study is Al-5052-H39. The mechanical properties of Al-5052-H39 and the polycarbonate material can be seen in Table 2-1.

Table 2-1: Mechanical properties of Al-5052-H39 and polycarbonate material

Materials	Young's modulus, E (GPa)	Poisson's ratio, v	Density, ρ (kg/m^3)
Al-5052-H39	68.97	0.34	2700
Polycarbonate	2.07	0.37	1200

The viscoelastic property of the polycarbonate material is defined by the shear relaxation of the material in the time domain.

For a small strain, the viscoelastic material model is defined as

$$\tau(t) = \int_0^t G_R(t-s)\dot{\gamma}(s)ds$$

where $\gamma(t)$ is the shear strain, $\tau(t)$ is the shear stress, $G_R(t)$ is the time-dependent shear relaxation modulus. For a constant strain γ, which is applied suddenly and held for a long time, the shear stress can be given as

$$\tau(t) = G_R(t)\gamma$$

For this condition, $G_R(t) \to G_\infty$ as time goes to infinity. Therefore, the shear modulus is given by

$$G_R(t) = g_R(t)G_0$$

For a large strain, the stress is given by

$$\tau(t) = G_0(\gamma + \int_0^t \dot{g}_R(s)\gamma(t-s)ds)$$

where G_0 is the instantaneous shear modulus.

Prony series expansion is used in defining the property.

$$g_R(t) = 1 - \sum_{i=1}^{N} g_i(1 - e^{-t/\tau_i})$$

The shear relaxation modulus for a linear elastic material can be derived using the relation mentioned above

$$G_R(t) = G_0(1 - \sum_{i=1}^{N} g_i(1 - e^{-t/\tau_i}))$$

where N , g_k , τ_k are material constants. The instantaneous shear modulus of polycarbonate can be defined from the instantaneous Young's modulus E_0 and Poisson's ratio v_0 shown in Table 2-1. The long-term moduli is defined by

$$G_\infty = G_0(1 - \sum_{i=1}^{N} g_i)$$

In this study, the frequency response of the honeycomb sandwich plate is taken more consideration. Therefore, the Prony series terms expressed using frequency dependent test data is more important. The expressions for the shear moduli are given by

$$G_s(\omega) = G_\infty + G_0 \sum_{i=1}^{N} \frac{g_i \tau_i^2 \omega^2}{1 + \tau_i^2 \omega^2}$$

$$G_l(\omega) = G_0 \sum_{i=1}^{N} \frac{g_i \tau_i \omega}{1 + \tau_i^2 \omega^2}$$

where $G_s(\omega)$ is called the storage modulus and $G_l(\omega)$ is called the loss modulus. Therefore, the shear modulus can be written in a complex form

$$G_m(\omega) = G_s(\omega) + iG_l(\omega)$$

The imaginary part of the complex shear modulus is where the energy dissipation of the system comes from. The ratio of the loss modulus to the storage modulus, η, is often called the loss factor which is mentioned in the first chapter.

$$G_m(\omega) = G_s(\omega)(1 + i\eta(\omega))$$

For viscoelastic materials the loss factor in frequency dependent. The prony series data to express the viscoelastic property of the polycarbonate can be found in Table 2-2.

Table 2-2: Prony series material constants

i	g_i	τ_i
1	0.0601089	0.0015332
2	0.84558	2.1425
3	0.0906806	19.791

The figures of the shear relaxation modulus are plotted numerically using the method and data shown above. The results are normalized to the instantaneous shear modulus. The figures are shown below in Figure 2.7 and Figure 2.8.

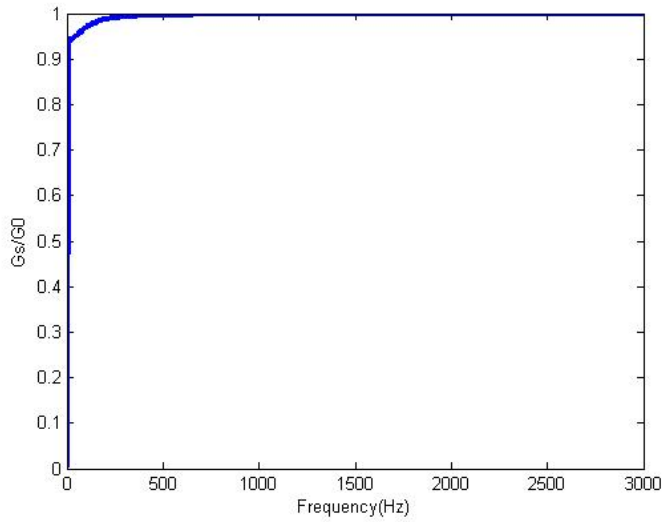

Figure 2.7: Normalized shear storage modulus via frequency

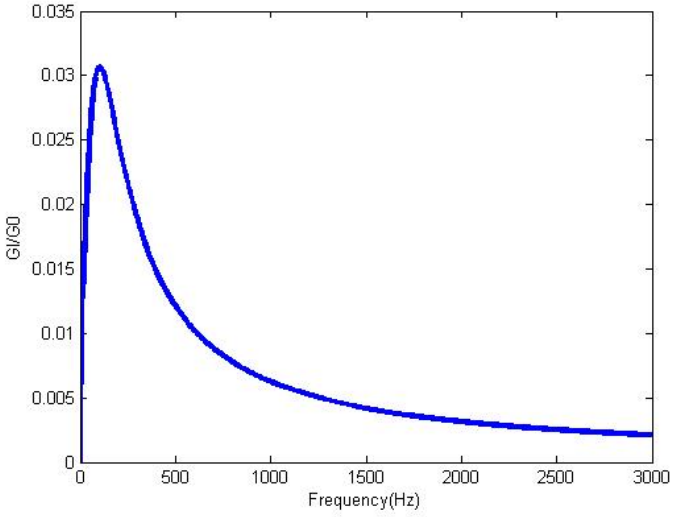

Figure 2.8: Normalized shear loss modulus via frequency

The frequency dependent Young's modulus is derived using the following relation.

$$E^*(\omega) = \frac{9K_0 G^*(\omega)}{3K_0 + G^*(\omega)}$$

where K_0 is the bulk modulus which is assumed to be a constant in this material model, K_0 is derived by

$$K_0 = \frac{E_0}{3(1-2\nu_0)}$$

The figures of the Young's modulus are shown in Figure 2.9 and Figure 2.10.

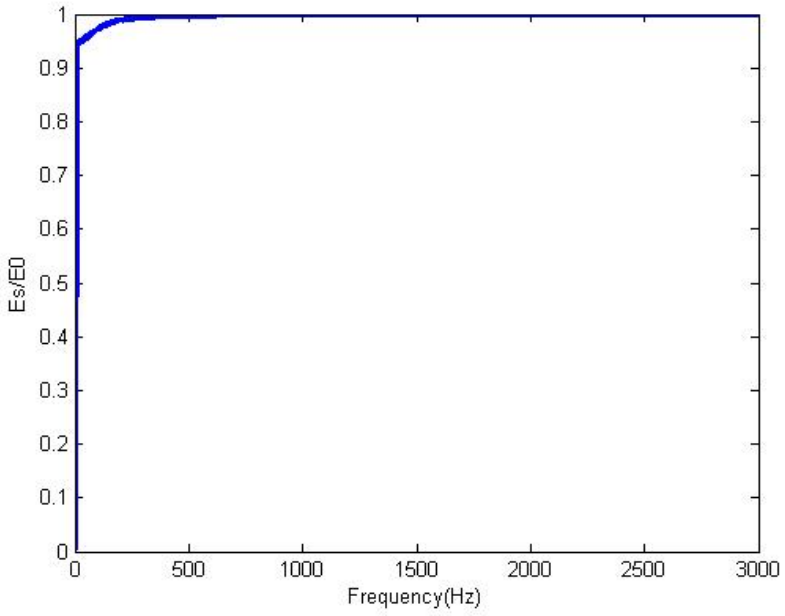

Figure 2.9: Normalized storage modulus of Young's modulus via frequency

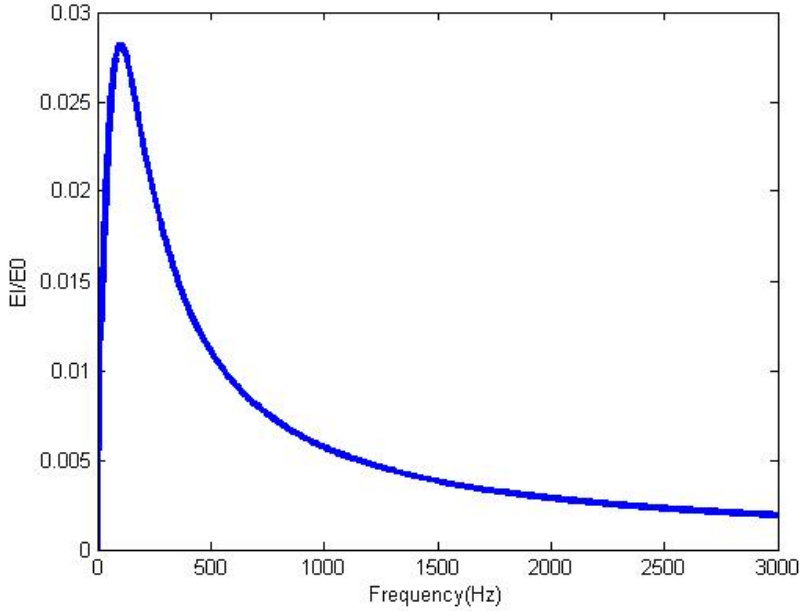

Figure 2.10: Normalized loss modulus of Young's modulus via frequency

The Poisson's ratio of the material can be derived using the following relation

$$\nu^*(\omega) = \frac{3K_0 - 2G^*(\omega)}{2(3K_0 + G^*(\omega))}$$

The figures of the Poisson's ratio are shown in Figure 2.11 and Figure 2.12.

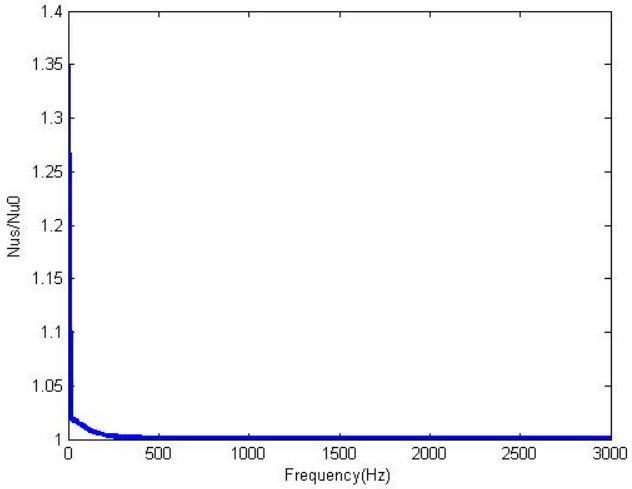

Figure 2.11: Normalized storage modulus of the Poisson's ratio via frequency

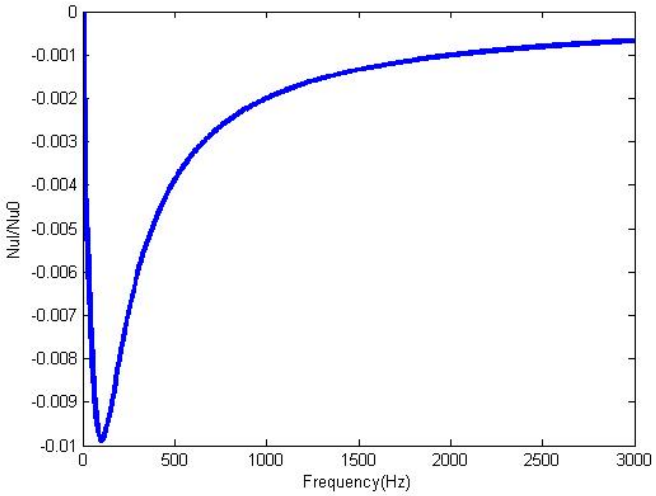

Figure 2.12: Normalized loss modulus of the Poisson's ratio via frequency

It is interesting to compare the figures of the Poisson's ratio with that of the shear modulus. The Poisson's ratio has an opposite tendency as the frequency increases considering the shear modulus.

Having the mechanical properties defined, the effective properties of a honeycomb layer can be determined.

The dimensions of the honeycomb structure mentioned in this study are defined as seen in Table 2-3

Table 2-3: Dimensions of the regular honeycomb structure

Dimensions	a	b	α	β	γ	t_c	t_f	θ	r
Value	0.5	0.5	1	0.12	12	0.012	0.001	30°	35.7

In Table 2-3, a stands for the length of the honeycomb sandwich plate. b is the width of the plate. $\gamma = t_c / t_f$, is the ratio of core thickness to face sheet thickness, where t_c is the core thickness. t_f is the thickness of the face sheet. θ is the cell wall angle. The ratio of the overall plate dimensions to out-of-plane total thickness is $r = a/(2t_f + t_c)$.

The effective density of the honeycomb layer and the total mass density per unit area ρ_t can be seen in Table 2-4. ρ_t is defined as

$$\rho_t = (2t_f)\rho_f + t_c\rho_c = t_f(2\rho_f + \gamma\rho_c)$$

where ρ_c is the density of the core material.

Table 2-4: Effective density and total mass density

	ρ_H (kg/m^3)	ρ_t (kg/m^2)
Aluminum face and polycarbonate core	166.2769	7.3953
Aluminum face and aluminum core	374.123	9.8895

The other effective properties of an Aluminum and polycarbonate honeycomb cores can be seen in Table 2-5.

Table 2-5: Effective density and total mass density

Regular hexagon	$E_1=E_2$ (MPa)	G_{13} (MPa)	G_{12} (MPa)	E_3 (MPa)	$\nu_{12}=\nu_{21}$
Aluminum core	253.65	1783	65.141	8276.4	0.9469
Polycarbonate core	7.6082	52.341	1.9539	248.4	0.9469

The effective properties for the polycarbonate core are derived by using the instantaneous modulus for comparison purpose. The moduli in the study are frequency dependent. All the properties are calculated using the refined theory. The regular hexagonal shaped honeycomb structure shows in-plane isotropic material property.

CHAPTER THREE - DERIVATION OF THE GOVERNING EQUATIONS OF A SANDWICH PLATE

3.1 Orthotropic material properties

As discussed in Chapter 2, the effective properties of honeycomb are characterized by orthotropic behavior. Orthotropic materials show different material behavior on orthogonal material directions which is also called orthogonal anisotropic. The elasticity tensor of an orthogonal material is defined as

$$\left[C_{ij}\right] = \begin{bmatrix} C_{11} & C_{12} & C_{13} & 0 & 0 & 0 \\ & C_{22} & C_{23} & 0 & 0 & 0 \\ & & C_{33} & 0 & 0 & 0 \\ & & & C_{44} & 0 & 0 \\ & sym & & & C_{55} & 0 \\ & & & & & C_{66} \end{bmatrix}$$

The stress-strain relationship is given by $\{\varepsilon\} = [C]\{\sigma\}$.

After standardized tensile tests [], anisotropic elastic material constants can be related to the compliance matrix [*C*], which is the inverse of the stiffness matrix.

$$\left[C_{ij}\right] = \begin{bmatrix} \frac{1}{E_1} & \frac{-\upsilon_{12}}{E_1} & \frac{-\upsilon_{13}}{E_1} & 0 & 0 & 0 \\ \frac{-\upsilon_{21}}{E_2} & \frac{1}{E_2} & \frac{-\upsilon_{23}}{E_2} & 0 & 0 & 0 \\ \frac{-\upsilon_{31}}{E_3} & \frac{-\upsilon_{32}}{E_3} & \frac{1}{E_3} & 0 & 0 & 0 \\ 0 & 0 & 0 & \frac{1}{G_{13}} & 0 & 0 \\ 0 & 0 & 0 & 0 & \frac{1}{G_{23}} & 0 \\ 0 & 0 & 0 & 0 & 0 & \frac{1}{G_{12}} \end{bmatrix}$$

Taking the inverse gives $\{\sigma\} = [Q]\{\varepsilon\}$. The stiffness matrix can be defined as $[Q] = [C]^{-1}$:

$$Q_{ij} = \begin{bmatrix} Q_{11} & Q_{12} & Q_{13} & 0 & 0 & 0 \\ Q_{12} & Q_{22} & Q_{23} & 0 & 0 & 0 \\ Q_{13} & Q_{23} & Q_{33} & 0 & 0 & 0 \\ 0 & 0 & 0 & Q_{44} & 0 & 0 \\ 0 & 0 & 0 & 0 & Q_{55} & 0 \\ 0 & 0 & 0 & 0 & 0 & Q_{66} \end{bmatrix}$$

The constants in the matrix are defined by material constants

$$\begin{aligned} Q_{11} &= E_1(1 - \nu_{23}\nu_{32}) / \Delta \\ Q_{22} &= E_2(1 - \nu_{13}\nu_{31}) / \Delta \\ Q_{33} &= E_3(1 - \nu_{12}\nu_{21}) / \Delta \\ Q_{12} &= (\nu_{21} + \nu_{31}\nu_{23})E_1 / \Delta = (\nu_{12} + \nu_{32}\nu_{13})E_2 / \Delta \\ Q_{13} &= (\nu_{31} + \nu_{21}\nu_{32})E_1 / \Delta = (\nu_{13} + \nu_{12}\nu_{23})E_3 / \Delta \\ Q_{23} &= (\nu_{32} + \nu_{12}\nu_{31})E_2 / \Delta = (\nu_{23} + \nu_{21}\nu_{13})E_3 / \Delta \\ Q_{66} &= G_{12} \\ Q_{44} &= G_{13} \\ Q_{55} &= G_{23} \end{aligned}$$

where

$$\Delta = 1 - \nu_{12}\nu_{21} - \nu_{23}\nu_{32} - \nu_{31}\nu_{13} - 2\nu_{21}\nu_{32}\nu_{13}$$

In the design process of a sandwich plate, the face sheet itself might be made of composite material composed of various laminae for certain purposes. These laminae may not share the same direction due to local coordinate systems which can be seen in Figure 3.1, which means that the stress generated on the principal geometric direction might be different for each laminae.

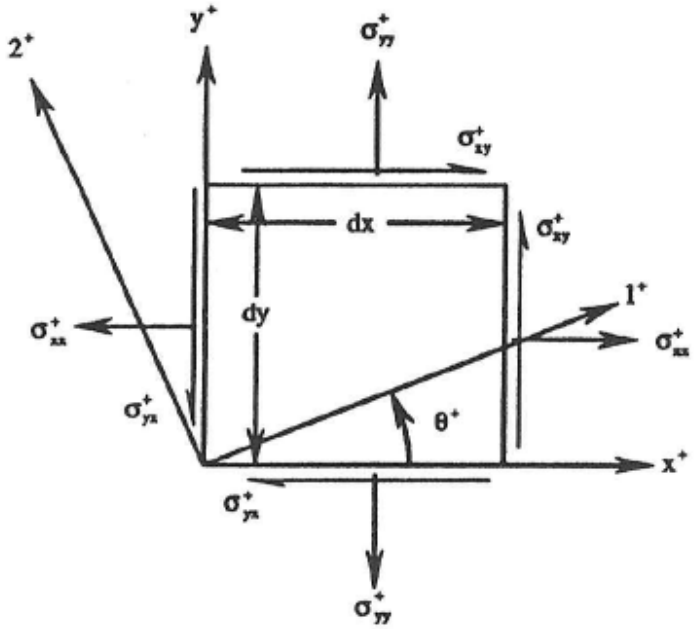

Figure 3.1: Stress coordinate system transformation

A transformation matrix is also used to add a stack of laminae, with different orthotropic directions in a common coordinate system. The transformation matrix can be derived by consideration of a sum of force components on cut free-body-diagrams on a stress element in directions defined by rotation of coordinates through an angle θ in the

plane of rotation. The transformation of stress components from a local lamina coordinates X_1, X_2 to rotated coordinates X, Y can be expressed as $\{\sigma\} = [T]\{\sigma'\}$. The transformation matrix is given by

$$[T] = \begin{bmatrix} m^2 & n^2 & 0 & 0 & 0 & 2mn \\ n^2 & m^2 & 0 & 0 & 0 & -2mn \\ 0 & 0 & 1 & 0 & 0 & 0 \\ 0 & 0 & 0 & m & -n & 0 \\ 0 & 0 & 0 & n & m & 0 \\ -mn & mn & 0 & 0 & 0 & m^2 - n^2 \end{bmatrix}$$

where $m = \cos\theta$ and $n = \sin\theta$. The relation between stress and strain for a typical laminate, in the geometric (x, y) coordinate system can then be expressed as

$$\begin{Bmatrix} \sigma_x \\ \sigma_y \\ \sigma_z \\ \sigma_{xz} \\ \sigma_{yz} \\ \sigma_{xy} \end{Bmatrix}_k = \begin{bmatrix} \bar{Q}_{11} & \bar{Q}_{12} & \bar{Q}_{13} & 0 & 0 & \bar{Q}_{16} \\ & \bar{Q}_{22} & \bar{Q}_{23} & 0 & 0 & \bar{Q}_{26} \\ & & \bar{Q}_{33} & 0 & 0 & \bar{Q}_{36} \\ & & & \bar{Q}_{44} & \bar{Q}_{45} & 0 \\ & sym & & & \bar{Q}_{55} & 0 \\ & & & & & \bar{Q}_{66} \end{bmatrix}_k \begin{Bmatrix} \varepsilon_x \\ \varepsilon_y \\ \varepsilon_z \\ 2\varepsilon_{xz} \\ 2\varepsilon_{yz} \\ 2\varepsilon_{xy} \end{Bmatrix}_k$$

where

$$[\bar{Q}] = [T]^{-1}[Q][T]$$

and *k* means the *k*th lamina of the composite.

3.2 Kinematic Displacement and Strains for Laminate

In the present work, a linear strain-displacement relation is used. For small strains, the strain components are defined by derivatives of displacement components. In index notation, the strain tensor components are given by

$$\varepsilon_{ij} = \frac{1}{2}(u_{i,j} + u_{j,i})$$

where *i*, *j*, are indices ranging from 1 to 3. The numerical indices correspond to component directions *x*, *y*, *z* in a Cartesian coordinate field. The comma means partial differentiation with respect to the coordinate after the comma. Expanding, the normal and shear components can be expressed as

$$\varepsilon_x = \frac{\partial u}{\partial x},$$
$$\varepsilon_y = \frac{\partial v}{\partial y},$$
$$\varepsilon_z = \frac{\partial w}{\partial z}$$
$$\gamma_{xz} = 2\varepsilon_{xz} = \frac{\partial u}{\partial z} + \frac{\partial w}{\partial x},$$
$$\gamma_{yz} = 2\varepsilon_{yz} = \frac{\partial v}{\partial z} + \frac{\partial w}{\partial y},$$
$$\gamma_{xy} = 2\varepsilon_{xy} = \frac{\partial u}{\partial y} + \frac{\partial v}{\partial x}$$

where *u*, *v* and *w* are displacements in *x*, *y* and *z* directions respectively. γ_{yz} and γ_{xz} are out-of-plane transverse shear strain components, while γ_{xy} is the in-plane shear strain component.

In the first order shear deformation theory, it is assumed that the displacement through the thickness is linear and there is only one element through the thickness. Only one translational and one rotational degree of freedom per direction are considered in the displacement field. Therefore, the displacement can be given in the following form

$$u(x,y,z) = u_0(x,y) + z\alpha(x,y)$$
$$v(x,y,z) = v_0(x,y) + z\beta(x,y)$$
$$w(x,y,z) = w(x,y)$$

In the classical theory, the rotational terms are defined as the derivative of the out-of-plane displacement, $\alpha = -\frac{\partial w}{\partial x}, \beta = -\frac{\partial w}{\partial y}$. This implies that transverse shear deformation is neglected. However, in the first shear deformation theory, transverse shear deformation is not zero. For composites constructed from a stack of lamina, where some layers with soft material are sandwiched between stiffer layers, it is important to model shear deformation in order to accurately capture the behavior under loading. Also first-order shear deformation theory gives more accurate stress values compared to classical theory. Using these first-order deformation assumptions, the thru thickness normal strain component is assumed to be zero. Substituting the displacement field into the linear strain-displacement relation gives

$$\varepsilon_x = \frac{\partial u_0}{\partial x} + z\frac{\partial \alpha}{\partial x},$$
$$\varepsilon_y = \frac{\partial v_0}{\partial y} + z\frac{\partial \beta}{\partial y},$$
$$\varepsilon_z = 0$$
$$\gamma_{xz} = 2\varepsilon_{xz} = \alpha + \frac{\partial w}{\partial x},$$
$$\gamma_{yz} = 2\varepsilon_{yz} = \beta + \frac{\partial w}{\partial y}$$
$$\gamma_{xy} = 2\varepsilon_{xy} = \left(\frac{\partial u_0}{\partial y} + \frac{\partial v_0}{\partial x}\right) + z\left(\frac{\partial \alpha}{\partial y} + \frac{\partial \beta}{\partial x}\right)$$

From these equations, it is clear in the case of classical theory, the transverse shear strains γ_{xz} and γ_{yz} are zero. The mid-surface strains can be written as

$$\varepsilon_{x_0} = \frac{\partial u_0}{\partial x}, \quad \varepsilon_{y_0} = \frac{\partial v_0}{\partial y}, \quad \varepsilon_{xy_0} = \frac{1}{2}\left(\frac{\partial u_0}{\partial y} + \frac{\partial v_0}{\partial x}\right)$$

The curvatures are given by

$$\kappa_x = \frac{\partial \alpha}{\partial x}, \quad \kappa_y = \frac{\partial \beta}{\partial y}, \quad \kappa_{xy} = \frac{1}{2}\left(\frac{\partial \alpha}{\partial y} + \frac{\partial \beta}{\partial x}\right)$$

Using the first-order deformation theory, the stress-strain relation for lamina can be rewritten as

$$\begin{Bmatrix} \sigma_x \\ \sigma_y \\ \sigma_{xz} \\ \sigma_{yz} \\ \sigma_{xy} \end{Bmatrix}_k = [\bar{Q}]_k \begin{Bmatrix} \varepsilon_{x_0} + z\kappa_x \\ \varepsilon_{y_0} + z\kappa_y \\ \gamma_{xz} \\ \gamma_{yz} \\ 2(\varepsilon_{xy_0} + z\kappa_{xy}) \end{Bmatrix}$$

3.3 Stiffness matrix relating resultants for a composite laminate

Figure 3.2 shows a stack of lamina forming a composite plate with individual positions relative to the common midsurface.

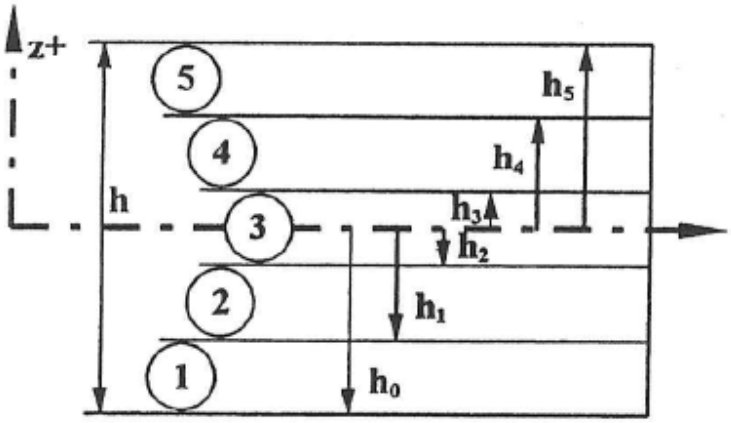

Figure 3.2: Composite plate with lamina positions measured from midsurface

The stress resultants $\{N\}$, stress couples $\{M\}$, and transverse shear resultants $\{Q\}$, all per unit width are defined as

$$\begin{Bmatrix} N_x \\ N_y \\ N_{xy} \end{Bmatrix} = \int_{-h/2}^{h/2} \begin{Bmatrix} \sigma_x \\ \sigma_y \\ \sigma_{xy} \end{Bmatrix} dz,$$

$$\begin{Bmatrix} Q_x \\ Q_y \end{Bmatrix} = \int_{-h/2}^{h/2} \begin{Bmatrix} \sigma_{xz} \\ \sigma_{yz} \end{Bmatrix} dz,$$

$$\begin{Bmatrix} M_x \\ M_y \\ M_{xy} \end{Bmatrix} = \int_{-h/2}^{h/2} \begin{Bmatrix} \sigma_x \\ \sigma_y \\ \sigma_{xy} \end{Bmatrix} z\, dz$$

It is shown in Figure 3.2 that every coordinate in the transverse direction below the mid surface is negative. Every coordinate above the mid surface is positive. For a sandwich plate, the stress resultants, stress couples and transverse shear resultants can be integrated for each laminae and then added together. The stress-strain relation can be substituted into the equations above. For N laminae,

$$\begin{bmatrix} N_x \\ N_y \\ N_{xy} \end{bmatrix} = \sum_{k=1}^{N} \int_{h_{k-1}}^{h_k} \begin{bmatrix} \sigma_x \\ \sigma_y \\ \sigma_{xy} \end{bmatrix}_k dz = \sum_{k=1}^{N} \left(\int_{h_{k-1}}^{h_k} [\bar{Q}]_k \begin{bmatrix} \varepsilon_{x_0} \\ \varepsilon_{y_0} \\ 2\varepsilon_{xy_0} \end{bmatrix} dz + \int_{h_{k-1}}^{h_k} [\bar{Q}]_k \begin{bmatrix} \kappa_x \\ \kappa_y \\ 2\kappa_{xy} \end{bmatrix} z\, dz \right)$$

Since α, β and $\bar{Q}$ are not functions of *z*, these terms can be moved outside the integrals, and the equation above can be written as

$$\begin{bmatrix} N_x \\ N_y \\ N_{xy} \end{bmatrix} = \left(\sum_{k=1}^{N} [\bar{Q}]_k \int_{h_{k-1}}^{h_k} dz \right) \begin{bmatrix} \varepsilon_{x_0} \\ \varepsilon_{y_0} \\ 2\varepsilon_{xy_0} \end{bmatrix} + \left(\sum_{k=1}^{N} [\bar{Q}]_k \int_{h_{k-1}}^{h_k} z dz \right) \begin{bmatrix} \kappa_x \\ \kappa_y \\ 2\kappa_{xy} \end{bmatrix}$$

The equation above can be written in short form as

$$\{N\} = [A]\{\varepsilon_0\} + [B]\{\kappa\}$$

After integrating thru the thickness of each laminae, the *A* and *B* matrix are given by

$$A_{ij} = \sum_{k=1}^{N} \left(\bar{Q}_{ij} \right)_k (h_k - h_{k-1})$$

$$B_{ij} = \frac{1}{2} \sum_{k=1}^{N} \left(\bar{Q}_{ij} \right)_k (h_k^{\,2} - h_{k-1}^{\,2})$$

for *i, j*=1, 2, 6

Similarly, the stress couples can be written in the form

$$\{M\} = [B]\{\varepsilon_0\} + [D]\{\kappa\}$$

where

$$D_{ij} = \frac{1}{3} \sum_{k=1}^{N} \left(\bar{Q}_{ij} \right)_k (h_k^{\,3} - h_{k-1}^{\,3})$$

The stress couples and stress resultants can be written together as

$$\begin{Bmatrix} N_x \\ N_y \\ N_{xy} \\ M_x \\ M_y \\ M_{xy} \end{Bmatrix} = \begin{Bmatrix} A_{11} & A_{12} & A_{16} & B_{11} & B_{12} & B_{16} \\ A_{12} & A_{22} & A_{26} & B_{12} & B_{22} & B_{26} \\ A_{16} & A_{26} & A_{66} & B_{16} & B_{26} & B_{66} \\ B_{11} & B_{12} & B_{16} & D_{11} & D_{12} & D_{16} \\ B_{12} & B_{22} & B_{26} & D_{12} & D_{22} & D_{26} \\ B_{16} & B_{26} & B_{66} & D_{16} & D_{26} & D_{66} \end{Bmatrix} \begin{Bmatrix} \varepsilon_{x_0} \\ \varepsilon_{y_0} \\ 2\varepsilon_{xy_0} \\ \kappa_x \\ \kappa_y \\ 2\kappa_{xy} \end{Bmatrix}$$

where [*A*] is the extensional stiffness matrix relating in-plane stress resultants to in-plane strain components. [*D*] is the flexural stiffness matrix, relating stress couples to curvature components, and [*B*] is the matrix coupling bending and stretching. The stiffness coefficients depend on both the material properties and thicknesses of the laminae.

The transverse shear resultants can be related to the shear strains using the same way

$$\begin{bmatrix} Q_x \\ Q_y \end{bmatrix} = \sum_{k=1}^{N} \int_{h_{k-1}}^{h_k} \begin{bmatrix} \sigma_{xz} \\ \sigma_{yz} \end{bmatrix}_k dz = \sum_{k=1}^{N} \left(\int_{h_{k-1}}^{h_k} \begin{bmatrix} \bar{Q}_{44} \\ \bar{Q}_{45} \end{bmatrix}_k \gamma_{xz} dz + \int_{h_{k-1}}^{h_k} \begin{bmatrix} \bar{Q}_{45} \\ \bar{Q}_{55} \end{bmatrix}_k \gamma_{yz} dz \right)$$

where $\gamma_{xz} = 2\varepsilon_{xz}$ and $\gamma_{yz} = 2\varepsilon_{yz}$. After integrating thru the thickness of each layer,

$$\begin{bmatrix} Q_x \\ Q_y \end{bmatrix} = \begin{bmatrix} A_{44} & A_{45} \\ A_{45} & A_{55} \end{bmatrix} \begin{bmatrix} \gamma_{xz} \\ \gamma_{yz} \end{bmatrix}$$

where A_{ij} for $i, j = 4, 5$ is given by

$$A_{ij} = \sum_{k=1}^{N} \left(\bar{Q}_{ij} \right)_k [h_k - h_{k-1}]$$

When the laminae are symmetric about the midsurface, then the coupling matrix [*B*] is zero. Even in the case of symmetric laminae thickness about the midsurface, material differences in two opposite laminae will cause [B] to be nonzero, resulting in a bending-stretching coupling effect. Therefore, to let [*B*] become zero, the laminae

properties, fiber orientation, laminae thickness and location should be symmetric from the mid surface.

3.4 Stiffness matrices for a sandwich plate

The honeycomb sandwich plate in this study is defined by a three-layer symmetric (Figure 3.3), meaning that the origin of the axis for transverse coordinate is at the mid surface through the thickness. The laminates above and below this mid surface are arranged in a symmetric way, with the same thickness respectively.

For a sandwich composite plate shown in Figure 3.3, the [*A*], [*B*], [*D*] stiffness matrices can be derived in detail using the definitions discussed above.

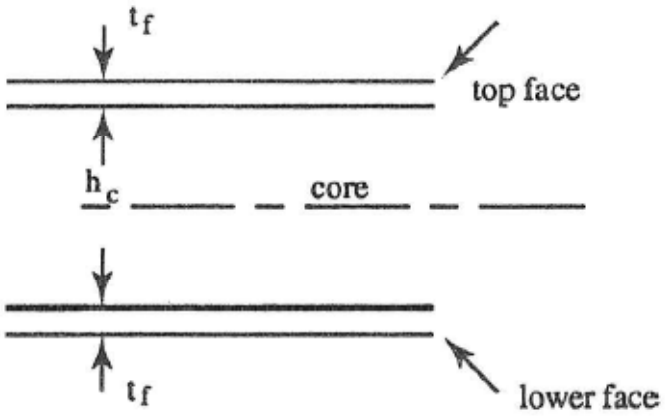

Figure 3.3: The cross section of a sandwich plate showing thicknesses of the symmetric face sheets and core

For the sandwich composite plate, the face sheets are assumed to be isotropic and the core is orthotropic. In this case, the material coefficients simplify to $[\bar{Q}_{ij}]=[Q_{ij}]$, and the stiffness matrix $[A_{ij}]$ specializes with $N=3$, and symmetry $h_3=-h_0$, and $h_2=-h_1$, to

$$A_{ij} = \sum_{k=1}^{3} (Q_{ij})_k (h_k - h_{k-1})$$
$$= (Q_{ij})_f [-\frac{t_c}{2} - (-\frac{t_c}{2} - t_f)] + (Q_{ij})_c [\frac{t_c}{2} - (-\frac{t_c}{2})] + (Q_{ij})_f [(\frac{t_c}{2} + t_f) - (\frac{t_c}{2})]$$
$$= (Q_{ij})_f (2t_f) + (Q_{ij})_c (t_c)$$

where $t_c = h_2 - h_1 = 2h_2$, and $t_f = h_3 - h_2 = h_1 - h_0$.

For isotropic materials, the compliance matrix relating in-plane strain to stress components is defined by the generalized Hooke's law for plain-stress

$$\begin{bmatrix} \varepsilon_{11} \\ \varepsilon_{22} \\ 2\varepsilon_{12} \end{bmatrix} = \frac{1}{E} \begin{bmatrix} 1 & -\nu & 0 \\ -\nu & 1 & 0 \\ 0 & 0 & 2(1+\nu) \end{bmatrix} \begin{bmatrix} \sigma_{11} \\ \sigma_{22} \\ \sigma_{12} \end{bmatrix}$$

The inverse relation is given by

$$\begin{bmatrix} \sigma_{11} \\ \sigma_{22} \\ \sigma_{12} \end{bmatrix} = \frac{E}{1-\nu^2} \begin{bmatrix} 1 & \nu & 0 \\ \nu & 1 & 0 \\ 0 & 0 & \frac{1-\nu}{2} \end{bmatrix} \begin{bmatrix} \varepsilon_{11} \\ \varepsilon_{22} \\ 2\varepsilon_{12} \end{bmatrix}$$

For isotropic materials for the face sheets with *i, j* = 1, 2.

$$(Q_{11})_f = (Q_{22})_f = \frac{E_f}{1-\nu_f{}^2}, \quad (Q_{12})_f = \frac{\nu E_f}{1-\nu_f{}^2}$$

Also, the shear modulus of the face sheets is $G_f = \dfrac{E_f}{2(1+\nu_f)}$.

For the orthotropic core with effective properties for the regular or auxetic honeycomb core, $E_c = E_1 = E_2$, $\nu_c = \nu_{12} = \nu_{21}$, $\nu_{13} = \nu_{23} \approx 0$, then

$$(Q_{11})_c = (Q_{22})_c = \frac{E_c}{1-\nu_c{}^2}, \qquad (Q_{12})_c = \frac{\nu_c E_c}{1-\nu_c{}^2}$$

After calculation, each member of [A] can be given in detail by

$$A_{11} = A_{22} = \frac{E_f}{1-\nu_f{}^2}(2t_f) + \frac{E_c}{1-\nu_c{}^2}t_c$$
$$A_{12} = \frac{\nu_f E_f}{1-\nu_f{}^2}(2t_f) + \frac{\nu_c E_c}{1-\nu_c{}^2}t_c$$
$$A_{66} = G_f(2t_f) + G_{12}t_c$$

In the above, $A_{11} = A_{22}$, and A_{12}, are the in-plane effective membrane stiffness coefficients which depend on the material properties and thickness of the face sheets, and the effective properties and thickness of the honeycomb core. Also G_{12} is the effective in-plane shear modulus for honeycomb, and $(Gt)_{12} \triangleq A_{66}$ is the effective in-plane shear stiffness for the composite sandwich plate. From these equations, the multi-scale aspect of the honeycomb sandwich plate is evident. Using the simple honeycomb cellular model discussed earlier, for regular honeycomb, $\nu_c = \nu_{12} = \nu_{21} = 1$, and cannot used since the effective stiffness equation for the sandwich composite will be singular. To correct this difficulty, we use the refined honeycomb model, which includes effects of transverse shear and axial effects in the honeycomb cells, and gives $\nu_{12} = \nu_{21} \neq 1$.

The bending stiffness coefficients [D_{ij}] can be specialized for a symmetric sandwich composite,

$$D_{ij} = \frac{1}{3}\sum_{k=1}^{3}(Q_{ij})_k(h_k^{\,3} - h_{k-1}^{\,3})$$
$$= \frac{1}{3}(Q_{ij})_f[(-\frac{h_c}{2})^3 - (-\frac{h_c}{2} - t_f)^3] + \frac{1}{3}(Q_{ij})_c[(\frac{h_c}{2})^3 - (-\frac{h_c}{2})^3] + \frac{1}{3}(Q_{ij})_f[(\frac{h_c}{2} + t_f)^3 - (\frac{h_c}{2})^3]$$
$$= \frac{1}{3}\left\{2(Q_{ij})_f\left[\frac{3}{2}t_c t_f^{\,2} + \frac{3}{4}t_c^{\,2}t_f + t_f^{\,3}\right] + (Q_{ij})_c\frac{t_c^{\,3}}{4}\right\}$$

for *i, j* = 1, 2. For isotropic face sheets and effective properties for regular and auxetic honeycomb, the bending stiffness coefficients are given by

$$D_1 = D_2 = \frac{1}{3}\left\{\frac{2E_f}{1-\nu_f^{\,2}}\left[\frac{3}{2}t_c t_f^{\,2} + \frac{3}{4}t_c^{\,2}t_f + t_f^{\,3}\right] + \frac{E_c}{1-\nu_c^{\,2}}\frac{t_c^{\,3}}{4}\right\}$$

$$D_{12} = \frac{1}{3}\left\{\frac{2\nu_f E_f}{1-\nu_f^{\,2}}\left[\frac{3}{2}t_c t_f^{\,2} + \frac{3}{4}t_c^{\,2}t_f + t_f^{\,3}\right] + \frac{\nu_c E_c}{1-\nu_c^{\,2}}\frac{t_c^{\,3}}{4}\right\}$$
$$D_{66} = \frac{1}{3}\left\{2G_f\left[\frac{3}{2}t_c t_f^{\,2} + \frac{3}{4}t_c^{\,2}t_f + t_f^{\,3}\right] + G_{12}\frac{t_c^{\,3}}{4}\right\}$$

In some studies, the second term involving the core properties is neglected since it is relatively small compared the first term involving the face shear materials. In this study, however, terms involving the core properties will be kept.

Transverse shear stiffness coefficients for the honeycomb sandwich composite, A_{44} and $A_{55,}$ are defined in a similar way by

$$A_{44} = G_f(2t_f) + G_{13}t_c$$
$$A_{55} = G_f(2t_f) + G_{23}t_c$$

These are important to model shear deformation in sandwich plates. For regular honeycomb, $G_{13} = G_{23}$, so that the transverse shear stiffness $A_{44} = A_{55}$. In the case of auxetic honeycomb, $G_{13} \neq G_{23}$, and $A_{44} \neq A_{55}$.

The governing dynamic equations are derived for symmetric sandwich plates by using the first order shear deformation theory. Stress resultants, stress couples and stress-strain-displacement relations will be used to derive the equations. A simplified form for beam problems will also be given. A continuum theory is used in deriving the equations.

The governing dynamic equations are derived starting from Newton's balance laws in the three component directions [?]:

$$\frac{\partial \sigma_x}{\partial x}+\frac{\partial \sigma_{yx}}{\partial y}+\frac{\partial \sigma_{zx}}{\partial z}+b_x=\rho\frac{\partial^2 u}{\partial t^2},$$

$$\frac{\partial \sigma_{xy}}{\partial x}+\frac{\partial \sigma_y}{\partial y}+\frac{\partial \sigma_{zy}}{\partial z}+b_y=\rho\frac{\partial^2 v}{\partial t^2},$$

$$\frac{\partial \sigma_{xz}}{\partial x}+\frac{\partial \sigma_{yz}}{\partial y}+\frac{\partial \sigma_z}{\partial z}+b_z=\rho\frac{\partial^2 w}{\partial t^2}$$

For simplicity in the body forces b_x, b_y, b_z are not included in the discussion, but can be included. Considering the first component equation and integrate thru the thickness for each laminae gives

$$\sum_{k=1}^{N}\int_{h_{k-1}}^{h_k}\frac{\partial(\sigma_x)_k}{\partial x}dz+\sum_{k=1}^{N}\int_{h_{k-1}}^{h_k}\frac{\partial(\sigma_{yx})_k}{\partial y}dz+\sum_{k=1}^{N}\int_{h_{k-1}}^{h_k}\frac{\partial(\sigma_{zx})_k}{\partial z}dz=\sum_{k=1}^{N}\int_{h_{k-1}}^{h_k}\rho_k\frac{\partial^2 u}{\partial t^2}dz$$

Changing the order of integration and differentiation in the first two terms gives

$$\frac{\partial}{\partial x}[\sum_{k=1}^{N}\int_{h_{k-1}}^{h_k}(\sigma_x)_k\,dz]+\frac{\partial}{\partial y}[\sum_{k=1}^{N}\int_{h_{k-1}}^{h_k}(\sigma_{yx})_k\,dz]+\sum_{k=1}^{N}(\sigma_{zx})_k\,|_{h_{k-1}}^{h_k}=\left[\sum_{k=1}^{N}\rho_k(h_k-h_{k-1})\right]\frac{\partial^2 u_0}{\partial t^2}$$

On the left-hand-side, the terms inside the brackets are in-plane stress resultants. The shear stress which is the third will cancel each other between laminae. Therefore, only

two shear tractions will remain which are applied on the bottom and top surface. The inertia term is specialized using symmetry about the midsurface.

Then the equation can be written as

$$\frac{\partial N_x}{\partial x} + \frac{\partial N_{xy}}{\partial y} + \tau_{top_x} - \tau_{bottom_x} = \rho_t \frac{\partial^2 u_0}{\partial t^2}$$

The equation in the *y* direction can be given in a similar way

$$\frac{\partial N_{xy}}{\partial x} + \frac{\partial N_y}{\partial y} + \tau_{top_y} - \tau_{bottom_y} = \rho_t \frac{\partial^2 v_0}{\partial t^2}$$

In the *z* direction, the equation is given by

$$\frac{\partial Q_x}{\partial x} + \frac{\partial Q_y}{\partial y} + p_{top} - p_{bottom} = \rho_t \frac{\partial^2 w}{\partial t^2}$$

where p_{top} and p_{bottom} are pressures in the *z* direction.

In the above equations, ρ_t is the total mass density per unit area for the symmetric sandwich plate with honeycomb core and face sheets derived earlier and repeated here:

$$\rho_t = \sum_{k=1}^{N} \rho_k (h_k - h_{k-1}) = (2t_f)\rho_f + t_c \rho_c$$

Moment equations about the mid-surface are derived by

$$\sum_{k=1}^{N} \int_{h_{k-1}}^{h_k} \frac{\partial (\sigma_x)_k}{\partial x} z dz + \sum_{k=1}^{N} \int_{h_{k-1}}^{h_k} \frac{\partial (\sigma_{yx})_k}{\partial y} z dz + \sum_{k=1}^{N} \int_{h_{k-1}}^{h_k} \frac{\partial (\sigma_{zx})_k}{\partial z} z dz = \sum_{k=1}^{N} \int_{h_{k-1}}^{h_k} \rho_k \frac{\partial^2 \alpha}{\partial t^2} z^2 dz$$

The third term can be integrated by parts and becomes

$$\frac{h}{2}(\tau_{top_x} + \tau_{bottom_x}) - Q_x$$

where Q_x is the transverse shear resultant, and h is the total plate thickness, and the first two terms are moments about the mid-surface produced surface tractions. A similar moment equation can derived, and expressing these in terms of stress couples, gives

$$\frac{\partial M_x}{\partial x}+\frac{\partial M_{xy}}{\partial y}+\frac{h}{2}(\tau_{top_x}+\tau_{bottom_x})-Q_x=\frac{1}{3}\sum_{k=1}^{N}\rho_k({h_k}^3-{h_{k-1}}^3)\frac{\partial^2\alpha}{\partial t^2}$$

$$\frac{\partial M_{xy}}{\partial x}+\frac{\partial M_y}{\partial y}+\frac{h}{2}(\tau_{top_y}+\tau_{bottom_y})-Q_y=\frac{1}{3}\sum_{k=1}^{N}\rho_k({h_k}^3-{h_{k-1}}^3)\frac{\partial^2\beta}{\partial t^2}$$

where $I=\frac{1}{3}\sum_{k=1}^{N}\rho_k({h_k}^3-{h_{k-1}}^3)$ is the rotary inertia term of the composite plate.

From these five dynamic equations, and the composite stiffness properties, the governing equations of the sandwich plate can be written in terms of five degrees of freedom (u_0, v_0, w, α and β). As discussed earlier, for the symmetric sandwich plate, there is no coupling between in-plane force resultants and curvature, and no coupling between moment resultants and in-plane strains, i.e. [B]=0. This situation occurs when the laminates are organized with symmetric layers. For regular and auxetic honeycomb core with special orthotropic effective properties, $E_c=E_1=E_2$, $G_{13}=G_{23}$, $\nu_c=\nu_{12}=\nu_{21}$, $\nu_{13}=\nu_{23}\approx 0$, the stress components can be specialized to,

$$N_x = A_{11}\varepsilon_{x_0} + A_{12}\varepsilon_{y_0}$$
$$N_y = A_{12}\varepsilon_{x_0} + A_{22}\varepsilon_{y_0}$$
$$N_{xy} = 2A_{66}\varepsilon_{xy_0}$$
$$M_x = D_{11}\kappa_x + D_{12}\kappa_y$$
$$M_y = D_{12}\kappa_x + D_{22}\kappa_y$$
$$M_{xy} = 2D_{66}\kappa_{xy}$$
$$Q_x = A_{55}(\alpha + \frac{\partial w}{\partial x})$$
$$Q_y = A_{44}(\beta + \frac{\partial w}{\partial y})$$

After substituting these stiffness relations into the moment equations and the shear force equation, assuming no surface shear tractions, the governing equations of the sandwich plates with transverse loading are given by

$$D_{11}\frac{\partial^2\alpha}{\partial x^2} + D_{66}\frac{\partial^2\alpha}{\partial y^2} + (D_{12} + D_{66})\frac{\partial^2\beta}{\partial x\partial y} - A_{44}(\alpha + \frac{\partial w}{\partial x}) = I\frac{\partial^2\alpha}{\partial t^2}$$
$$(D_{12} + D_{66})\frac{\partial^2\alpha}{\partial x\partial y} + D_{66}\frac{\partial^2\beta}{\partial x^2} + D_{22}\frac{\partial^2\beta}{\partial y^2} - A_{55}(\beta + \frac{\partial w}{\partial y}) = I\frac{\partial^2\beta}{\partial t^2}$$
$$A_{44}(\frac{\partial\alpha}{\partial x} + \frac{\partial^2 w}{\partial x^2}) + A_{55}(\frac{\partial\beta}{\partial y} + \frac{\partial^2 w}{\partial y^2}) + p(x,y) = \rho_t\frac{\partial^2 w}{\partial t^2}$$

In the first two equations, the rotary inertia can be specialized for a symmetric sandwich plate which is given by

$$I = \frac{1}{3}\left\{\rho_f\left[\frac{3}{2}h_c{}^2 t_f + 3h_c t_f{}^2 + 2t_f{}^3\right] + \frac{1}{4}\rho_c h_c{}^3\right\}$$

Another two equations are given for in-plane extensions which are derived by stress resultant equilibrium equations and the in-plane stiffness relations

$$A_{11}\frac{\partial^2 u_0}{\partial x^2}+A_{66}\frac{\partial^2 v_0}{\partial y^2}+(A_{12}+A_{66})\frac{\partial^2 v_0}{\partial x\partial y}=\rho_t\frac{\partial^2 u_0}{\partial t^2}$$
$$(A_{12}+A_{66})\frac{\partial^2 u_0}{\partial x\partial y}+A_{66}\frac{\partial^2 v_0}{\partial x^2}+A_{22}\frac{\partial^2 v_0}{\partial y^2}=\rho_t\frac{\partial^2 v_0}{\partial t^2}$$

3.5 Specialization to Cylindrical Bending problem

The governing equations of the general plate can be simplified to apply for a problem having an infinite length on one direction, such that plate deformation is considered independent of the length. Therefore, the governing equations across the width direction of the plate can be written by

$$D_{11}\frac{\partial^2\alpha}{\partial x^2}-A_{44}(\alpha+\frac{\partial w}{\partial x})=I\frac{\partial^2\alpha}{\partial t^2}$$
$$A_{44}(\frac{\partial\alpha}{\partial x}+\frac{\partial^2 w}{\partial x^2})+p=\rho_t\frac{\partial^2 w}{\partial t^2}$$

In this form it is clear that D_{11} is the bending stiffness, and A_{44} is the transverse shear stiffness. The sandwich plate is assumed to be simply supported on side edges, which is defined as

$$w(0)=0,\quad w(a)=0,$$
$$\frac{\partial\alpha}{\partial x}(0)=0,\quad \frac{\partial\alpha}{\partial x}(a)=0$$

where a is the width of the plate. Therefore, for harmonic response, the displacement field can be written in the following form

$$w=\bar{w}e^{i\omega t}=(\sum_{m=1}^{k}A_m\sin\frac{m\pi x}{a})e^{i\omega t}$$
$$\alpha=\bar{\alpha}e^{i\omega t}=(\sum_{m=1}^{k}B_m\cos\frac{m\pi x}{a})e^{i\omega t}$$

where ω is the frequency in rad/sec, and m is the mode number.

After taking partial differentiation with respect to every coordinate, the following forms are derived for the degrees of freedom

$$\frac{\partial \alpha}{\partial x} = \sum_{m=1}^{k} (-\frac{m\pi}{a} B_m \sin\frac{m\pi x}{a}) e^{i\omega t}$$
$$\frac{\partial^2 \alpha}{\partial x^2} = \sum_{m=1}^{k} (-\frac{m^2\pi^2}{a^2} B_m \cos\frac{m\pi x}{a}) e^{i\omega t}$$
$$\frac{\partial w}{\partial x} = \sum_{m=1}^{k} (\frac{m\pi}{a} A_m \cos\frac{m\pi x}{a}) e^{i\omega t}$$
$$\frac{\partial^2 w}{\partial x^2} = \sum_{m=1}^{k} -(\frac{m^2\pi^2}{a^2} A_m \sin\frac{m\pi x}{a}) e^{i\omega t}$$
$$\frac{\partial^2 w}{\partial t^2} = -\omega^2 \sum_{m=1}^{k} (A_m \sin\frac{m\pi x}{a}) e^{i\omega t} = -\omega^2 w$$

Substituting these forms into the governing equations for an infinite plate using the orthogonality characteristic between different modes enables solving the modal amplitudes A_m and B_m in terms of p. The orthogonality condition is

$$\int_0^a \sin\frac{m\pi x}{a} \sin\frac{n\pi x}{a} dx = \frac{a}{2}\delta_{mn}$$

For the second equation,

$$(-A_{44}B_m \frac{m\pi}{a} - A_{44}A_m \frac{m^2\pi^2}{a^2} + \rho_t A_m \omega^2) \int_0^a \sin\frac{m\pi x}{a} \sin\frac{n\pi x}{a} dx = -\int_0^a p \sin\frac{n\pi x}{a} dx$$

For constant uniform pressure,

$$(-A_{44}B_m \frac{m\pi}{a} - A_{44}A_m \frac{m^2\pi^2}{a^2} + \rho_t A_m \omega^2) \frac{a}{2} = p\frac{a}{m\pi}(\cos m\pi - 1)$$

A similar form can be written for the first equation. Summarizing in matrix form

$$\begin{bmatrix} -(\frac{D_{11}m^2\pi^2}{a^2}+A_{44})+I\omega^2 & -\frac{A_{44}m\pi}{a} \\ -\frac{A_{44}m\pi}{a} & -(\frac{A_{44}m^2\pi^2}{a^2})+\rho_t\omega^2 \end{bmatrix}\begin{bmatrix} B_m \\ A_m \end{bmatrix}=\begin{bmatrix} 0 \\ 2p\frac{(-1)^m-1}{m\pi} \end{bmatrix}$$

The uniform distributed pressure loading p is set to be 1MPa , and A_m and B_m are solved numerically using the sandwich plate dimensions given in Table 2-3. The A_m and B_m are plotted in the form given below via frequency.

$$|\bar{w}|=\left|\sum_{m=1}^{k}A_m\sin\frac{m\pi x}{a}\right|$$
$$|\bar{\alpha}|=\left|\sum_{m=1}^{k}B_m\cos\frac{m\pi x}{a}\right|$$

3.5.1 Aluminum face sheet and Aluminum Honeycomb core

The honeycomb sandwich plate model is studied firstly using Aluminum for both core and face sheet with no viscoelastic damping material property. The composite material stiffness coefficients used in this problem are A_{44} and D_{11}. The values are shown in Table 3-1.

Table 3-1: Values for [A] and [D] matrices and the mass density (Al core, η=0)

	D_{11}	A_{44}	ρ_t (kg/m^2)
Regular	6956.2	72.866×10^6	9.8895
Auxetic I	6875.3	72.866×10^6	11.386
Auxetic II	6802.6	67.517×10^6	9.8895

The figure of the translational degree of freedom at the center of the plate is shown in Figure 3.5 which is plotted using MATLAB. Only five modes are taken into consideration. The rotary inertia term in the governing equations is neglected at the moment. It will be added back in later studies. The values on the ordinate axis are divided by the absolute value of w_{static} which is the value of w when the frequency is zero. The result is then taken by $dB = 20\log(\frac{|w|}{|w_{static}|})$.

To study the effect that damping may bring to the system, an imaginary part is then added to the shear modulus of the material, which is given by

$$G_m = G_{real} + iG_{real}\eta$$

This shear modulus is frequency independent. The shear modulus is added to the honeycomb core. η is chosen to be 0, 0.2, and 0.4 respectively in Figure 3.4.

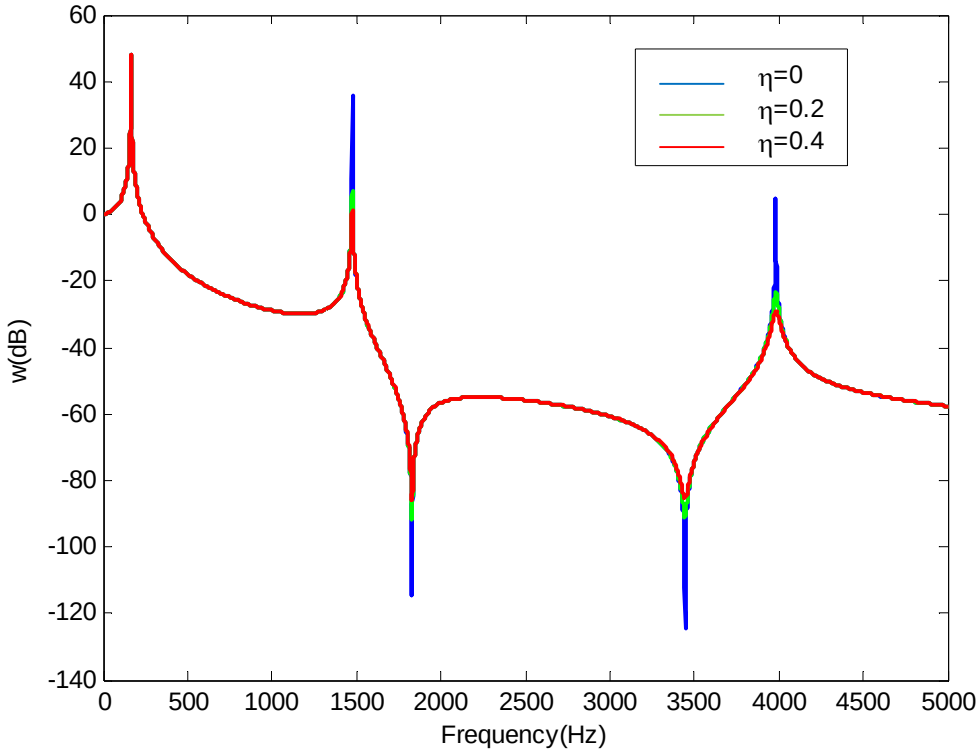

Figure 3.4: w via frequency at plate center

Obvious damping effect can be seen in Figure 3.4 when the damping coefficient is added to the system comparing to the undamped system. Damping becomes more obvious as the damping coefficient becomes larger. The frequency response of the rotational degree of freedom is shown in Figure 3.6.

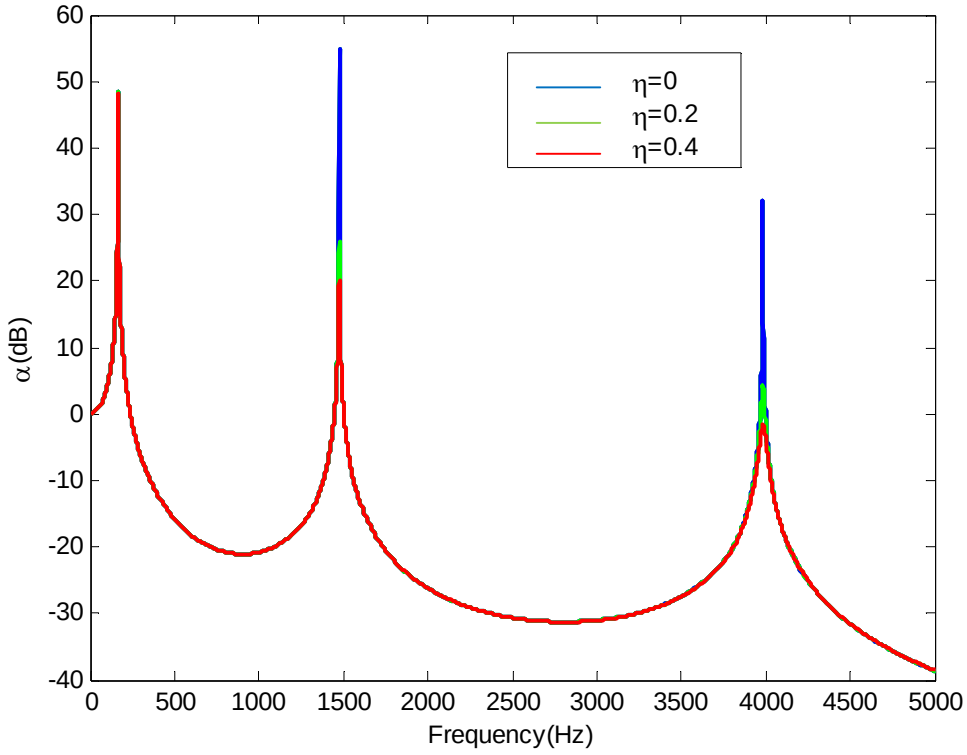

Figure 3.5: α via frequency at plate center

Although damping effect is observed in Figure 3.4 and Figure 3.5, the damping of translational and rotational degrees of freedom around the first natural frequency is not obvious. Therefore, Figure 3.6 is plotted in the frequency domain ranging from 0 to 200Hz. The increment is much smaller than Figure 3.4 and Figure 3.5. Therefore, a more specific frequency response of the plate could be observed around the first natural frequency.

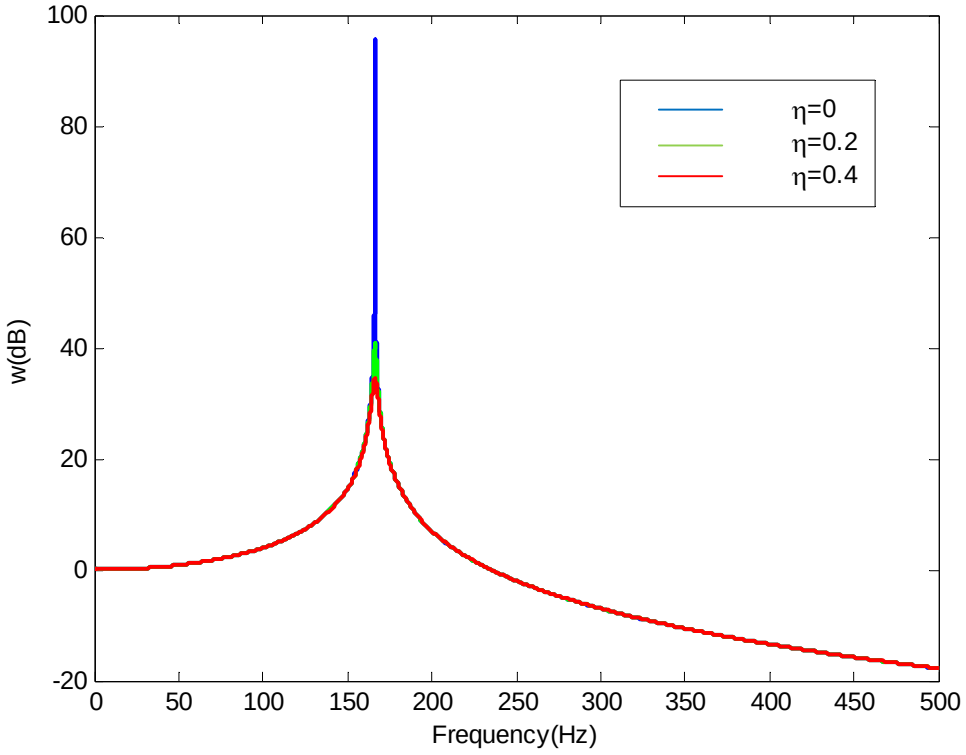

Figure 3.6: w at the first natural frequency

With much smaller frequency increment in the MATLAB code, it can be seen that the peak value of the undamped system for the first natural frequency changed. Damping can be found for systems with damping coefficients. The same plot is also given for the rotaional degree of freedom in Figure 3.7.

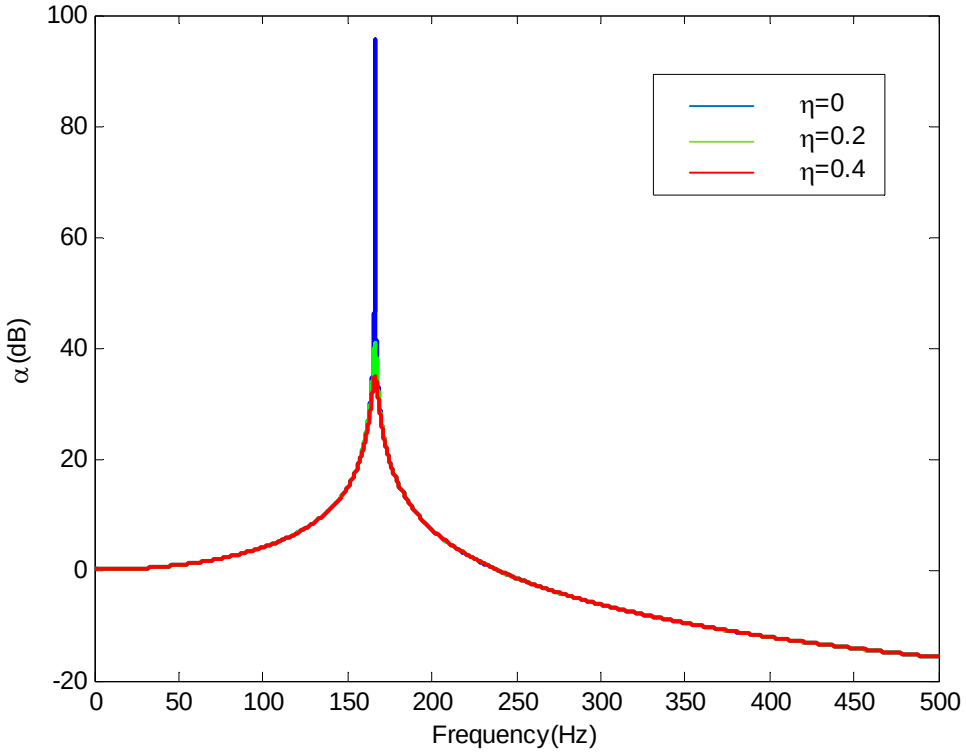

Figure 3.7: α at the first natural frequency

From the figures shown above, it can be concluded that damping has significant effect in the behavior of a honeycomb sandwich plate. It also proves that this is a viable way to add damping to the sandwich plate system.

The study above has neglected the rotary inertia term. In the following study, this term is added back to the system to see what change it may bring to the system.

Figure 3.8 shows the undamped system with the rotary inertia term added back. It is compared with the undamped system without rotary inertia which is also shown in Figure 3.4.

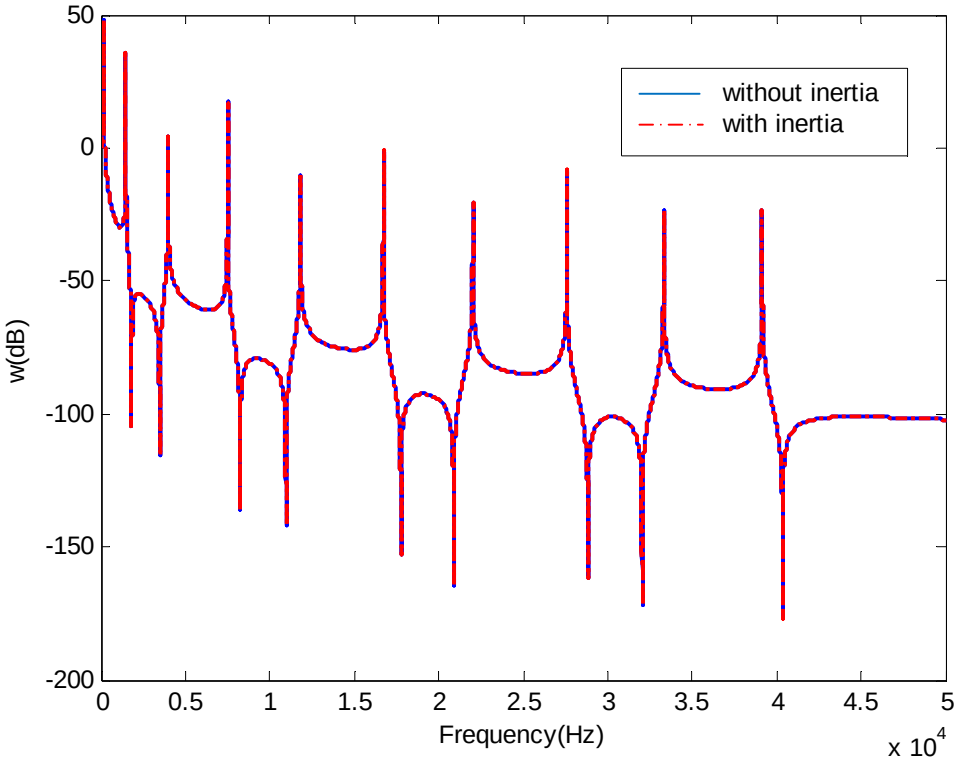

Figure 3.8: w via frequency, undamped

It is found that the difference between the system with rotary inertia and the one without inertia is so small that no difference could be realized if the figures are plotted with even twenty modes included in a frequency range of 0-50000Hz. Therefore, the rotary inertia term does not have a major effect in the frequency response of the beam. The compare is also made when $\eta = 0.2$ in Figure 3.9.

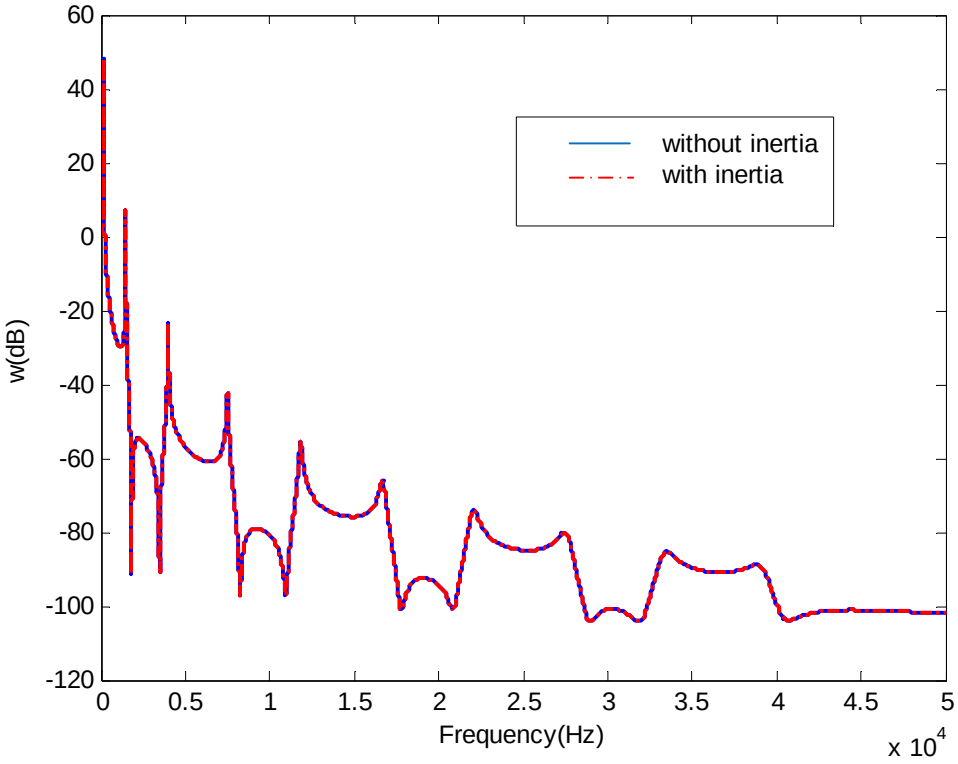

Figure 3.9: w via frequency, η=0.2

It can be seen that for the systems with η=0.2, the difference between the system with rotary inertia and the one without inertia is even smaller.

3.5.2 The study of the natural frequency

It is known that the natural frequency of the system can be found from the free vibration problem which means to set the external loadings to zero. Then the matrices formed governing equations can be rewritten as

$$\begin{bmatrix} -(\frac{D_{11}m^2\pi^2}{a^2}+A_{44})+I\omega^2 & -\frac{A_{44}m\pi}{a} \\ -\frac{A_{44}m\pi}{a} & -(\frac{A_{44}m^2\pi^2}{a^2})+\rho_t\omega^2 \end{bmatrix}\begin{bmatrix} B_m \\ A_m \end{bmatrix}=\begin{bmatrix} 0 \\ 0 \end{bmatrix}$$

without considering the rotary inertia term. This turns the equations into an eigenvalue problem. It is noted that the rotary inertia term can make the characteristic equation be quartic. The solution of the characteristic equation is obtained from the determinate of the coefficient matrix and is given by

$$\omega_m=\sqrt{\frac{D_{11}A_{44}m^4\pi^4}{a^2\rho_t(D_{11}m^2\pi^2+A_{44}a^2)}}$$

For the first five modes, the natural frequencies can be found in Table 3-2. It is noted that frequency $f_m=\omega_m/(2\pi)$ in cycles per second.

Table 3-2: Natural frequencies for the cylindrical bending problem, Aluminum (Hz)

f_1	f_2	f_3	f_4	f_5
166.3264	661.5899	1474.9	2589.3	3982.6

It can be seen from Figure 3.5 and Figure 3.6 that the peak values in these figures happen at the first, third and fifth natural frequencies. The translational and rotational displacements are derived based on a mode superposition method.

3.5.3 Aluminum face sheet and polycarbonate core

A study including the frequency dependent damping effect is needed after studying the case of no damping effect and frequency independent damping effect for

cylindrical bending problem. As having discussed in chapter two, the polycarbonate material which has linear viscoelastic characteristic is used in this study. The frequency dependent characteristic of the shear modulus and the storage and loss modulus features give this material unique damping property. The viscoelastic property can be applied simply by replacing the original material properties with the new ones which will make [A] and [D] matrices become frequency dependent. Therefore, the study including the polycarbonate core can be initiated using the same way. First of all, the polycarbonate core without viscoelastic property is compared with the one which has viscoelastic property. When the viscoelastic property is turned off, the values of stiffness coefficients can be found in Table 3-3

Table 3-3: Values for [A] and [D] matrices and the mass density (Poly core with no viscoelastity)

	D_{11}	A_{44}	ρ_t (kg/m^2)
Regular	6613.3	52.098×10^6	7.3953
Auxetic I	6610.9	52.098×10^6	8.0604
Auxectic II	6608.7	51.941×10^6	7.3953

It is noted that the rotary inertia term is neglected at the moment. The figure for the translational displacement at the center of the plate is given in Figure 3.10.

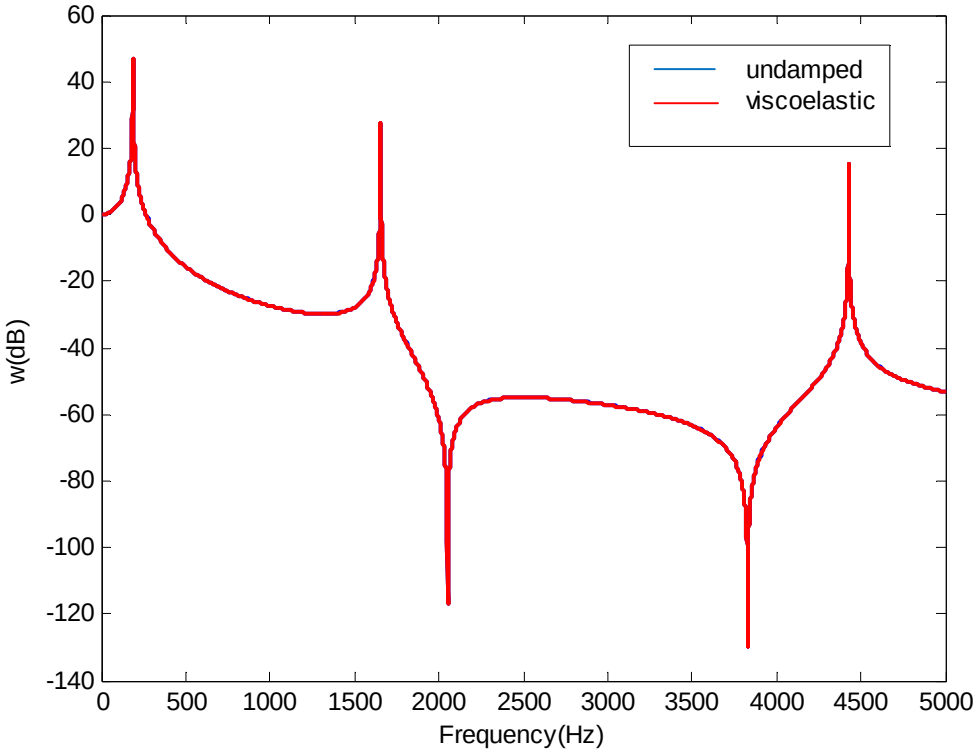

Figure 3.10: w via frequency for a polycarbonate core

The small increment is used again because of the slight difference between the two figures. As we can see from Figure 3.10, the two curves overlapped.

The rotational degree of freedom is plotted in Figure 3.11.

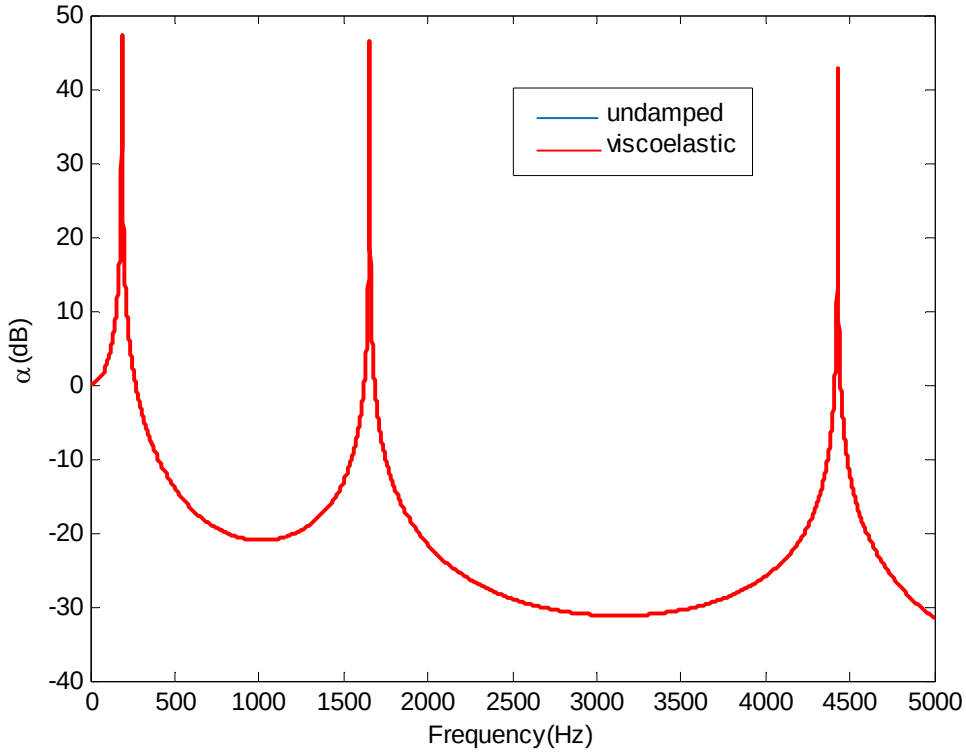

Figure 3.11: α via frequency for a polycarbonate core

A compare is given in Figure 3.12 between honeycomb sandwich plate with a polycarbonate core (viscoelasticity turned off) and a honeycomb sandwich plate with an aluminum core with no damping ratio in the shear modulus.

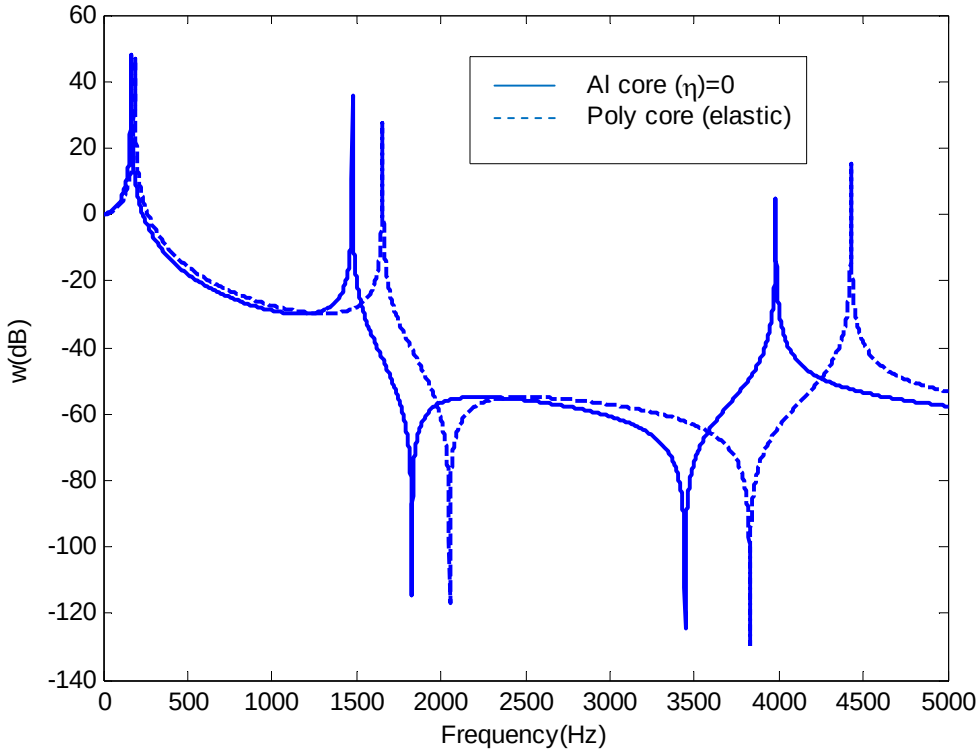

Figure 3.12: w, Compare between polycarbonate core (viscoelasticity turned off) and aluminum core (η=0)

The compare of the rotational degree of freedom between the two systems is given in Figure 3.13.

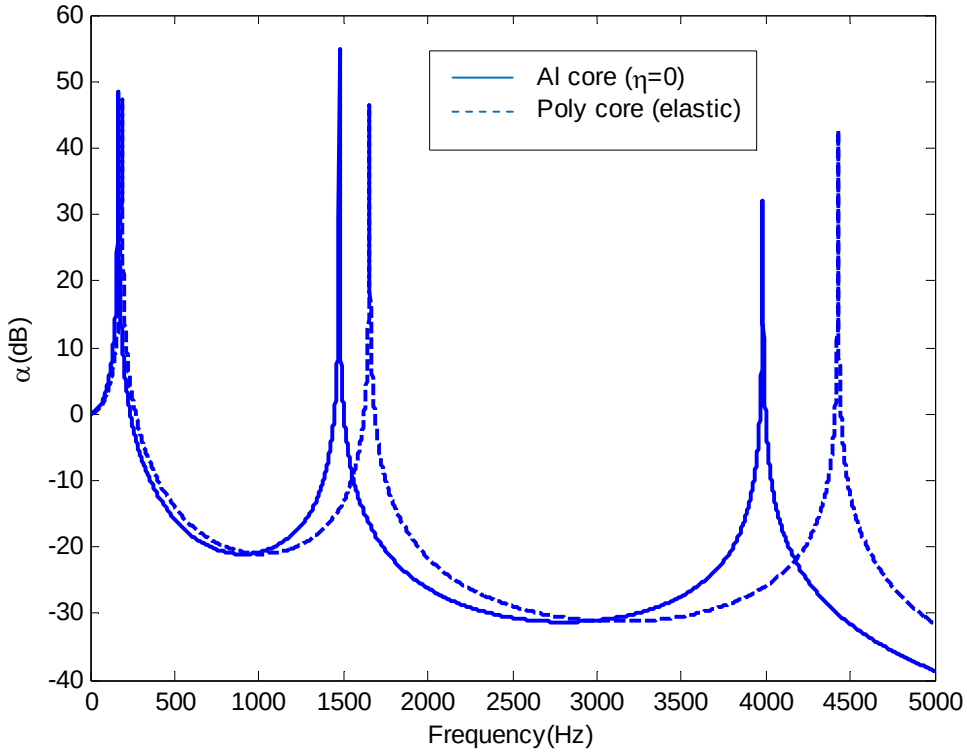

Figure 3.13: α, Compare between polycarbonate core (viscoelasticity turned off) and aluminum core (η=0)

It is found in Figure 3.12 and Figure 3.13 that the sandwich plate with polycarbonate core has larger natural frequencies comparing to the one with aluminum core.

The next compare is made between sandwich plate with aluminum core (η=0.2) and polycarbonate with viscoelastic property considered. The results are shown in Figure 3.14 and Figure 3.15.

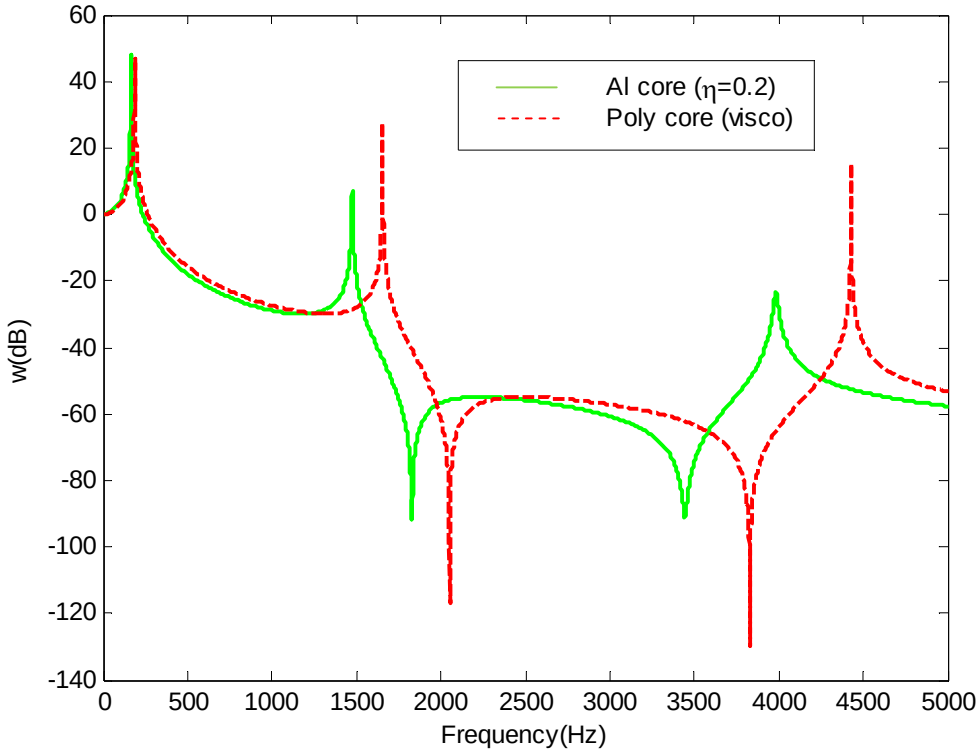

Figure 3.14: w, Compare between polycarbonate core (viscoelasticity turned on) and aluminum core (η=0.2)

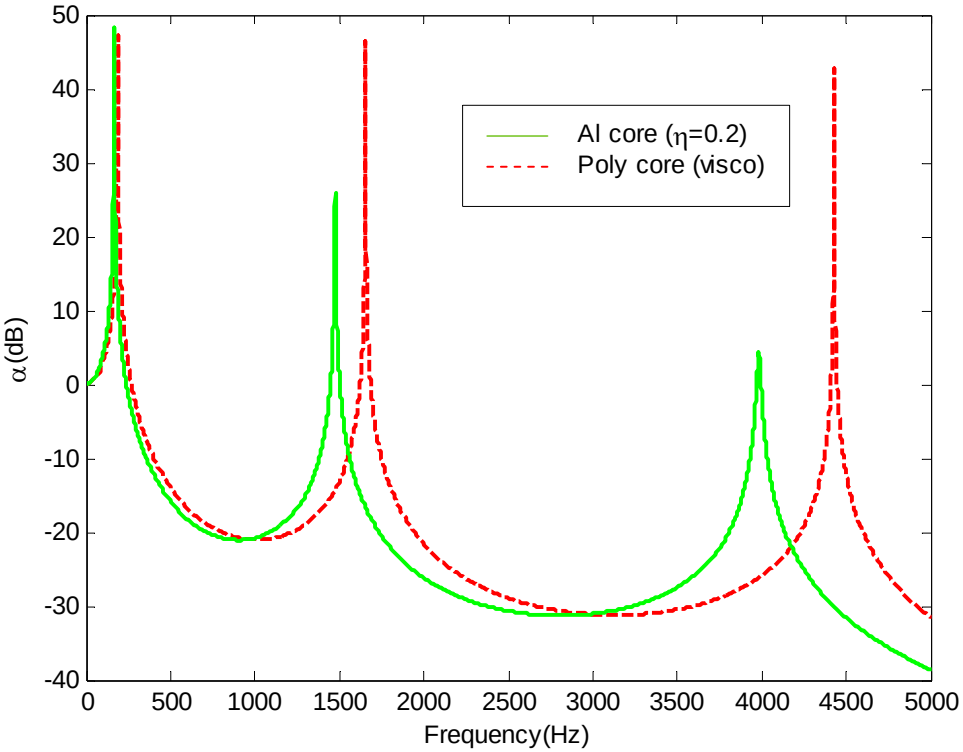

Figure 3.15: α, Compare between polycarbonate core (viscoelasticity turned on) and aluminum core (η=0.2)

From Figure 3.14 and Figure 3.15, it can be found that the sandwich plate with aluminum (η=0.2) shows much better damping behavior than the polycarbonate one with viscoelastic property.

The natural frequency of the sandwich plate with polycarbonate core can be studied using the same way which is shown in Table 3-4.

Table 3-4: Natural frequencies for the cylindrical bending problem, polycarbonate (Hz)

f_1	f_2	f_3	f_4	f_5
187.4245	744.1527	1654.2	2892.6	4428.1

In the above study, the inertia term is neglected. Figure 3.16 shows a compare between sandwich plates (polycarbonate core, viscoelasticity turned on) with inertia and without inertia.

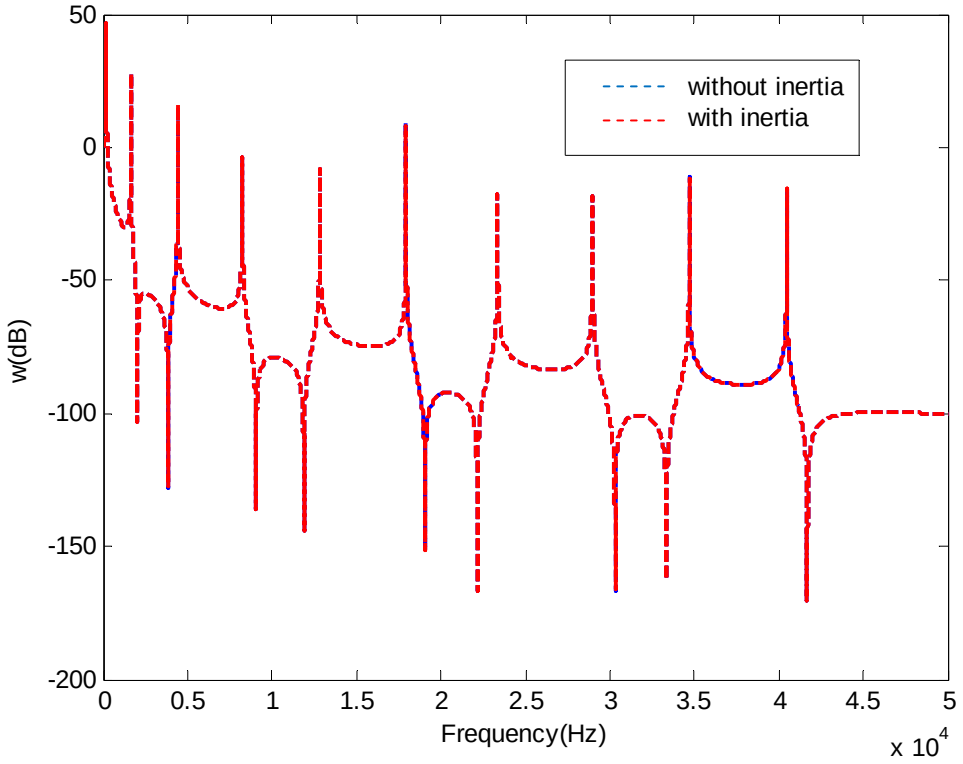

Figure 3.16: w via frequency, with viscoelastic property

It is found in Figure 3.14 that the difference between the two systems is very small.

3.6 Simply supported sandwich plate

The cylindrical problem can then be generalized to a 2D plate problem as described in chapter 3.4. Firstly, the two equations for in-plane extension will be neglected for simplicity. The governing equations are repeated here

$$D_{11}\frac{\partial^2\alpha}{\partial x^2}+D_{66}\frac{\partial^2\alpha}{\partial y^2}+(D_{12}+D_{66})\frac{\partial^2\beta}{\partial x\partial y}-A_{44}(\alpha+\frac{\partial w}{\partial x})=I\frac{\partial^2\alpha}{\partial t^2}$$

$$(D_{12}+D_{66})\frac{\partial^2\alpha}{\partial x\partial y}+D_{66}\frac{\partial^2\beta}{\partial x^2}+D_{22}\frac{\partial^2\beta}{\partial y^2}-A_{55}(\beta+\frac{\partial w}{\partial y})=I\frac{\partial^2\beta}{\partial t^2}$$

$$A_{44}(\frac{\partial\alpha}{\partial x}+\frac{\partial^2 w}{\partial x^2})+A_{55}(\frac{\partial\beta}{\partial y}+\frac{\partial^2 w}{\partial y^2})+p(x,y)=\rho_t\frac{\partial^2 w}{\partial t^2}$$

The simply supported boundary condition on four edges is given by

at $x=0,\quad x=a$

$$w=0,\quad \text{and}\quad M_y=D_{12}\frac{\partial\alpha}{\partial x}+D_{22}\frac{\partial\beta}{\partial y}=0$$

at $y=0,\quad y=b$

$$w=0,\quad \text{and}\quad M_x=D_{11}\frac{\partial\alpha}{\partial x}+D_{12}\frac{\partial\beta}{\partial y}=0$$

The displacement field, according to the boundary condition, could be given by

$$w=\bar{w}e^{i\omega t}=(\sum_{m=1}^{k}\sum_{n=1}^{k}A_{mn}\sin\frac{m\pi x}{a}\sin\frac{n\pi y}{b})e^{i\omega t}$$

$$\alpha=\bar{\alpha}e^{i\omega t}=(\sum_{m=1}^{k}\sum_{n=1}^{k}B_{mn}\cos\frac{m\pi x}{a}\sin\frac{n\pi y}{b})e^{i\omega t}$$

$$\beta=\bar{\beta}e^{i\omega t}=(\sum_{m=1}^{k}\sum_{n=1}^{k}C_{mn}\sin\frac{m\pi x}{a}\cos\frac{n\pi y}{b})e^{i\omega t}$$

which conforms the boundary condition.

Again, the governing equations can be written in the matrix form for further study. The matrix form is given below after substituting the degrees of freedom into the governing equations.

$$\begin{bmatrix} -(D_{11}\frac{m^2\pi^2}{a^2}+D_{66}\frac{n^2\pi^2}{b^2}+A_{55})+I\omega^2 & -(D_{12}+D_{66})\frac{mn\pi^2}{ab} & -A_{55}\frac{m\pi}{a} \\ -(D_{12}+D_{66})\frac{mn\pi^2}{ab} & -(D_{66}\frac{m^2\pi^2}{a^2}+D_{22}\frac{n^2\pi^2}{b^2}+A_{44})+I\omega^2 & -A_{44}\frac{n\pi}{b} \\ -A_{55}\frac{m\pi}{a} & -A_{44}\frac{n\pi}{b} & -(A_{55}\frac{m^2\pi^2}{a^2}+A_{44}\frac{n^2\pi^2}{b^2}-\rho_t\omega^2) \end{bmatrix} \begin{bmatrix} B_{mn} \\ C_{mn} \\ A_{mn} \end{bmatrix} = \begin{bmatrix} 0 \\ 0 \\ \frac{4p}{mn\pi^2}((-1)^n-1)(1-(-1)^m) \end{bmatrix}$$

In this model, only bending behavior is considered. Therefore, another rotational degree of freedom is added to the system. The translational displacement at the center of the plate is shown in Figure 3.17 for an aluminum core. The shear modulus is added to the honeycomb core. η is chosen to be 0, 0.2, and 0.4 respectively in Figure 3.17.

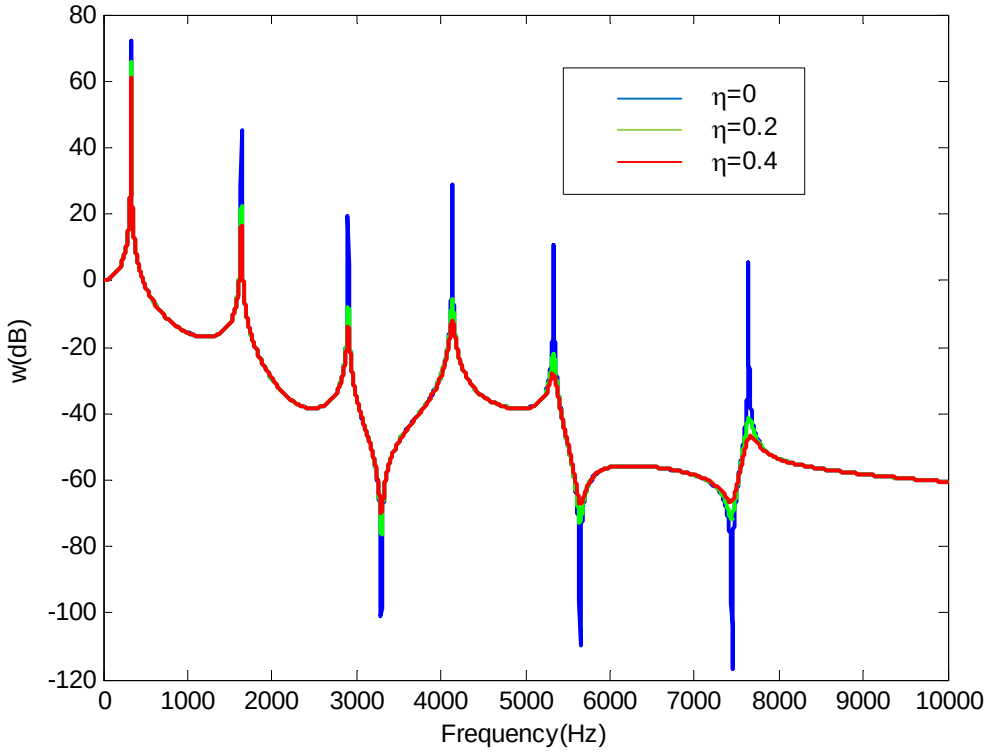

Figure 3.17: w via frequency at plate center

The results for two rotational degrees of freedom are given in Figure 3.18 and Figure 3.19.

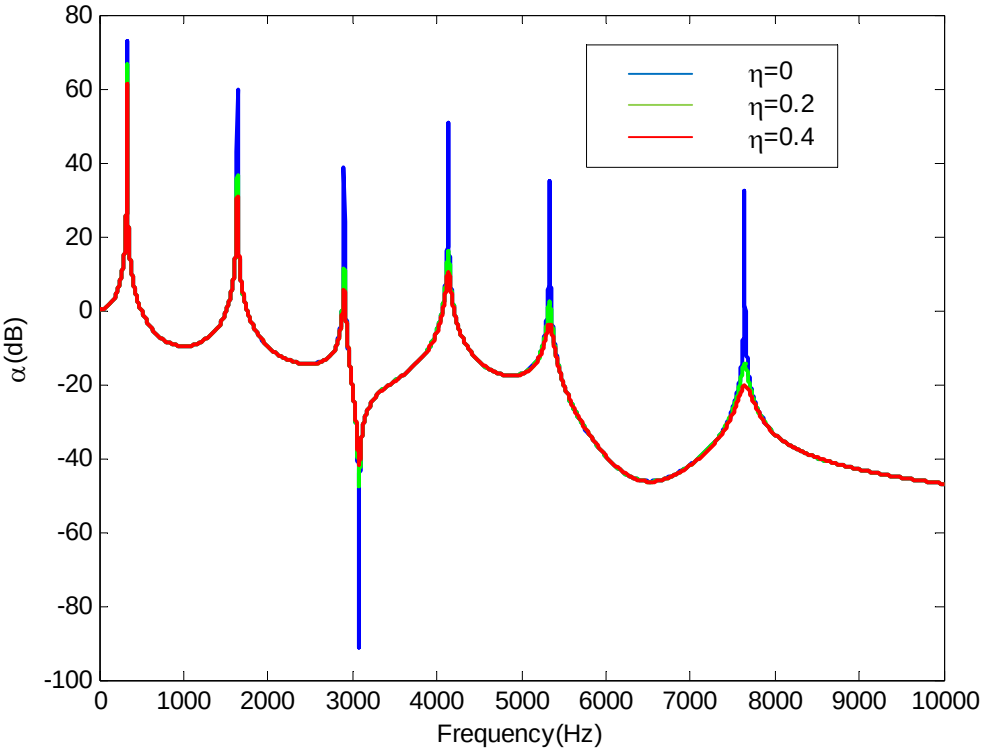

Figure 3.18: α via frequency for plate problem (Al core)

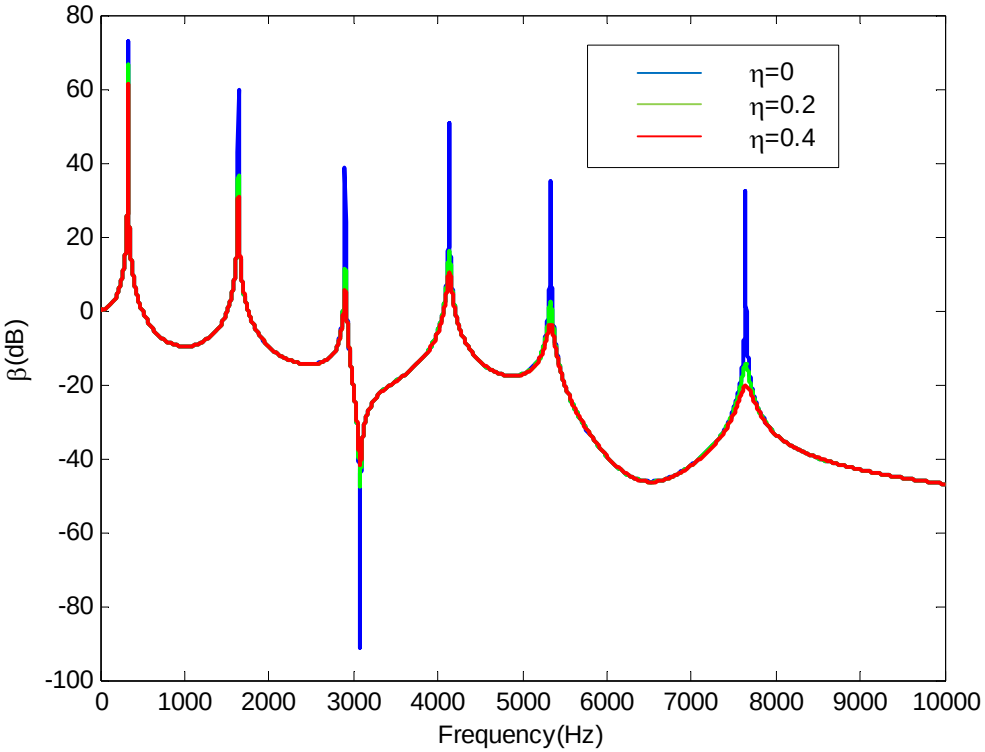

Figure 3.19: β via frequency for plate problem (Al core)

It is found that Figure 3.18 and Figure 3.19 are identical to each other. This is due to the fact that the point being studied is the center of the plate. The external loading is a pressure distributed on the whole plate. The plate is simply-supported on all edges. Therefore, the two degrees of freedom have the same behavior.

The study above has neglected the rotary inertia term. In the following study, this term is added back to the system to see what change it may bring to the system.

Figure 3.20 shows the undamped system with the rotary inertia term added back. It is compared with the undamped system without rotary inertia which is also shown in Figure 3.17.

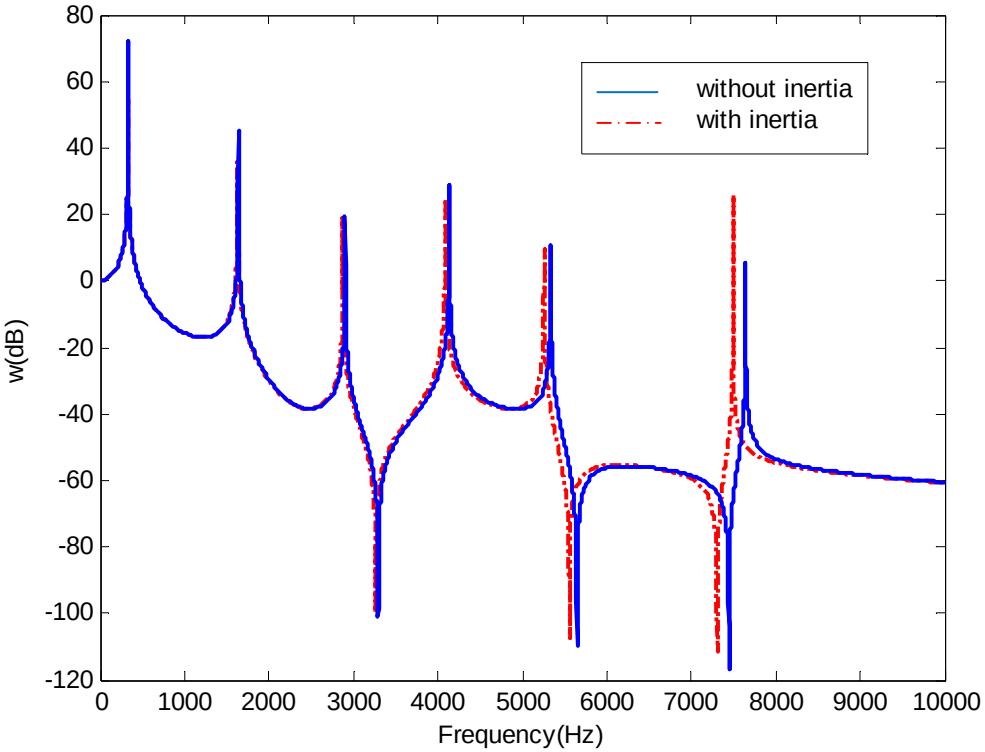

Figure 3.20: w via frequency (Al core, undamped)

The case when η=0.2 is given in Figure 3.21.

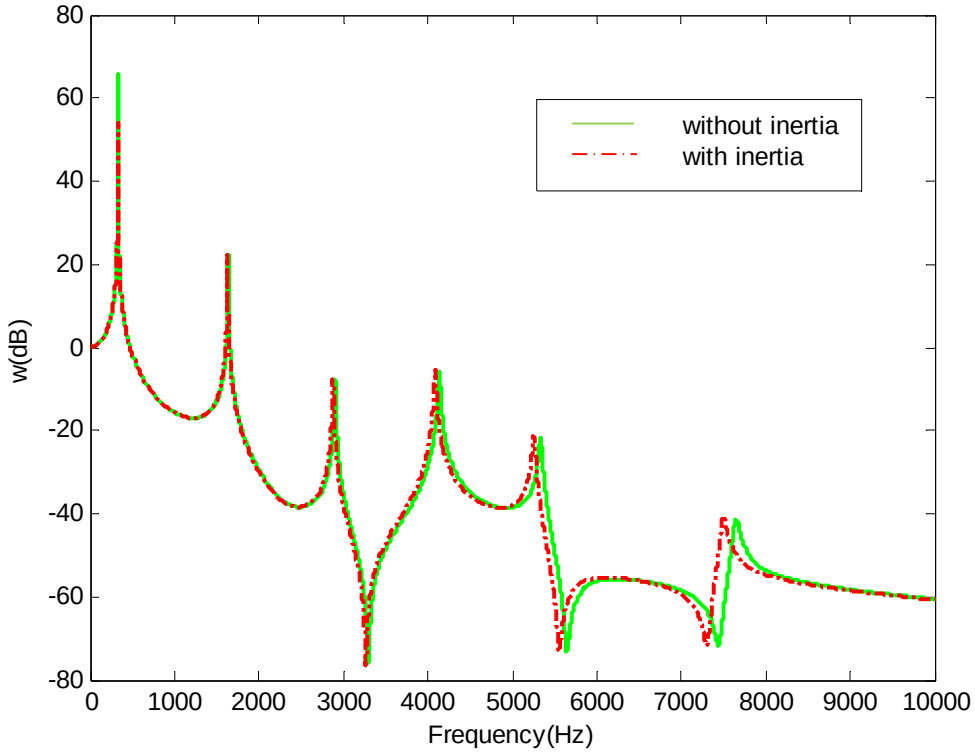

Figure 3.21: w via frequency (Al core, η=0.2)

It can be seen from Figure 3.20 and Figure 3.21 that without the rotary inertia, the first two peaks match the model with the rotary inertia, but for higher modes, the natrual frequencies shift to the left for the model with rotary inertia with the peak values being the same. Therefore, rotary inertia is important in simulating plate behavior.

Figure 3.22 shows the compare between a sandwich plate with polycarbonate core without viscoelastic property and a one which has viscoelastic property. It is noted that the rotary inertia is added in the following compares.

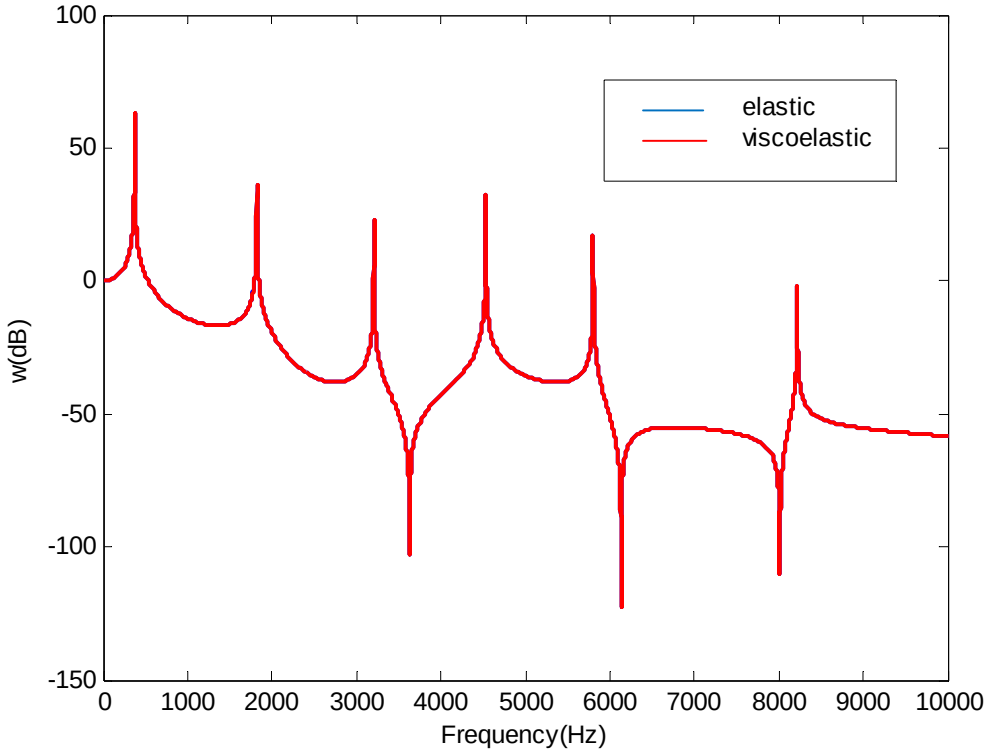

Figure 3.22: w via frequency at the first natural frequency (Poly core)

It is found that the difference is small between the viscoelastic polycarbonate core and the elastic polycarbonate core.

Figure 3.23 shows a compare between aluminum core with η=0 and polycarbonate core without viscoelastic property

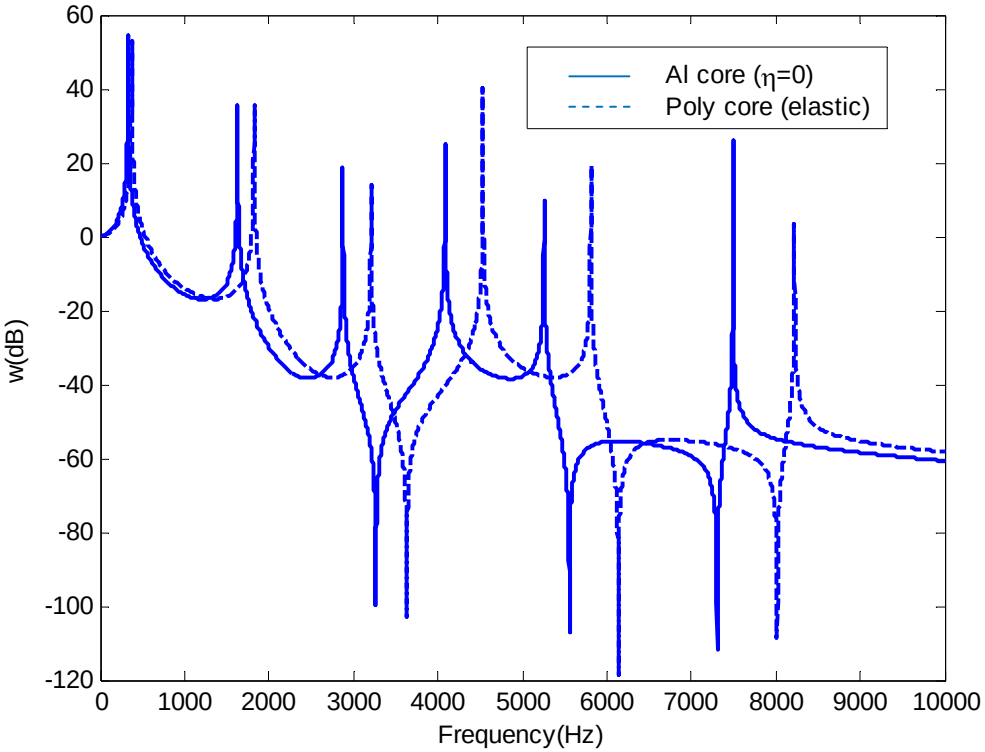

Figure 3.23: w, Compare between polycarbonate core (viscoelasticity turned off) and aluminum core (η=0)

Figure 3.24 shows a compare between aluminum core with η=0.2 and polycarbonate core with viscoelastic property.

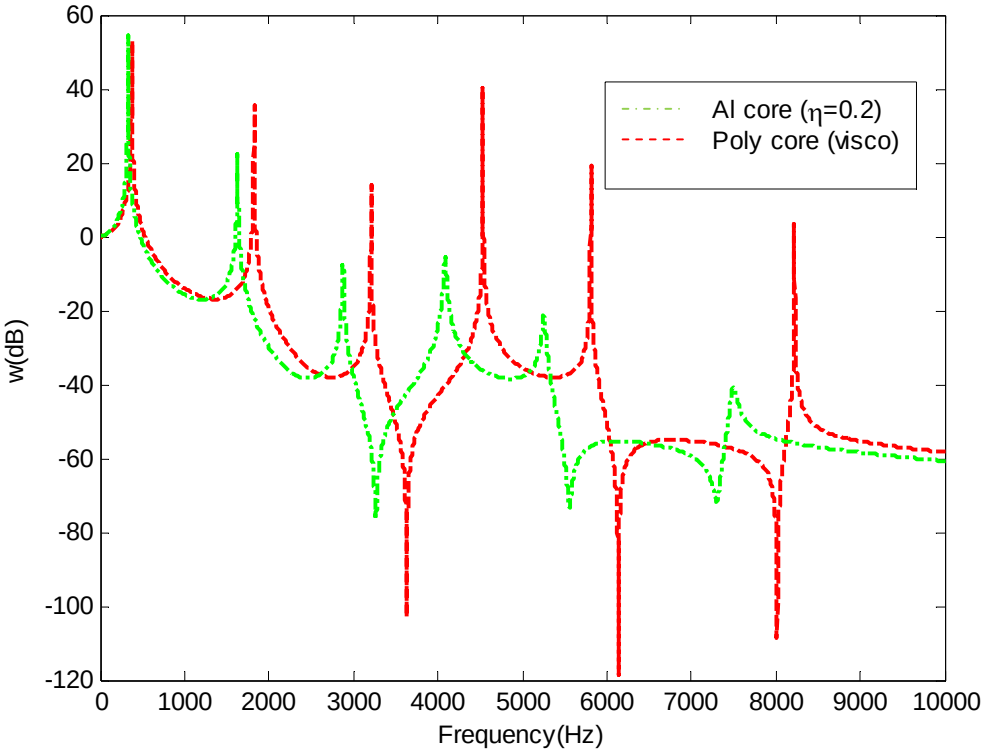

Figure 3.24: w, Compare between polycarbonate core (viscoelasticity turned on) and aluminum core (η=0.2)

The natural frequency of the system could be derived using the same way as discussed in chapter 3.5.2. For simplicity, the matrices formed governing equations could be written in the following form [2].

$$\begin{bmatrix} L_{11} & L_{12} & L_{13} \\ L_{12} & L_{22} & L_{23} \\ L_{13} & L_{23} & L_{33} - \rho_t \omega^2 \end{bmatrix} \begin{bmatrix} B_{mn} \\ C_{mn} \\ A_{mn} \end{bmatrix} = \begin{bmatrix} 0 \\ 0 \\ 0 \end{bmatrix}$$

According to the complete form of the governing equations, there will be two rotary inertia terms on L_{11} and L_{22}. However, they are neglected because including them will make the characteristic equation become difficult to solve. The natural frequency can be given in the following form

$$\omega_{mn} = \sqrt{(QL_{33} + 2L_{12}L_{23}L_{13} - L_{22}L_{13}^{\ 2} - L_{11}L_{23}^{\ 2})/(\rho_t Q)}$$
$$Q = L_{11}L_{22} - L_{12}^{\ 2}$$

The natural frequencies for the first ten modes are given in Table 3-5.

Table 3-5: Natural frequencies, Al (Hz)

f_1	f_2	f_3	f_4	f_5	f_6	f_7	f_8	f_9	f_{10}
332.0425	825.4761	825.4761	1313.5	1635.9	1635.9	2115.2	2115.2	2746.3	2746.3

It is interesting to find that the mode number m=3, n=3 (2902.8Hz) has larger frequency than the mode number m=4, n=1 and m=1, n=4 (2746.3Hz) which equal to each other.

The natural frequencies of the first ten modes for a sandwich plate with polycarbonate core are given in Table 3-6.

Table 3-6: Natural frequencies, Polycarbonate (Hz)

f_1	f_2	f_3	f_4	f_5	f_6	f_7	f_8	f_9	f_{10}
373.9184	927.9150	927.9150	1473.9	1833.6	1833.6	2366.7	2366.7	3066.2	3066.2

3.7 Comparison with Auxetic honeycomb cores

In addition to the regular honeycomb case discussed above, two auxetic honeycomb cores are provided in this part.

The type-I auxetic honeycomb has θ = -30°, and α = 2.

The type-II auxetic honeycomb has θ= -30°, α = 2 and β=0.09, since the wall thickness of the honeycomb is cut to 75% of the original one.

For the cylindrical bending case, the three types of honeycomb are compared using a sandwich plate with aluminum core and η=0. The response is shown in Figure 3.25

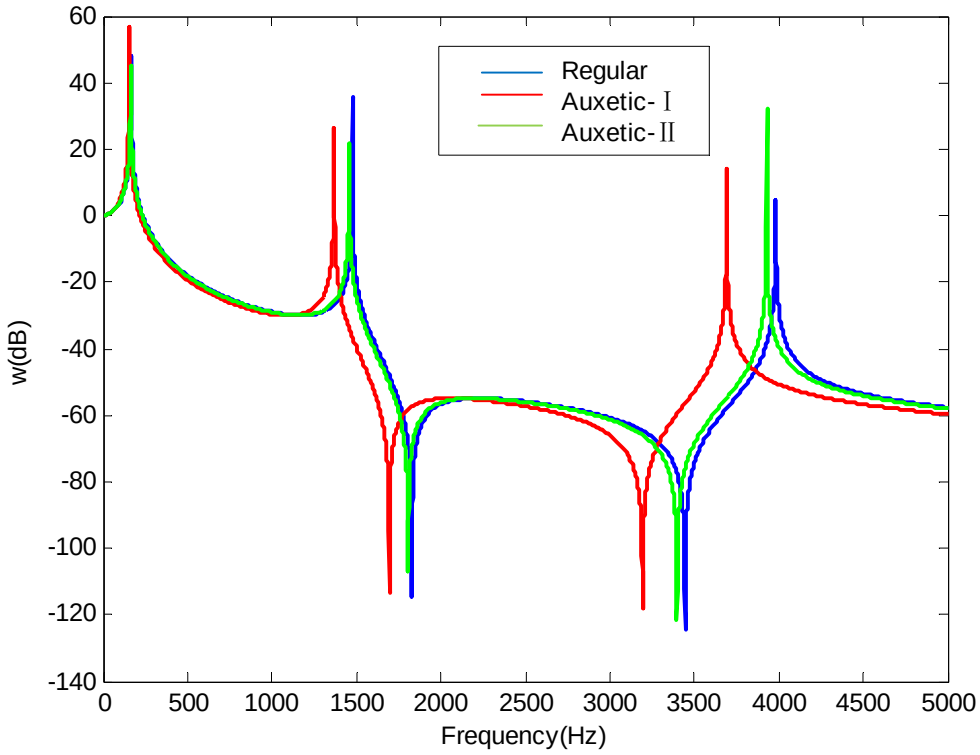

Figure 3.25: w via frequency, aluminum core (η=0)

It is found from Figure 3.25 that type-I auxetic honeycomb has the lowest natural frequencies on same modes comparing to the other two honeycomb cores. However it also has the highest first peak value. Figure 3.26 shows the damped response when η=0.2

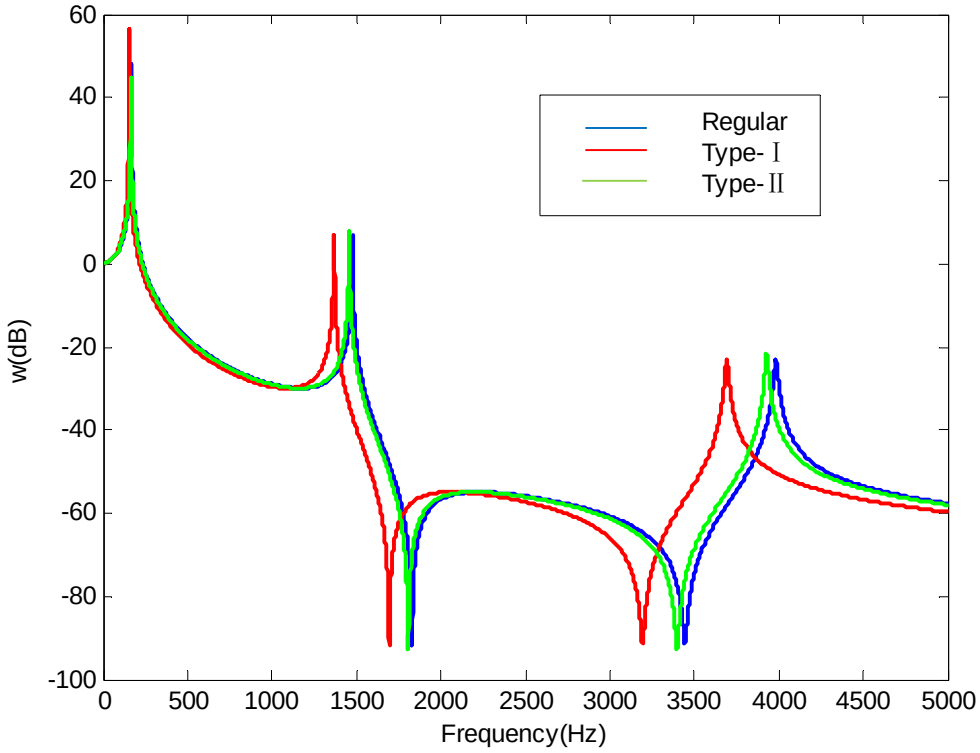

Figure 3.26: w via frequency, aluminum core (η=0.2)

It is found that type-I auxetic honeycomb has the lowest natural frequency and the highest first peak value. The undamped natural frequencies of type-I auxetic honeycomb and type-II auxetic honeycomb are shown in Table 3-7.

Table 3-7: Natural frequencies for the cylindrical bending problem, Aluminum (Hz)

	f_1	f_2	f_3	f_4	f_5
type-I	155.0111	616.5816	1374.6	2413.2	3711.7
type-II	165.2106	656.9148	1463.7	2567.5	3945.3

The results are then compared for polycarbonate cores. Figure 3.27 shows the sandwich plates with polycarbonate cores when the viscoelasticity is not included.

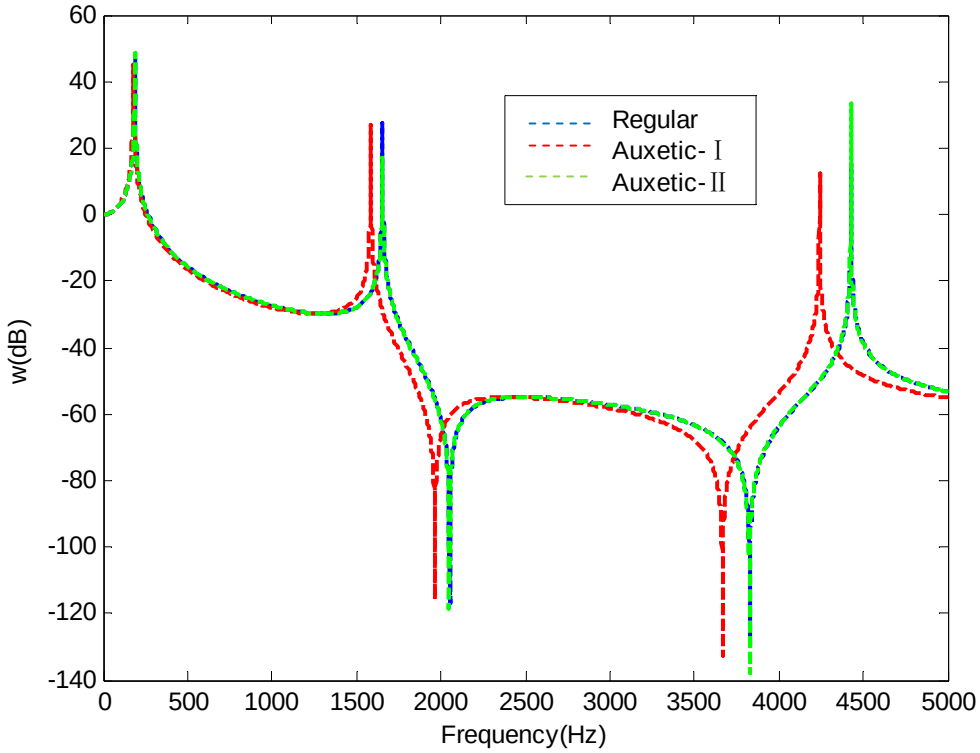

Figure 3.27: w via frequency, polycarbonate core (without viscoelastic property)

It can be seen from Figure 3.27 that the response around the first natural frequency for all three types are almost the same. For higher modes, type-I auxetic honeycomb still has the lowest natural frequencies. type-II auxetic honeycomb and regular honeycomb have very similar response except for the value of the second peak. Viscoelastic property is then included in Figure 3.28

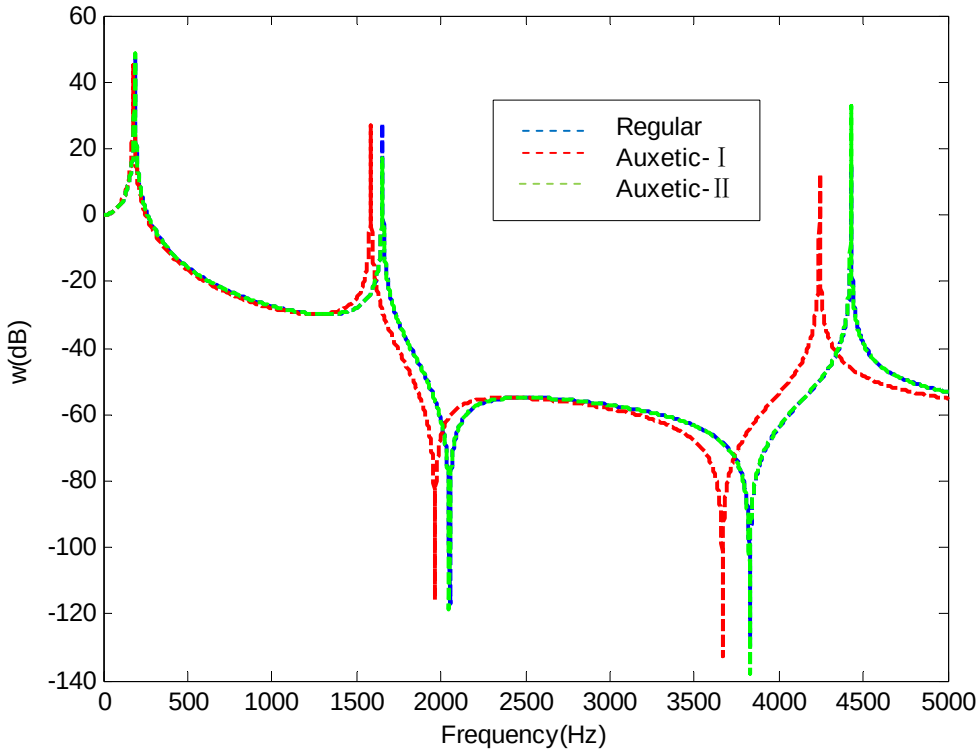

Figure 3.28: w via frequency, polycarbonate core (with viscoelastic property)

Table 3-8 shows the undamped natural frequencies of type-I auxetic honeycomb and type-II auxetic honeycomb with polycarbonate core

Table 3-8: Natural frequencies for the cylindrical bending problem, Polycarbonate (Hz)

	f_1	f_2	f_3	f_4	f_5
type-I	179.4926	712.6617	1584.2	2770.2	4240.8
type-II	187.3581	743.8763	1653.5	2891.3	4426.0

The compares are then made between plates with different types of honeycomb core. Figure 3.29 shows a compare using a sandwich plate with aluminum core and η=0

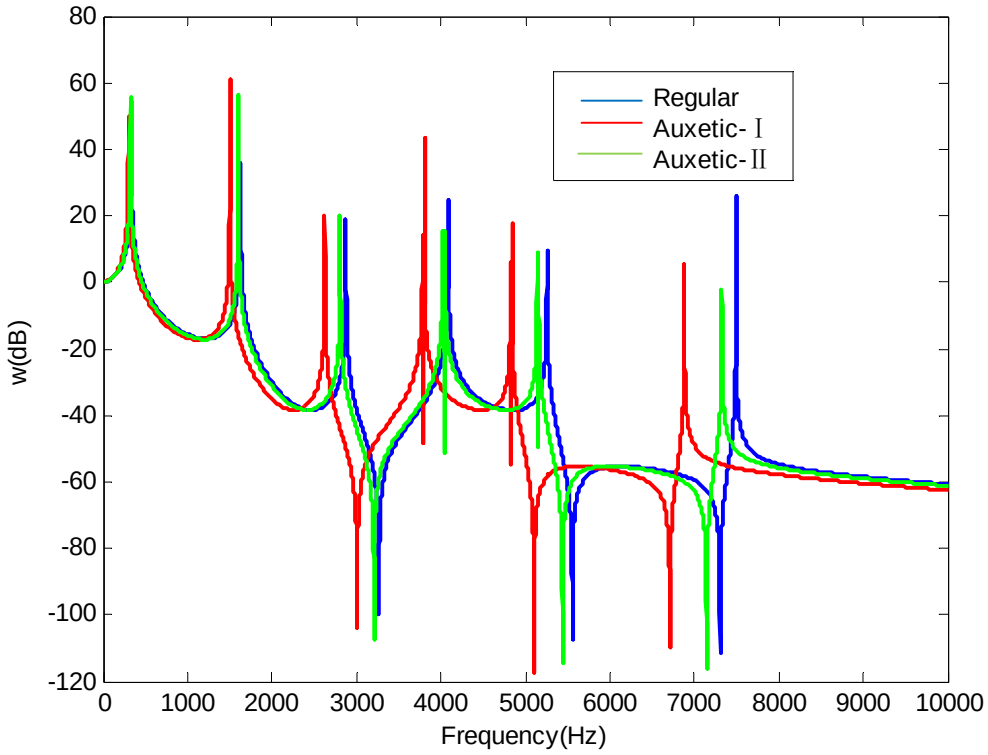

Figure 3.29: w via frequency, plate, Al core (η=0)

Figure 3.30 shows a compare using a sandwich plate with aluminum core and η=0.2

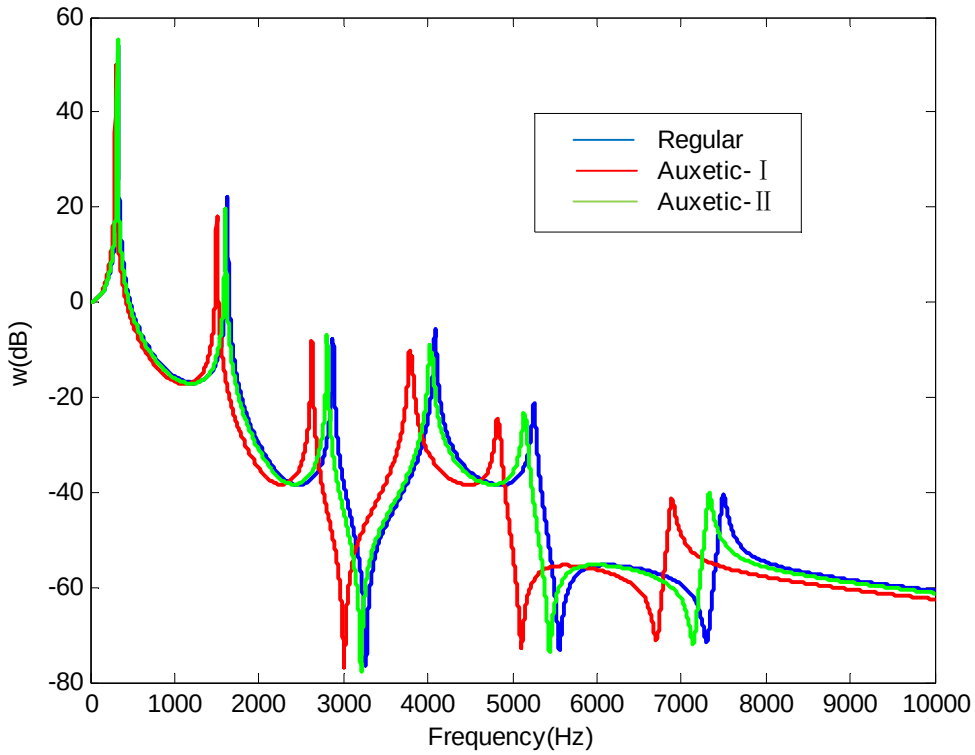

Figure 3.30: w via frequency, plate, Al core (η=0.2)

The undamped natural frequencies of type-I auxetic honeycomb and type-II auxetic honeycomb are shown in Table 3-9.

Table 3-9: Natural frequencies, Al (Hz)

	f_1	f_2	f_3	f_4	f_5	f_6	f_7	f_8	f_9	f_{10}
I	301.8213	756.5158	756.5158	1195.6	1509.9	1509.9	1934.4	1934.4	2535.8	2535.8
II	323.6310	809.3170	809.3170	1280.9	1608.4	1608.4	2066.4	2066.4	2703.7	2703.7

Figure 3.31 and Figure 3.32 show the response for the sandwich plate with polycarbonate core

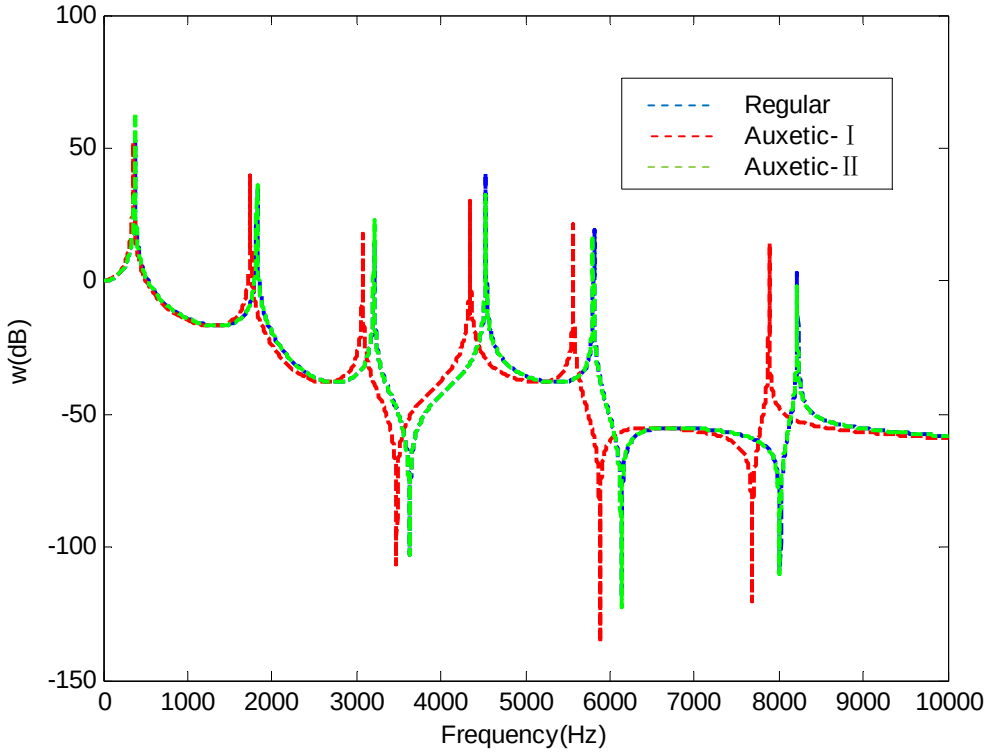

Figure 3.31: w via frequency, plate, Poly core (without viscoelasticity)

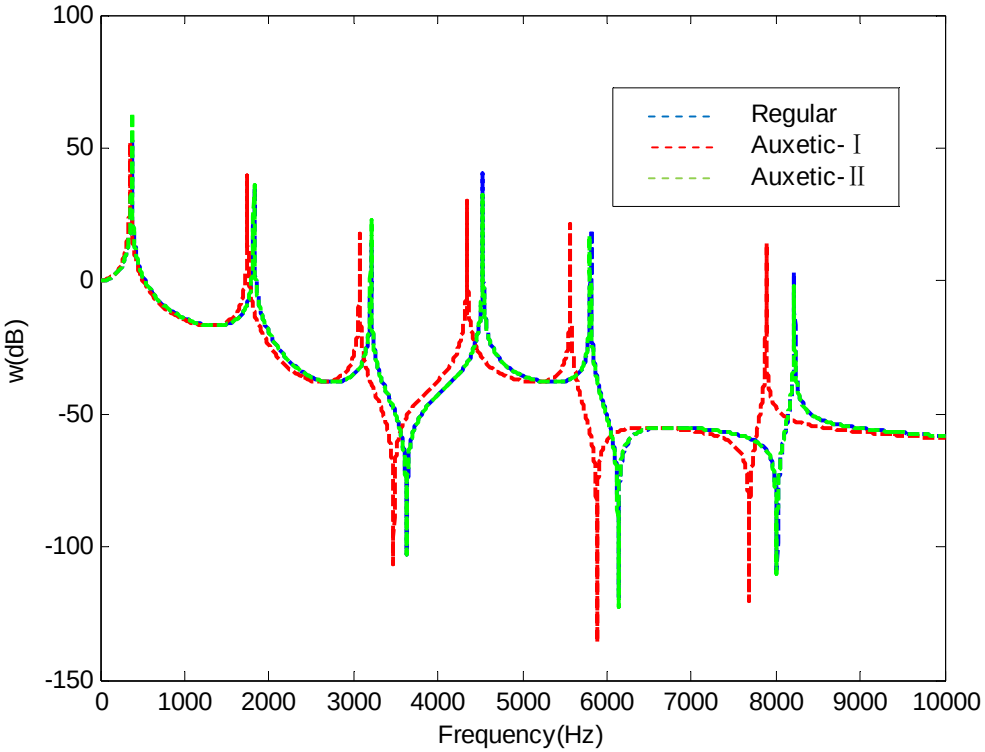

Figure 3.32: w via frequency, plate, Poly core (with viscoelasticity)

The undamped natural frequencies of type-I auxetic honeycomb and type-II auxetic honeycomb are shown in Table 3-10.

Table 3-10: Natural frequencies, Polycarbonate (Hz)

	f_1	f_2	f_3	f_4	f_5	f_6	f_7	f_8	f_9	f_{10}
I	357.8885	888.3845	888.3845	1410.8	1755.6	1755.6	2265.7	2265.7	2936.2	2936.2
II	373.6240	927.3202	927.3202	1472.8	1832.6	1832.6	2365.0	2365.0	3064.7	3064.7

CHAPTER FOUR – A HIGHER ORDER SHEAR DEFORMATION THEORY

It is known that the first order shear deformation theory is always used for its simplicity and low computational consumption. However, it is not accurate for composite material sometimes in that it assumes the same shear deformation for all layers which is not correct in many cases. Therefore, researchers have been studied for many years on developing new methods to simulate the behavior of the composite material more accurately. In this chapter, a higher order shear deformation theory [11] will be introduced. Compares will be made between this theory and FSDT for the cylindrical bending problem.

4.1 Derivation of the governing equation

The unique feature of this theory is that it does not take rotational degrees of freedom into consideration. Instead of that, it assumes different displacements on the top and bottom surfaces. Therefore, the displacement filed has three translational degrees of freedom which are u_1, u_3, and the transverse displacement w which is shown in Figure 4.1.

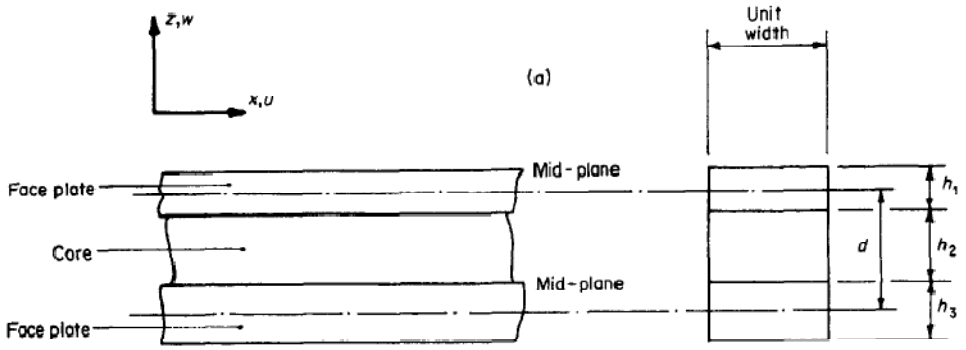

Figure 4.1: Coordinate system of the HSDT

The displacement field used in this theory is shown in Figure 4.2.

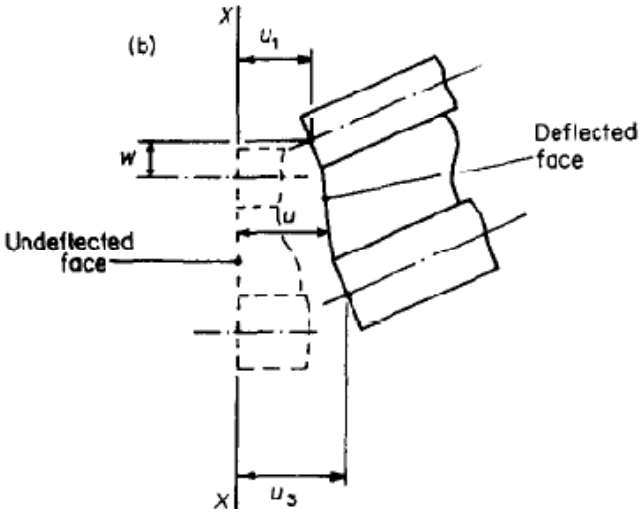

Figure 4.2: The displacement field for HSDT

Several assumptions are given below. Firstly, the core carries shear stress only. Secondly, face sheets have no shear strains.

As mentioned in Chapter 3, the transverse shear strain is given by

$$\gamma_{xz} = 2\varepsilon_{xz} = \frac{\partial w}{\partial x} + \frac{\partial u}{\partial z}$$

Based on the geometry given in Figure 4.1 and Figure 4.2, the shear strain can be derived as

$$\gamma = \frac{d}{h_2}\frac{\partial w}{\partial x} + \frac{u_1 - u_3}{h_2}$$

The shear stress is given by

$$\tau = G^* \gamma$$

where G^* can be the frequency dependent shear modulus. Figure 4.3 shows the forces and moments applied in a plate section.

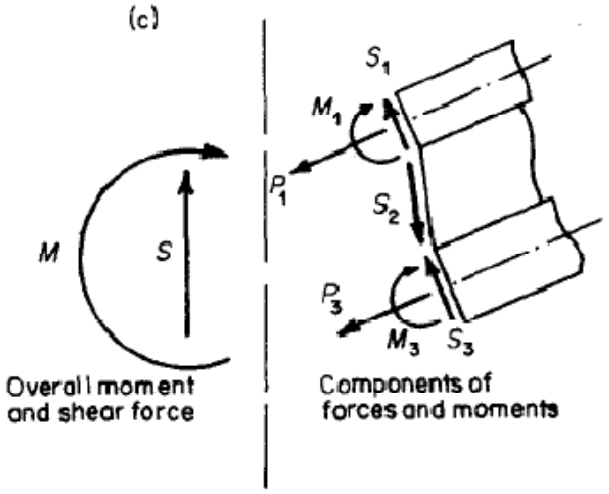

Figure 4.3: Forces and moments in a plate section

The total shear force S can be derived by

$$S = S_1 + S_2 + S_3 = D_1 \frac{\partial^3 w}{\partial x^3} - \tau d + D_3 \frac{\partial^3 w}{\partial x^3}$$

The relation between the total shear force and the external loading is given in a similar way considering Chapter 3.

$$\frac{\partial S}{\partial x} = -\rho_t \frac{\partial^2 w}{\partial t^2} + p$$

where p is the external transverse loading.

Another relation is established by using the normal forces which is shown below

$$\tau = -\frac{\partial P_3}{\partial x} = -\frac{\partial}{\partial x}(E_3 h_3 \frac{\partial u_3}{\partial x})$$

This can be related to the equation for the shear stress given above, which gives

$$\frac{\partial^2 u_3}{\partial x^2} - g u_3 = -gY \frac{D_t}{E_3 h_3 d} \frac{\partial w}{\partial x}$$

where the coefficients are defined by

$$g = \frac{G^*}{h_2}\left(\frac{1}{E_1 h_1} + \frac{1}{E_3 h_3}\right)$$
$$Y = \frac{d^2}{D_t}\left(\frac{E_1 h_1 E_3 h_3}{E_1 h_1 + E_3 h_3}\right)$$
$$D_t = D_1 + D_3 = (E_1 h_1^{\,3} + E_3 h_3^{\,3})/12$$

After combining the two relations together, the governing equation of the system in terms of w is given by

$$\frac{\partial^6 w}{\partial x^6} - g(1+Y)\frac{\partial^4 w}{\partial x^4} + \frac{m}{D_t}(\frac{\partial^4 w}{\partial x^2 \partial t^2} - g\frac{\partial^2 w}{\partial t^2}) = \frac{1}{D_t}(\frac{\partial^2 p}{\partial x^2} - gp)$$

where the transverse translational degree of freedom w can be simulated by using the same way as defined in chapter three for simply supported honeycomb sandwich plates. Then the system can be studied numerically using MATLAB.

The simply supported boundary condition of the beam is given by

$$w(0) = 0, \quad w(a) = 0$$
$$\frac{\partial^2 w}{\partial x^2}(0) = 0, \quad \frac{\partial^2 w}{\partial x^2}(a) = 0$$

The displacement field can then be written in the following form

$$w = \bar{w} e^{i\omega t} = (\sum_{m=1}^{k} A_m \sin\frac{m\pi x}{a}) e^{i\omega t}$$

The figure for the transverse displacement of the center is given below in Figure 4.4 for a honeycomb sandwich plate with polycarbonate core. It is compared with the Figure plotted using FSDT when other conditions are same. The displacement is not normalized to the static value in order to compare. The first five modes are being plotted.

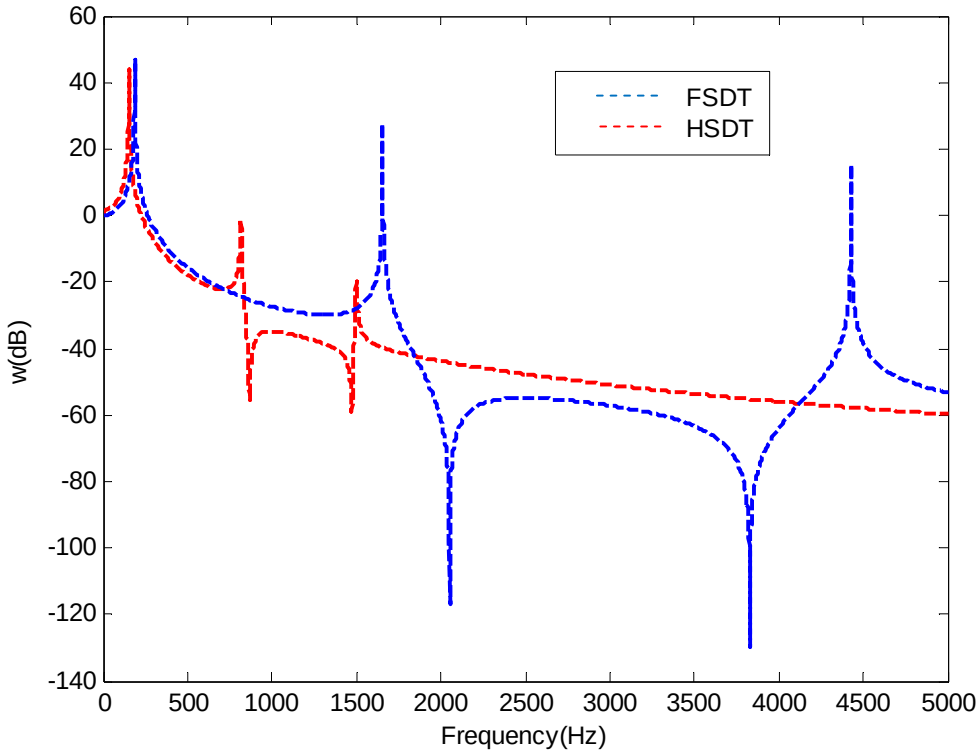

Figure 4.4: w via frequency (HSDT and FSDT)

It can be seen clearly that the displacement derived by higher order shear deformation theory has lower natural frequencies at the same mode comparing to the first order shear deformation theory. It can also be found that the peaks for the third and fifth

natural frequency are much lower for the HSDT. But the peaks for the first natural frequency are almost the same for both theories.

For further study, the property of the honeycomb core needs to be changed. In Figure 4.5, $\gamma = 1$ with the thickness of the face sheet being the same as the previous study. This means that the honeycomb core is set to be much thinner.

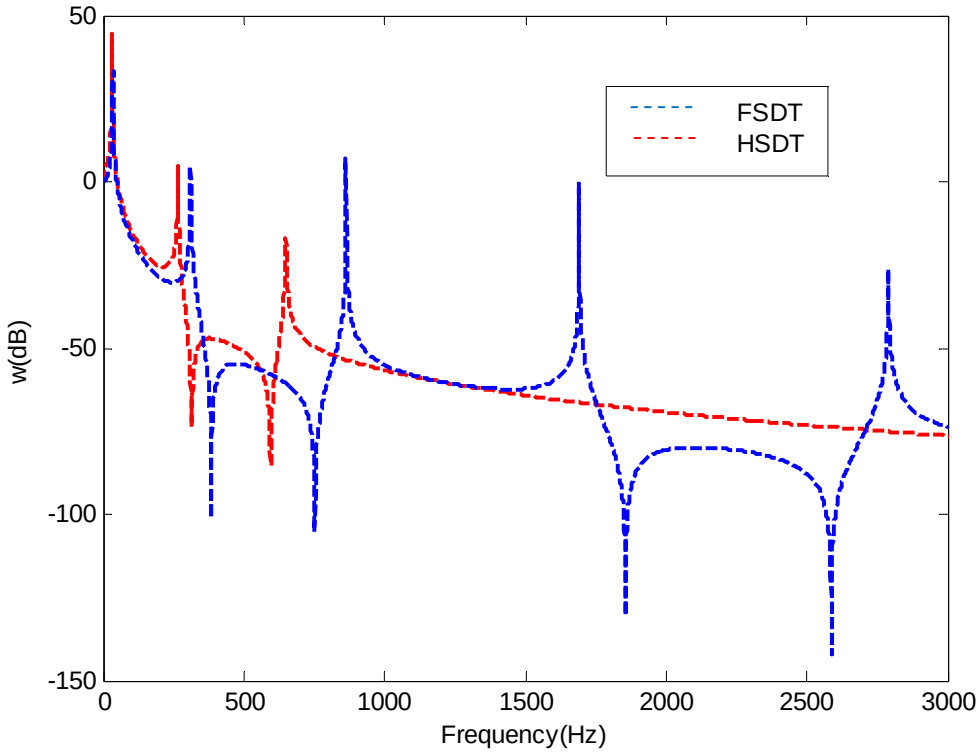

Figure 4.5: w via frequency (HSDT and FSDT) with γ = tc/tf = 1

From Figure 4.5, it is seen that the two plots using different theories become closer. It is also found that the natural frequencies for a thinner plate become much lower than thicker plates. The peak value at each natural frequency also gets much larger which

means that the vibration is more severe. In Figure 4.6, the thickness of the face sheet t_f is set to be 0.0001 and $\gamma = 1$. In Figure 4.7, the two theories are compared using the original dimensions with aluminum core.

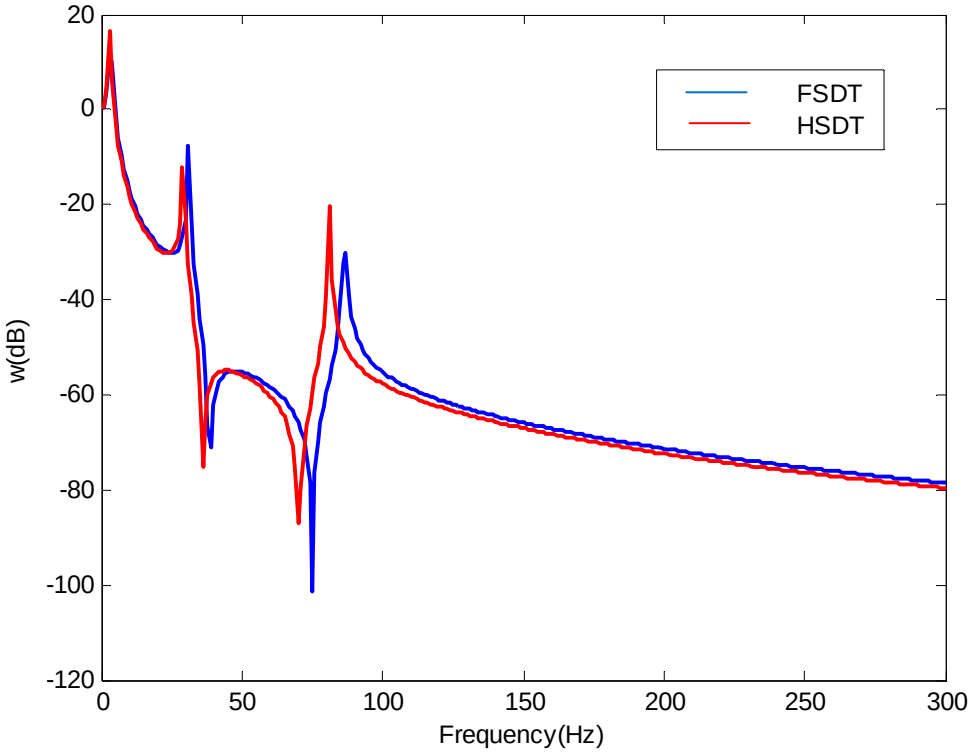

Figure 4.6: w via frequency (HSDT and FSDT) with γ = 1 and tf = 0.0001

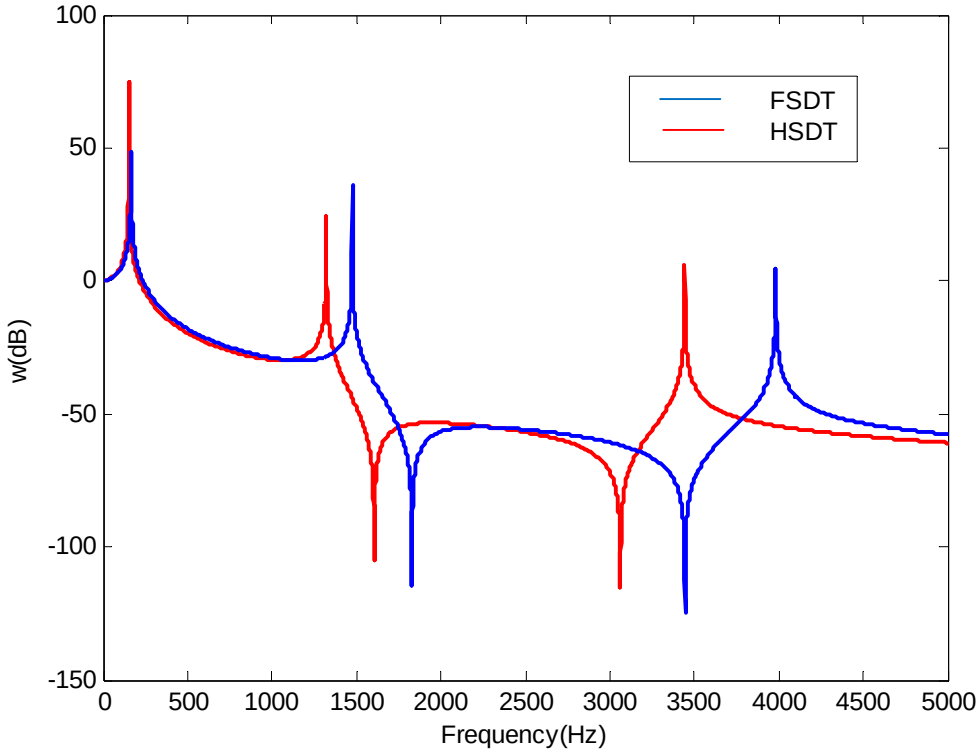

Figure 4.7: w via frequency (HSDT and FSDT Al core)

It can be seen in Figure 4.6 that the two plots are almost identical. This proves that the first order shear deformation theory is more feasible for modeling thin plates with stiff cores. For thick plates with soft cores, it can only give the correct peak for the first natural frequency. The damping effect of viscoelastic material is also not well modeled using FSDT. But FSDT is feasible for modeling stiffer cores made of aluminum. It is also known from the above compares that the HSDT is much better in honeycomb sandwich plate modeling. Another compare is made between HSDT for sandwich plate with polycarbonate core and aluminum core which has 0.2 in damping ratio. It is shown in Figure 4.8.

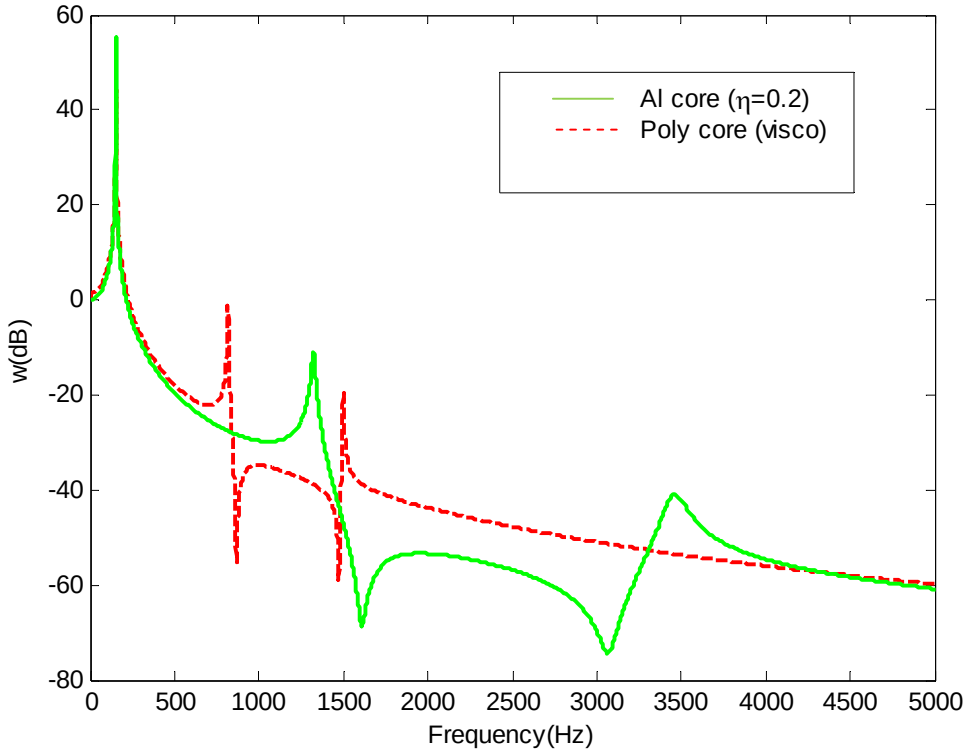

Figure 4.8: w via frequency (HSDT polycarbonate core and Al core with 0.2 damping ratio)

It is shown in Figure 4.8 that the viscoelastic property is modeled in a much better way using the HSDT comparing to Figure 3.11. Therefore, HSDT is a much better theory to model the honeycomb sandwich plate. It is also much better to use the HSDT to study the damping property of the plate when the geometry of the honeycomb core is changed.

In this study, for Auxetic type-I core, the cell wall angle is chosen to be $\theta = -30^{\circ}$ and $\alpha = 2$ with other dimensions remain the same.

The Auxetic type-II core is given by reducing 25% of the cell wall thickness which are $\alpha = 2$, $\theta = -30^{\circ}$ and $\beta = 0.09$.

The results are shown in Figure4.9 and Figure 4.10.

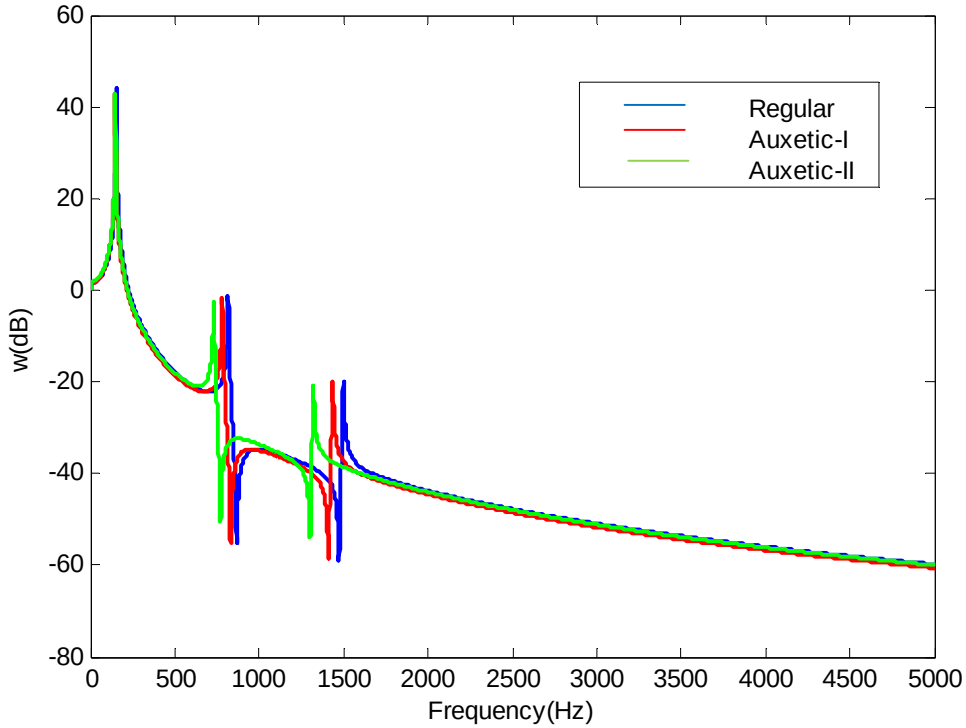

Figure 4.9: w via frequency, Poly (Auxetic cores and Regular core)

The first five modes are plotted in Figure 4.9. It can be seen that the natural frequencies of the Auxetic type-II core are lower than those of the regular honeycomb core and Auxetic type-I core.

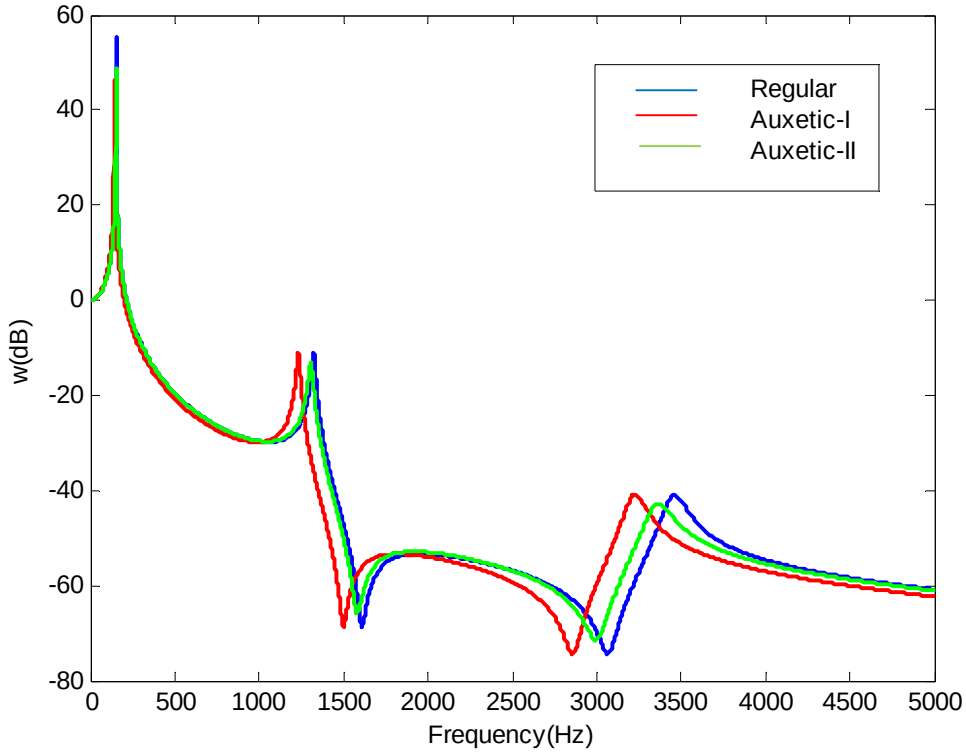

Figure 4.10: w via frequency, Al core, η=0.2 (Auxetic cores and Regular core)

Although the natural frequencies for Auxetic type-II core are higher than those of Auxetic type-I core. Better damping behavior could be found in Auxetic type-II core.

From Table 3-1 and Table 3-3, it is found that D_{11} for poly is similar to D_{11} stiffness for aluminum honeycomb core because, D_{11} is dominated by the stiffness of the aluminum face sheets, and not the core. That's why some researchers neglect the effect of core when calculating D_{11}. In contrast, A_{44} is greatly affected by the polycarbonate core stiffness, and thus changes significantly from aluminum core. However, the face sheet and the core take shear strain, and the shear modulus of the face sheet G_f(Al, 2.57×10^{10})

is much larger than that of the core G_c (poly core, 5.23×10^7). Although the face sheet are relatively thin comparing to the core thickness, the product of $2t_fG_f$ is still about 100 times larger than t_cG_c, which makes the face sheet still be the dominant factor in forming A_{44}. That's why there is not a significant change in A_{44} for Auxetic-II core comparing to regular core. As we know the natural frequency is determined by both stiffness and mass, $\omega=\sqrt{k/m}$. This explains why there is not much change from Auxetic-II core to regular core (Figure 3.27). This also explains why damping is not obvious in Figure 3.10. However, when the core is aluminum, the product of t_cG_c becomes much larger than the polycarbonate core. Therefore, the effect of core in A_{44} becomes much larger which makes A_{44} much smaller for Auxetic-II core comparing to regular core. Then the Auxetic-II becomes much softer than the regular core with the same mass. That's why for aluminum core, the figure shifts to the left in Figure 3.25.

For Auxetic-I core, D_{11} and A_{44} are identical to the coefficients of regular core. The little difference in the D_{11} is caused by the refined theory, which makes the Poisson's ratio for Auxetic-I not equal to each other ($\nu_{12}=-0.9469,\quad \nu_{21}=-0.9169$). The Auxetic-I core has heavier mass, which also cause the natural frequencies to shift to the left comparing to regular core.

From the above discussion, it is seen that the first order shear deformation theory has the drawback that it let the face sheet carry too much shear strain, which is corrected in the HSDT. In HSDT, only the core takes shear stress which makes it more sensitive to

the change in the core material. In Figure 4.10, unlike FSDT (Figure 3.27), significant shift can be seen in the curve for Auxetic-II core from regular core. This is due to the fact that the core takes major effect in the shear stiffness. Therefore, a change in the stiffness from regular core to Auxetic-II core is expressed in Figure 4.10. It is also interesting to see that the curves in Figure 4.11 keep the same sequence as Figure 3.26. This is due to the reason that the shear stiffness of aluminum core is much larger than polycarbonate core. Therefore, without significant reduction in the shear stiffness, the HSDT plot matches the FSDT plot in curve sequence.

CHAPTER FIVE – FEM MODELING USING ANSYS

As described in the first chapter, there are several ways to model the honeycomb sandwich plate using ANSYS. In this chapter, the model is established using the homogeneous plate method with effective honeycomb properties input before modeling. A SHELL281 element is used in the modeling. The original dimensions are used for compare. The aluminum core and face sheet are used in the analysis. The polycarbonate core is not used in that ANSYS does not allow users to add viscoelastic material property for modal analysis and time harmonic analysis. The plate is established using shell section lay-up method in preprocessing. It is also viable to using the pre-integrated method which means to input the [*A*], [*B*] and [*D*] matrices directly. There are 400 elements in total. The boundary condition is simply supported with no external loading in modal analysis. Firstly, a modal analysis is taken to extract natural frequencies. Ten natural frequencies are extracted for the first ten modes which are shown in Table 5-1.

Table 5-1: Natural frequencies (Hz)

f_1	f_2	f_3	f_4	f_5	f_6	f_7	f_8	f_9	f_{10}
329.32	**809.15**	**809.15**	**1273.2**	**1574.6**	**1574.6**	**2015.1**	**2015.1**	**2583.4**	**2583.4**

The figure for the deformed shape of the transverse translational degree of freedom for each mode is given below in Table 5.1.

Table 5-2: Mode shapes

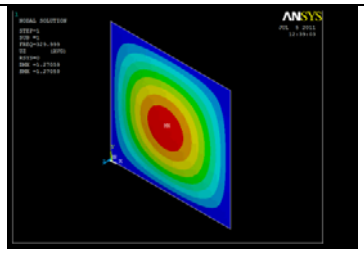 Mode 1	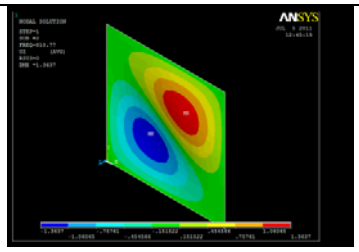 Mode 2
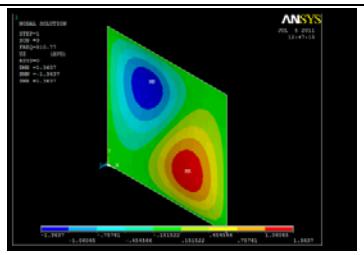 Mode 3	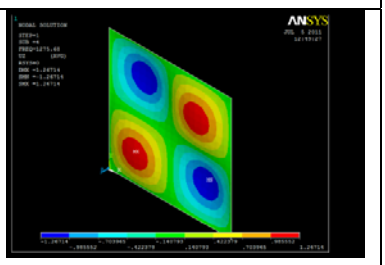 Mode 4
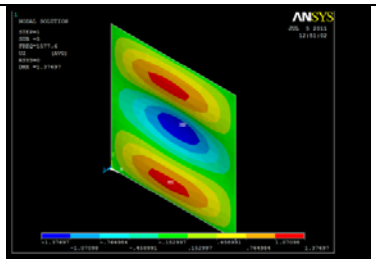 Mode 5	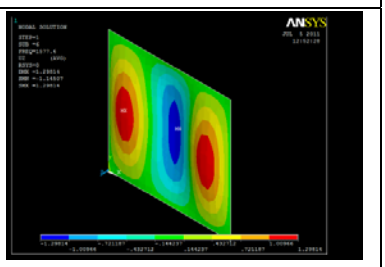 Mode 6
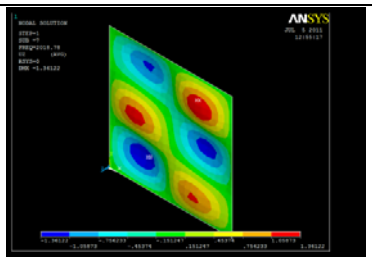 Mode 7	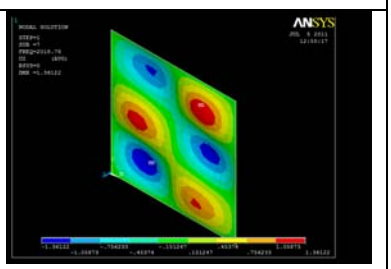 Mode 8
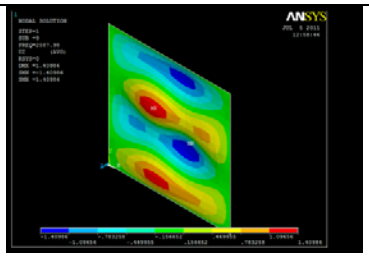 Mode 9	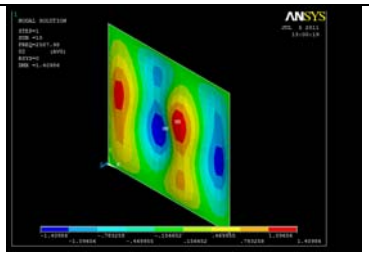 Mode 10

It can be seen from Table 5-2 that there are similar mode shapes when the natural frequencies for different modes are same, but the mode shapes have different directions. This happens when $m = i$, $n = j$ and $m = j$, $n = i$, where m, n are mode numbers. This is due to the simply supported boundary conditon.

The result for w at the center of the plate is shown in Figure 5.1.

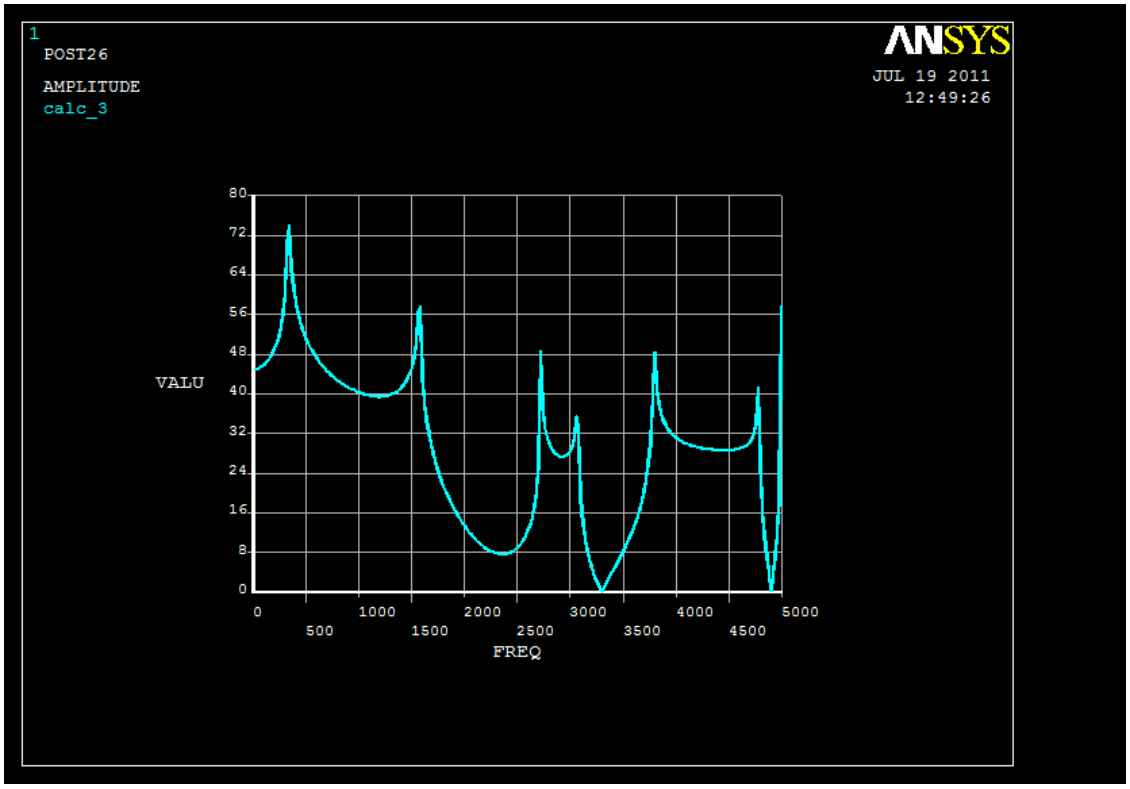

Figure 5.1: w via frequency at the center of the plate (ANSYS)

Comparing to Figure 3.13, it can be found that the peak values happen at the same frequencies.

CHAPTER SIX – CONCLUSIONS

6.1 Effective honeycomb core mechanical property study and material selection

In Chapter 2, the unique mechanical property of the honeycomb core is studied. The popular way to derive the effective properties, the CMT theory, is introduced. It is found that the density of the honeycomb core is significantly reduced comparing to the building material, which creates a huge weight loss in designing. While the in-plane moduli are much reduced, the moduli in the out-of-plane direction remain relatively high which proves the high stiffness-to-weight ratio of a honeycomb sandwich plate. The honeycomb core with a regular hexagonal shape shows interesting mechanical property. The effective Young's modulus in X_1 direction is equal to that of X_2 direction. The Poisson's ratio also shows the same value.

Aluminum is always used by composite material manufacturers as the building material for honeycomb sandwich plates, because aluminum has a low density and low price considering other metals. It is also easy to process. Therefore, it is worthwhile to study aluminum honeycomb sandwich plates.

The damping property is a very important characteristic of the honeycomb sandwich plate. That's why the polycarbonate material is chosen for the study. It is interesting to know the behavior of a sandwich plate when frequency dependent viscoelastic damping property is added to the system. The way how frequency affects the shear modulus of the polycarbonate material is introduced in Chapter 2. This effect is then generalized to other modulus of the polycarbonate material and to the effective

modulus of the honeycomb core. It is found when comparing to the aluminum core with the same dimension that the polycarbonate core is much softer.

6.2 FSDT theory, governing equations for beam and plate

In Chapter 2, the governing equations of the sandwich plate are derived using the first order shear deformation theory. The governing equations are derived using the stress-strain-displacement relations. In the process of deriving the equations, the [A], [B] and [D] matrices are introduced based on the relation between stress resultants and stresses. The governing equations are then simplified to a form for solving 1D beam problems. For simplicity, the in-plane extensional equations and terms as well as the rotary inertia are neglected. It is interesting to study the behavior of the sandwich plate with a soft core and stiff face sheets and make compares with the plate built by aluminum core. It is shown that the FSDT is not good for modeling polycarbonate cores since it is known that a polycarbonate core is much softer. Therefore, the system built by a polycarbonate core should have much lower natural frequency for the same mode than the aluminum core. However, it is seen in Chapter 3 that the frequencies of the polycarbonate core are much higher. Only the first mode might be accurate. So the FSDT is not a good choice when high accuracy is needed in modeling.

6.3 HSDT and compares

Because of the imperfection of the FSDT, HSDT is needed in modeling soft cores. It is introduced in detail in Chapter 3. Other than FSDT, HSDT does not consider the rotational degree of freedoms. It uses different translational displacement on the top and

the bottom surfaces of the plate and assumes different shear strain in the transverse direction. After comparing with the FSDT, it is found that the polycarbonate core modeled by the HSDT is much more accurate. The limited cases are taken. It is found in these cases that the FSDT and HSDT become similar when the total thickness of the plate is very small.

6.4 FEM solution using ANSYS

In Chapter 5, the plate is modeled using ANSYS for compare. Only aluminum core is studied in that the viscoelastic property of the polycarbonate core will be neglected in modal analysis and time harmonic analysis. The first ten modes of the plates are extracted using modal analysis.

6.5 Future work

In the present work, the viscoelastic damping is studied. In the future work, it is interesting to know the effect that the change of plate dimensions can bring to the system. Using the analytical models developed in this work, comparisons between Regular and Auxetic honeycomb effective properties could also be compared. The effective properties of honeycomb can easily be changed in the models by simply changing the angles and length ratios the unit cell geometry. It is also interesting to study the damping optimization of the system, by varying the geometric properties of the honeycomb cells.

The HSDT is used in the study. This theory needs to be refined in the future study by adding rotational degree of freedom into the displacement field.

A new method shall be developed for ANSYS to take nonlinearity into consideration during modal analysis and time harmonic analysis.

REFERENCES

1. Scarpa, F. and Tomlinson, G., "Theoretical Characteristics of the Vibration of Sandwich Plates with In-Plane Negative Poisson's Ratio Values," *Journal of Sound and Vibration*, Vol. 230(1), Jun. 1999, pp. 45-67.
2. Dobyns, A. L., "Analysis of Simply-Supported Orthotropic Plates Subject to Static and Dynamic Loads," *AIAA Journal*, Vol. 19, pp. 642-650.
3. Chandra, R., Singh, S. P. and Gupta, K., "Damping Studies in Fiber-Reinforced Composites-a Review," *Composite Structures*, Vol. 46, 1999, pp. 41-51.
4. Latheswary, S., Valsarajan, K. V. and Sadasiva Rao, Y. V. K., "Dynamic Response of Moderately Thick Composite Plates," *Jouranal of Sound and Vibration*, Vol. 270, 2004, pp. 417-426.
5. Araújo, A. L., Martins, P., Mota Soares, C. M., Mota Soares, C.A. and Herskovits, J., "Damping Optimization of Viscoelastic Laminated Sandwich Composite Structures," *Struct Multidisc Optim*, Vol. 39, 2009, pp. 569-579.
6. Meunier, M. and Shenoi, R. A., "Dynamic Analysis of Composite Sandwich Plates with Damping Modeled Using High-Order Shear Deformation Theory," *Composite Structures*, Vol. 54, 2001, pp. 243-254.
7. Nayak, A. K., Shenoi, R. A. and Moy, S. S. J., "Analysis of Damped Composite Sandwich Plates Using Plate Bending Elements with Substitute

Shear Strain Fields Based on Reddy's Higher-Order Theory," *Proc Instn Mech Engrs*, Vol. 216(Part C), 2002, pp. 591-606.

8. Makhecha, D. P., Ganapathi, M. and Patel, B. P., "Vibration and Damping Analysis of Laminated/Sandwich Composite Plates Using Higher-Order Theory," *Journal of Reinforced Plastics and Composites*, Vol. 21, 2002, pp. 559-575.
9. Siala, W., Abdennadher, M., Hammami, L. and Haddar, M., "Modal Damping Prediction of Sandwich Panel with Visco-Elastic Thick Core," *Proceedings of the Institution of Mechanical Engineers, Part C: Journal of Mechanical Engineering Science*, Vol. 222, 2008, pp. 2077-2086.
10. Zhu, D., "Modeling and Parameters Identification of Dynamic Properties of Paper Honeycomb Panel," *International Conference on Computer Science and Software Engineering*, 2008.
11. Mead, D. J., Markus, S., "The Forced Vibration of a Three-Layer, Damped Sandwich Beam with Arbitrary Boundary Conditions," *Journal of Sound and Vibration*, Vol. 10(2), 1969, pp. 163-175.
12. Sadasiva Rao, Y. V. K., "Vibrations of Unsymmetrical Sandwich Beams and Plates with Viscoelastic Cores," *Journal of Sound and Vibration*, Vol. 34(3), 1974, pp. 309-326.
13. Greenberg, J. B. and Stavsky, Y., "Vibration of axially compressed laminated orthotropic cylindrical shells, including transverse shear deformation," *Acta Mechanica*, Vol. 37, 1980, pp. 13-28.

14. Mercier, J. P., Aklonis, J. J., Litt, M. and Tobolsky, A. V., "Viscoelastic Behavior of the Polycarbonate of Bisphenol A," *Journal of Applied Polymer Science*, Vol. 9, 1965, pp. 447-459.
15. Gibson, L. J. and Ashby, M. F., *Cellular Solids*: *Structure* & *Properties*, Pergamon Press, Oxford, 1997.
16. ABAQUS CAE/User's Manual
17. ANSYS 13.0 Help, 2010 SAS IP, Inc.
18. http://en.wikipedia.org/wiki/Composite_material
19. http://www.grc.nasa.gov/WWW/RT/2006/RX/RX11C-hurwitz1.html
20. http://www.archiexpo.com/prod/multipanel-uk/composite-lightweight-sandwich-panels-60737-258830.html
21. http://www.netcomposites.com/newspic.asp?6698